THESIS FOR THE DEGREE OF DOCTOR OF PHILOSOPHY

Neutron Multiplicity Counting with the Analysis of Continuous Detector Signals

LAJOS NAGY

Department of Physics
Chalmers University of Technology
Gothenburg, Sweden

Faculty of Natural Sciences
Budapest University of Technology and Economics
Budapest, Hungary

March 2021

Cover:
Illustration of the voltage signal observed in a neutron detector. As the intensity of detections increases, individual voltage pulses start to overlap until they form a continuous fluctuating signal.

Neutron Multiplicity Counting with the Analysis of Continuous Detector Signals
LAJOS NAGY
Department of Physics
Chalmers University of Technology

Abstract

Neutron multiplicity counting is a non-destructive assay method for determining the mass of fissile materials (primarily plutonium) using the measured values of the singles, doubles and triples detection rates. Traditionally, the detection rates are obtained from the counting statistics of neutron detectors. The main problem with this approach is that it is sensitive to the overlapping of pulses which, especially at high count rates, lead to dead time losses in the counting electronics. This feature limits the applicability of the method to the measurement of samples with low emission intensities. To overcome this constraint, an alternative version of neutron multiplicity counting has been developed. The new approach is based on the direct analysis of the continuous voltage signals of the detectors (primarily fission chambers). Since the procedure does not rely on counting individual pulses, it is inherently free from dead time losses caused by their overlapping. As a result, the proposed method provides an alternative to traditional multiplicity counting, especially when measuring high intensity samples, like spent nuclear fuel. The thesis presents the complete process of establishing the new version of multiplicity counting. Based on a stochastic model of continuous detector signals, expressions are derived for some of their one- two and three-point (in time) moments (including their mean, covariance function and bicovariance function) and it is shown that the singles, doubles and triples detection rates can be recovered from them. In a computational study, detector signals are simulated and analysed in order to investigate the effect of certain parameters (the measurement time, the detection efficiency, the amplitude of the electronic noise and the intensity of non-neutron pulses) on the estimated values of the detection rates. To demonstrate the practical use of the proposed method, measurements have been performed using a ^{252}Cf source and the detection rates recovered from the moments of the recorded signals were compared with reference values obtained with pulse counting.

List of publications

This thesis is based on the work contained in the following papers:

[P1] I. Pázsit, L. Pál, and L. Nagy. "Multiplicity counting from fission chamber signals in the current mode". *Nuclear Instruments and Methods in Physics Research Section A: Accelerators, Spectrometers, Detectors and Associated Equipment* **839** (2016): 92-101.

[P2] L. Nagy, I. Pázsit and L. Pál, "An extended theory of multiplicity counting from fission chamber signals in the current mode". In: *International Conference on Mathematics and Computational Methods Applied to Nuclear Science and Engineering*, Jeju, Korea, April 16–20, 2017.

[P3] L. Nagy, I. Pázsit and L. Pál. "Multiplicity counting from fission detector signals with time delay effects". *Nuclear Instruments and Methods in Physics Research Section A: Accelerators, Spectrometers, Detectors and Associated Equipment* **884** (2018): 119-127.

[P4] L. Nagy, I. Pázsit and L. Pál. "Two-and three-point (in time) statistics of fission chamber signals for multiplicity counting with thermal neutrons". *Nuclear Instruments and Methods in Physics Research Section A: Accelerators, Spectrometers, Detectors and Associated Equipment* **929** (2019): 148-155.

[P5] L. Nagy, I. Pázsit, L. Pál, G. Klujber and M. Szieberth, "Multiplicity counting using the two- and three point statistics of fission chamber signals – theory and experimental demonstration". In: *International Conference on Mathematics and Computational Methods Applied to Nuclear Science and Engineering*, Portland, Oregon, USA, August 25–29, 2019.

[P6] L. Nagy, I. Pázsit, L. Pál, G. Klujber and M. Szieberth, "Measurements and simulations to investigate the feasibility of neutron multiplicity counting in the current mode of fission chambers". *EPJ Web of Conferences*. Vol. 225. EDP Sciences, 2020.

[P7] L. Nagy, G. Klujber, I. Pázsit, I. Barth, Y. Kitamura, T. Misawa and M. Szieberth, "Experimental Demonstration of Neutron Multiplicity Counting in the Current Mode of Fission Chambers". *INMM 61st Annual Meeting*, (Online), July 12–16, 2020.

[P8] L. Nagy, Y. Kitamura, I. Pázsit and M. Szieberth, "New Paradigm in Neutron Fluctuation Analysis: Extracting the Statistics of Discrete Detection Events from Time-resolved Signals of Fission Chambers". To appear in the *Proceedings of the International Conference on Mathematics and Computational Methods Applied to Nuclear Science and Engineering*, Raleigh, North Carolina, USA, October 3–7, 2021. (accepted)

[P9] M. Szieberth, L. Nagy, G. Klujber, Y. Kitamura, T. Misawa, I. Barth and I. Pázsit, "Experimental Demonstration of Neutron Fluctuation Analysis Based on the Continuous Signal of Fission Chambers: Neutron Multiplicity and Reactor Noise Measurements". To appear in the *Proceedings of the International Conference on Mathematics and Computational Methods Applied to Nuclear Science and Engineering*, Raleigh, North Carolina, USA, October 3–7, 2021. (accepted)

[P10] L. Nagy, G. Klujber, Y. Kitamura, T. Misawa, I. Barth, I. Pázsit and M. Szieberth. "Computational Investigation and Experimental Verification of Multiplicity Counting from the Continuous Signals of Fission Chambers". *Nuclear Instruments and Methods in Physics Research Section A: Accelerators, Spectrometers, Detectors and Associated Equipment.* (to be submitted)

[P11] L. Nagy, G. Klujber, Y. Kitamura, T. Misawa, I. Barth, I. Pázsit and M. Szieberth, "A Computational and Experimental Investigation of Multiplicity Counting with Continuous Fission Chamber Signals". *INMM and ESARDA Joint Annual Meeting*, (Online), August 21–26, 2021. (to be submitted)

Acknowledgements

First and foremost I would like to thank my supervisors, prof. Imre Pázsit, assoc. prof. Máté Szieberth and assoc. prof. Paolo Vinai for their guidance, encouragement and patience. I offer my special thanks to prof. Lénárd Pál, the creator of the mathematical formalism behind this work; he took an active part in overseeing the research but, unfortunately, he did not have the chance to see the final results. I am particularly grateful to my dear friends and colleges: Boglárka Babcsány and Zoltán Böröczki, who kept believing in me even when I could not believe in myself, and to Gergely Klujber without whom the experimental results presented in the thesis would not exist. I am also grateful to assoc. prof. Dávid Légrády for reviewing the thesis providing comments. Finally, I would like to express my deepest gratitude to my parents for their continuous support and never-ending love.

<div align="right">

Lajos Nagy
Budapest, March 2021

</div>

dedicated to Viktória

for guiding me towards an integrated sense of self

x

Contents

Chapter 1

Introduction

Neutron multiplicity counting is a widely used non-destructive assay method for measuring the mass of fissile materials (primarily plutonium) [1]. The goal in a measurement is to estimate the singles, doubles and triples detection rates which quantify the intensity of detecting one, two or three neutrons, respectively, from the same emission event. The sample mass can then be obtained from the detection rates with algebraic inversion. Traditionally, the measurement is performed with ^{3}He-gas-filled detectors and the detection rates are determined from their pulse counting statistics. This approach comes, however, with several practical difficulties. The major problem is caused by dead time originating from the overlapping of pulses, which leads to a loss of counts in the counting electronics. Although various dead time correction techniques are available [2], their use is limited to moderate count rates; at very high count rates, for example when measuring spent nuclear fuel [3], they break down completely. Another (purely technical) problem is the global shortage on ^{3}He, which is a key component of the neutron detectors used in the measurements [4].

To overcome the above problems, an alternative version of neutron multiplicity counting has been developed. Relying on a recently published stochastic model of continuous detector signals [5], the new method is based on the direct analysis of the continuous voltage signals of neutron detectors (primarily fission chambers). In applying the method, the values of the singles, doubles and triples detection rates are obtained from suitably chosen moments (cumulants) of the measured signals. Since this procedure does not rely on counting individual pulses, it is inherently free from dead time losses originating from their overlapping. As a result, the detection rates with the new method can be determined even at very high count rates, which makes it a viable alternative to traditional multiplicity counting, especially when measuring high intensity samples, like spent nuclear fuel.

The remaining part of the thesis is structured as follows. Chapter 2 begins with a general overview of the subject of fissile material measurement, which is followed by a detailed description the theoretical background and some experimental aspects of neutron multiplicity counting. Chapters 3–5 summarize the author's activity in developing the new version of neutron multiplicity counting by reviewing three aspects of this process.

Chapter 3 describes the theoretical basis of the method formed by a set of equations that relate certain moments of the continuous detector signals with the singles, doubles

and triples detection rates. The mathematical model behind these equations evolved through three stages. In each stage, expressions are derived for the moments in a master equation formalism and the ability to extract the detection rates from these moments is discussed. Then a set of formulas are presented that express the singles, doubles and triples detection rates with the appropriate moments of signals recorded by a large detector array, and that serve as a practical tool for analysing measurements.

Chapter 4 presents a computational study in which the properties of the new method are investigated from a practical aspect. A numerical algorithm for the efficient estimation of the moments of recorded signals is described along with a software tool that implements its. The impact of various parameters (the measurement time, the detection efficiency, the electronic noise as well as the non-neutron pulses) on the estimated detection rates is investigated by analysing a large number of simulated measurements. Additionally, the sensitivity of the traditional as well as the new method of multiplicity counting to dead time losses caused by the overlapping of pulses is compared.

Chapter 5 reports on experimental activities aiming to demonstrate the practical use of the new method. Measurements have been performed at the Kyoto University Critical Assembly (KUCA) facility on a ^{252}Cf sample using four fission chambers. The measurement set-up and the associated data acquisition system is described. The detection rates were estimated both from the moments of the continuous detector signals as well as using the traditional pulse counting approach. The applicability of the newly proposed method is assessed by comparing these two sets of values.

Finally, Chapter 6 summarizes the results presented in the preceding chapters and highlights the key achievements in the form of propositions.

Chapter 2

Overview of neutron multiplicity counting

2.1 Nuclear safeguards

The term *nuclear safeguards* refers to the means to ensure the peaceful use of nuclear energy and to prevent its use for military purposes. Two organizations are currently responsible for this activity: *Euratom*, which belongs under the European Commission, performs safeguards activities in countries of the European Union; the *International Atomic Energy Agency (IAEA)*, which reports to the United Nations, has a competence in almost every country. Since the two agencies have similar practices and cooperate within Europe, nuclear safeguards will be described from the aspect of the IAEA in the rest of this section. The discussion is largely based on References [6, 7].

From the technical point of view, nuclear safeguards is a set of practices and methods applied for "the timely detection of diversion of significant quantities of nuclear material from peaceful nuclear activities to the manufacture of nuclear weapons or of other nuclear explosive devices or for purposes unknown, and deterrence of such diversion by the risk of early detection" [6]. The legal basis of this activity is the *Treaty on the Non-Proliferation of Nuclear Weapons* [8] to which 190 states have joined as of February 2015. In the following, certain parts of the above description are elaborated in a little more detail.

The subject of nuclear safeguards are materials that can be used to manufacture nuclear explosive devices. Collectively, these are referred to as *nuclear materials*. Nuclear materials are divided into two categories: direct use materials and indirect use materials. From a direct use material a nuclear weapon can be produced without transmutation or further enrichment; it includes plutonium containing less than $80\,\%$ ^{238}Pu, highly enriched uranium and ^{233}U. Every nuclear material, which is not direct use material is called an indirect use material; it includes depleted, natural and low enriched uranium as well as thorium; these must be further processed in order to produce direct use materials.

For the production of a nuclear bomb, at least one critical mass of nuclear material must be available in a highly enriched metallic form. However, when utilized for peaceful purposes, nuclear materials are not in this form. Therefore, to manufacture a nuclear explosive device, a state must divert an appropriate amount of a nuclear material and

convert it into the required form. The amount of material for which the manufacturing of an explosive device cannot be excluded is referred to as a *significant quantity*, which takes into account unavoidable losses in the conversion and manufacturing processes, hence should not be confused with critical masses. Significant quantities of various nuclear materials are listed in Table 2.1. The time required to convert different forms of nuclear material to the metallic components of a nuclear explosive device is called the *conversion time*. Estimates for the conversion time of nuclear materials are listed in Table 2.2.

Table 2.1: Significant quantities of various nuclear materials. Values are taken from Reference [9].

category	material	quantity
direct use material	U $\left(^{235}\text{U} > 20\,\%\right)$	25 kg in ^{235}U
	^{233}U	8 kg
	Pu $\left(^{238}\text{Pu} < 80\,\%\right)$	8 kg
indirect use material	U $\left(^{235}\text{U} < 20\,\%\right)$	75 kg in ^{235}U (or 10 t natural U or 20 t depleted U)
	Th	20 t

Table 2.2: Conversion times of various nuclear materials. Values are taken from Reference [9].

material	conversion time
Pu, HEU, ^{233}U metal	7–10 days
PuO$_2$, Pu(NO$_3$)$_4$ or other pure Pu compounds	1–3 weeks
HEU or ^{233}U oxide or other pure U compounds	
MOX or other non-irradiated pure mixtures containing Pu, U $\left(^{233}\text{U} + ^{235}\text{U} \geq 20\,\%\right)$	
Pu, HEU and/or ^{233}U in scrap or other miscellaneous impure compounds	
Pu, HEU, ^{233}U in irradiated fuel	1–3 months
U $\left(< 20\,\%\ ^{235}\text{U}\right)$, ^{233}U, Th	3–12 months

To detect any of such diversion of nuclear materials, the IAEA makes regular inspections to all nuclear facilities of a state. The frequency of inspections is determined by the type and amount of nuclear material handled in the facility based on the conversion times listed in Table 2.2. The most important activity performed during the inspection is *nuclear material accountancy*. In applying nuclear material accountancy, inspectors

determine the amount of nuclear material present in the facility by counting items (e.g. fuel assemblies, bundles, rods or containers) and measuring their attributes with various techniques. Such measurement techniques are the topic of the next section.

2.2   Nuclear material measurement techniques

There are two fundamental groups of techniques for measuring the characteristics of nuclear materials: destructive techniques and nondestructive techniques. In this section the principal techniques of these two groups are summarized briefly based on references [3, 7, 10].

In destructive analysis, a small sample is taken from the nuclear material under investigation which is then submitted to a series of physical and/or chemical measurement procedures. The major advantage of destructive methods is that they provide the highest accuracy, typically less than 1 %. However, they require a fixed laboratory to which the samples need to be transported for analysis. As a result they are costly and time consuming. Moreover, destructive techniques can only be used on pure (homogeneous) materials so that the sample of the item represents well the entire item. The most frequently used destructive techniques are: gravimetry, titrimetry and mass spectrometry; a good summary of these methods can be found in [7].

Nondestructive techniques measure nuclear materials without altering or making direct contact with them. The advantage of nondestructive techniques is that they can be performed on site using portable (often online) systems. For this reason, they are faster, simpler and less expensive compared to destructive techniques. They are, however, less accurate: the usual measurement precision is in the order of 1 %. Nondestructive measurements are often performed, when it is either impossible or impractical to sample an item for destructive analysis; examples include fresh fuel assemblies or nuclear waste. Most techniques are based on detecting radiation emitted from the material; from all the possible radiation types, gamma ray, x ray and neutron are used for their large penetrability in bulk materials. There are two types of nondestructive assay techniques: active and passive. Passive techniques measure radiation that is spontaneously emitted during nuclear decay [3]; active techniques measure radiation that is stimulated by neutron or gamma-ray irradiation [11]. The principal nondestructive techniques are classified as gamma-ray spectroscopy, neutron counting and calorimetry. In the following, a brief description of neutron counting is given.

There are three sources of neutrons in a nuclear material: *a)* spontaneous fission of the (mainly even) isotopes of uranium and plutonium; *b)* fission induced on the fissile isotopes of uranium and plutonium by neutrons (including both internal and external sources); *c)* (α, n) reactions induced on light elements (such as oxygen and fluorine) by α particles from the decay of uranium and plutonium isotopes. Neutrons in fission are emitted in groups of 0–10 and generate correlated detections; the third process produces single neutrons which cause independent detections. The intensity of neutron counts in the detector carries information on the overall quantity of the fissile material. The masses of specific isotopes can be calculated when isotopic composition of the sample is known from e.g. gamma-ray spectroscopy or mass spectroscopy. The passive form of neutron counting relies on neutrons from spontaneous fission; it is used to analyze plutonium samples which have a high measurable spontaneous fission yield.

In active measurements, an isotopic neutron source (typically Am-Li) is used to induce fission reactions in the sample; this is used to measure uranium samples which have low spontaneous fission yield. In general, the advantage of neutron counting over gamma spectroscopy is that neutrons penetrate high density heavy materials much better than gamma rays, hence they can effectively be used to assay materials which are dense or stored in large containers.

There are three fundamental types of neutron counting measurements: total neutron counting, neutron coincidence counting and neutron multiplicity counting. Total neutron counting is responsive to all neutrons emitted from the sample. As a result, it cannot differentiate between the three sources of neutrons. For this reason, it is used to measure samples with one dominating neutrons source. For example: a highly enriched UF_6 or PuF_4 is dominated by the (α, n) source; a pure uranium or plutonium metal is dominated by the spontaneous fission source. Neutron coincident counting is responsive to correlated detection events originating from induced fission or spontaneous fission. As a result, it can be used to measure samples, which have a strong uncorrelated neutron background, but in which only one fission source dominates. For example: a small impure plutonium sample has a dominating spontaneous fission source with an (α, n) background; in the active assay of a pure uranium sample a dominated induced fission source is accompanied with a background from the driver isotopic neutron source. Neutron multiplicity counting is the extension of coincident counting, which can also differentiate between neutrons from induced fission and spontaneous fission. As a result, it is used to measure samples with all three neutron sources present. For example: highly heterogeneous Pu materials, including moist or impure Pu oxides or oxidized metal, or Pu waste.

The method presented in this thesis is closely related to neutron multiplicity counting. For this reason, a detailed description of multiplicity counting is given in the following section.

2.3 Neutron multiplicity counting

Neutron multiplicity counting is a well-established technique for the quantitative analysis of nuclear materials. Although in principle any material capable of fission (either spontaneously or induced by an external particle) can be characterized with this method, most items assayed are samples from fresh, spent or reprocessed reactor fuel, which are primarily composed of uranium and plutonium [3, 12]. The passive form of the measurement is used to analyze plutonium items; in case of uranium items, an active measurement is performed. Since this second type of analysis is relatively rare, the discussion in this section will focus exclusively on the passive assay of plutonium. The basic theory of active assays is described in Reference [13]; examples of practical applications can be found in [14–17].

2.3.1 Basic principles

The practical applicability of (passive) neutron multiplicity counting is based on the fact that the distribution of the number of neutrons produced in the fission of a plutonium nuclide is known from nuclear physics experiments. As a result, by measuring

the neutron radiation emitted from the sample, information can be obtained on the quantity of the plutonium present in it. Figure 2.1 shows the conceptual view of typical measurement setup. The measured sample is located inside sample cavity which is open to air at atmospheric pressure. The cavity is surrounded by a large number (usually several dozens) of neutron detectors, most often ^{3}He-filled proportional counters. The space between the detectors is filled with polyethylene to thermalize fast neutrons originating from fission. [1]
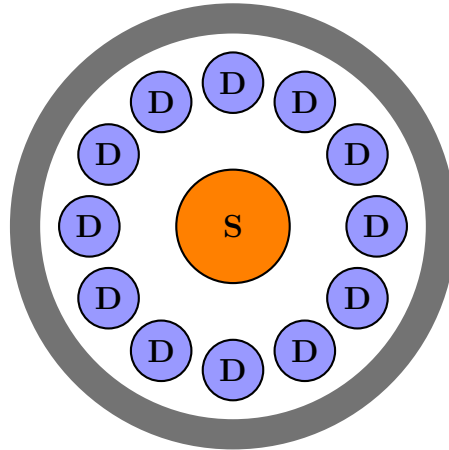
Figure 2.1: A conceptual view of the experimental setup of a multiplicity counting measurement, in which a heavy-nuclide sample (S), emitting neutrons spontaneously, is surrounded by a large number of neutron detectors (D).

As mentioned earlier, the majority of plutonium samples that are assayed with multiplicity counting originates from reactor fuel. As an illustration, Table 2.3 lists the typical plutonium compositions of low-, medium and high-burnup fuel from a light water reactors. It is seen that the plutonium content of such samples consists mainly of the isotope ^{239}Pu and smaller quantities of ^{240}Pu, ^{241}Pu, ^{242}Pu and ^{238}Pu. Among these, nuclides with an even mass number decay by spontaneous fission; they are: ^{238}Pu, ^{240}Pu, ^{242}Pu (see Table 2.4). Since multiplicity counting relies on neutrons produced in spontaneous fission, the method provides information on the quantities of these three isotopes only.

Table 2.3: Plutonium isotopic compositions representative of low-, medium and high-burnup fuel from light water reactor and the specific spontaneous neutron fission yield of each isotope. Table from Reference [3].

isotope	weight fraction of Pu (%)		
	low burnup	medium burnup	high burnup
^{238}Pu	0.024	0.059	1.574
^{239}Pu	89.667	82.077	57.342
^{240}Pu	9.645	16.297	24.980
^{241}Pu	0.556	1.231	10.560
^{242}Pu	0.109	0.336	5.545

As seen in Table 2.3, the major even component in plutonium samples is ^{240}Pu. For this reason, it is customary to introduce the so-called ^{240}Pu-*effective mass*. It is defined as the mass of ^{240}Pu that would give the same detector response as all the even isotopes in the measured sample. Denoting the mass of the plutonium isotope with mass number A by m_A, the ^{240}Pu-effective mass can be written as the following weighted linear sum [1]:

$$m_{240}^{\text{eff}} = 2.52\, m_{238} + m_{240} + 1.68\, m_{242}, \tag{2.1}$$

where the weights 2.52 and 1.69 account for the difference in the spontaneous fission neutron yields of the isotopes (see Table 2.4).

The ^{240}Pu-effective mass can be directly deduced from the measured detector response, hence it is the conventional target quantity of the assay. The quantity of the specific isotopes (both with even and odd mass numbers) can only be obtained in the knowledge of their relative composition within the sample; this information might be acquired by an independent gamma-ray spectroscopy or mass spectroscopy measurement. Denoting the weight fraction of the plutonium isotope with mass number A in the sample by f_A, the total mass of the even isotopes can be written as:

$$m_{\text{Pu}} = \frac{m_{240}^{\text{eff}}}{2.52\, f_{238} + f_{240} + 1.68\, f_{242}}. \tag{2.2}$$

Note that in most samples m_{240}^{eff} is somewhat larger than m_{Pu} [3].

As it will be seen in Section 2.3.5, the ^{240}Pu-effective mass is obtained from the counting statistics of the detection system in a measurement. Three quantities, in particular, are determined directly from the detector counts: the *singles*, *doubles* and *triples* detection rates. The singles rate (also referred to as the *totals rate*) gives the total number of registered detection events per unit time. The doubles rate (also referred to as the *reals rate* or *pairs rate*) gives the number of correlated detection event-pairs per unit time; these are induced by neutrons from the same spontaneous fission event. Analogously, the triples rate gives the number of correlated detection event-triplets per unit time. An analytical expression can be derived for the ^{240}Pu-effective mass as a function of the three detection rates as well as certain detector parameters and nuclear constants [1,18]. The effective mass of an unknown sample can then be calculated from the measured detection rates using this formula [19]. Most often, however, calibration curves are constructed for all three detection rates using simulations or reference standards with known compositions and masses. In this case, the effective mass of the unknown sample is obtained by simply locating the measured detection rates on the calibration curves [20–23].

2.3.2 The origin of neutrons in a sample

As we have noted above, the most important source of neutrons in a plutonium sample is spontaneous fission. The number of neutrons emitted in a fission event is called the multiplicity (hence the name *neutron multiplicity counting*) and it typically varies from 0 to 6 or more in individual events. Figure 2.2a shows the multiplicity distribution of the spontaneous fission of ^{240}Pu; the average multiplicity is around 2.156. The rate of spontaneous fission events, in general, shows a strong dependence on the

number of protons and neutrons in the nuclide: it is high for even-even isotopes but negligible in other cases. Table 2.4 shows the average spontaneous neutron yields of different plutonium isotopes. Combining with the data from Table 2.3, one can conclude that the primary source of spontaneous fission neutrons in most plutonium sample is ^{240}Pu. The energy spectrum of neutrons released in the spontaneous fission of ^{240}Pu is shown on Figure 2.3b; the average neutron energy is about 1.96 MeV [1].

Spontaneous fission is, however, not the only source of neutrons in a fissile sample. Almost all isotopes of plutonium listed in Table 2.3 decay also via alpha particle emission; the only exception is ^{241}Pu, which is primarily a beta particle emitter. The typical energy of the alpha particles from plutonium isotopes is around 5.2 MeV which is higher than the typical energies of fission neutrons and is suitable for causing (α, n) reaction on certain light elements, such as O, N, C or F, that are possibly present in the sample. This reaction will yield a single neutron. Clearly, the (α, n) neutron yield of a plutonium sample will strongly depend on its purity and chemical form. In pure metallic samples, every alpha particle is essentially absorbed in the heavy elements, hence no neutrons are produced in (α, n) reactions. However, plutonium often comes in the form of *plutonium dioxide* (PuO$_2$) used as reactor fuel and *plutonium tetrafluoride* (PuF$_4$) used in reprocessing plants. In these cases, additional neutrons might be produced in the following reactions: ^{18}O $+ \alpha \rightarrow$ ^{21}Ne $+ n$ and ^{19}F $+ \alpha \rightarrow$ ^{22}Na $+ n$. Typical values of the (α, n) neutron yields are listed in Table 2.4 for these two compounds. Note that the number of neutrons originating from (α, n) reactions can easily approach or even exceed those originating from spontaneous fission.

Table 2.4: Specific neutron yields of plutonium isotopes from spontaneous fission and from (α, n) reaction in oxide or fluoride form. Values are taken from Reference [3].

isotope	specific neutron yield (g^{-1}s^{-1})		
	from spontaneous fission	from (α, n) reaction	
		in PuO$_2$	in PuF$_4$
^{238}Pu	2590	13400	2200000
^{239}Pu	0.0218	38.1	5600
^{240}Pu	1020	141	21000
^{241}Pu	0.05	1.3	170
^{242}Pu	1720	2.0	270

Spontaneous fission and (α, n) reaction are the primary sources of neutrons in a plutonium sample. The primary neutrons, however, can participate in further reactions as they migrate through the sample; some of these create new neutrons, while others decrease their numbers. The most important reaction that populates neutrons is fission induced by neutrons (both primary or secondary) on the isotopes of plutonium. Due to its large weight fraction in samples, the most significant source of induced fission neutrons is ^{239}Pu. Just as in the case of spontaneous fission, the neutron multiplicity of induced fission is random and its distribution is shown on Figure 2.2b for one thermal and one fast neutron energy; the corresponding average multiplicities are 2.876 and 3.163, respectively. The spectrum of induced fission neutrons is similar to that of the

spontaneous fission neutrons in ^{240}Pu. Although it depends on the incident neutron energy, this dependence is generally weak. Figure 2.3b shows the neutron spectrum of the thermal induced fission of ^{239}Pu; the average neutron energy is around $2\,\text{MeV}$. Besides induced fission, $(n, 2n)$ reaction might also occur, though its threshold energy is higher than the typical energies of neutrons in the sample, hence it can usually be neglected. The most significant reaction that might decrease the neutron population in the sample is the (n, γ) reaction on plutonium isotopes. However, as seen from Figure 2.3a, the amount of neutrons lost due to capture is small compared to the amount of neutrons produced in induced fission at typical neutron energies of 1–5 MeV. In the theoretical description of multiplicity counting, the above mentioned secondary reactions are treated together and their overall effect is referred to as sample multiplication.
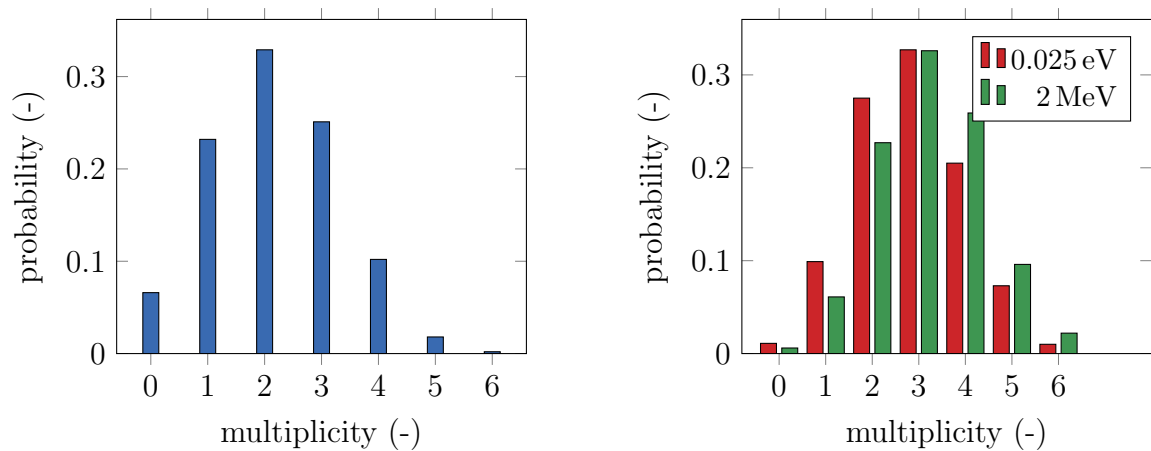
(a) Multiplicity distribution of ^{240}Pu spontaneous fission.

(b) Multiplicity distribution of ^{239}Pu induced fission at two incident neutron energies.

Figure 2.2: The multiplicity distribution of spontaneous and induced fission of some plutonium isotopes. Values are taken from [3].

According to what we have said so far, in terms of neutron emission a plutonium sample can be considered as a mix of three sources: a spontaneous fission source, an (α, n) source and a sample multiplication source. Clearly, each of them contributes to the overall neutron output, however, the individual contributions are generally not known when dealing with an unknown sample. One of the few exceptions to this is a pure metallic plutonium, in which case the (α, n) source is practically zero.

It is easy to see that the ^{240}Pu-effective mass, which is the target quantity of the assay, is directly related to the number of spontaneous fission events in the sample. For this reason, determining the ^{240}Pu-effective mass is equivalent to determining the strength of the spontaneous fission source. Neutron detectors, however, cannot directly differentiate between neutrons of different origins. As a consequence, the characterization of the spontaneous fission source can only be made on a statistical basis with a stochastic analysis of the measured detector response. Since, however, the three sources are not independent from each other (as it is clear from the discussion above), one essentially needs to quantify all three sources at once. Such an analysis of the detector response requires a stochastic mathematical model of the emission and detection process
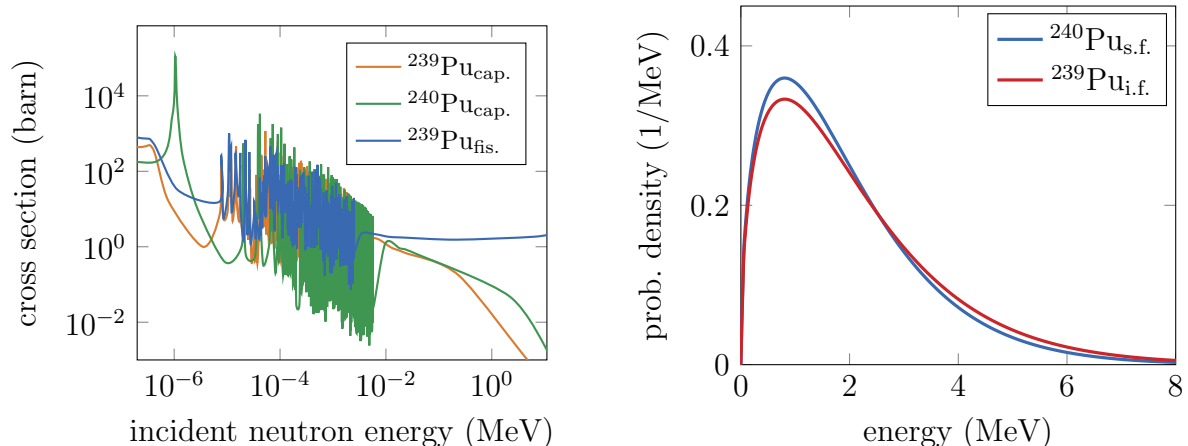
(a) Cross section of induced fission and radiative capture reactions in ^{239}Pu and ^{240}Pu isotopes. Values are taken from the ENDF/B-VIII.0 library [24].

(b) The energy spectrum of neutrons emitted in the spontaneous and thermal neutron induced fission of the ^{240}Pu and ^{239}Pu isotopes. Parameters for the Watt distribution are taken from the MCNPX manual [25, Appendix H.].

Figure 2.3: Some cross-section and neutron spectrum data of the ^{240}Pu and ^{239}Pu isotopes.

of neutrons. This is the topic of the following two sections.

2.3.3 Mathematical model of neutron emission – Böhnel moments

Based on the discussion in the previous section, the process of neutron emission in a plutonium sample can be summarized as follows. Primary source events occur spontaneously at random time instants. The primary source event is either a spontaneous fission or an (α, n) reaction, producing zero, one or more neutrons. As these neutrons migrate towards the surface of the sample, they engage in secondary reactions (including induced fission or radiative capture) in which some of them multiplicate while others disappear. As a net result, each primary source event is followed by the emission of a burst of neutrons from the entire sample. The complete process is illustrated on Figure 2.4.

Mathematically, the sample-wise emission of the neutrons can be described as a compound Poisson process with (unknown) parameters $\{Q_s, \boldsymbol{n}\}$. Here, Q_s is the intensity of the primary source events (spontaneous fission or (α, n) reaction) and $\boldsymbol{n}$ is the (random) number of neutrons released from the sample after each primary event; the probability mass function of this latter will be denoted by $P(n)$.

Expressions specifying Q_s and $P(n)$ were first given by Böhnel [26] as well as by Hage and Cifarelli [27, 28] independently. They all assumed a simple point model of the sample with no space or energy dependence (see the assumptions below). However, while Hage and Cifarelli follows a combinatorial approach resulting in complicated recurrence relations, Böhnel uses probability generating functions [29] which leads to

11
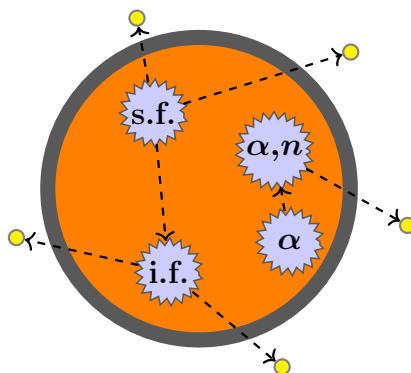
Figure 2.4: Illustration of the neutron emission process in a heavy-nuclide sample. A small number of neutrons are produced spontaneously via spontaneous fission of a heavy isotope or via (α, n) reaction of a light matrix isotope following the alpha-decay of a heavy isotope. These neutrons (and the induced ones as well) might either leave the sample, get captured (e.g.: in (n, γ) reaction), or undergo multiplication (e.g.: induced fission). The dashed lines represent the path of the neutrons.

.

compact and closed analytical formulas. Several extensions of Böhnel's model have been published [30–34] over the years. However, for its simplicity and because it forms the basis of the theory of multiplicity counting (see Section 2.3.4), the original version is presented in the following.

The key assumptions of the model can be summarized in three points, while also introducing the notations used:

1. The sample is a homogeneous mixture of ^{239}Pu, ^{240}Pu and possible light elements. The source of spontaneous fission is ^{240}Pu. The probability mass function of the multiplicity of spontaneous fission is denoted by $p_{\text{sf}}(n)$; its ith factorial moment is $\nu_{\text{sf},i}$. The total intensity of spontaneous fission in the sample is F. The source of induced fission is ^{239}Pu. The probability mass function of the multiplicity of induced fission is denoted by $p_{\text{if}}(n)$; its ith factorial moment is $\nu_{\text{if},i}$. The total intensity of the (α, n) reactions in the sample is denoted by S_α. Note that since $p_{\text{sf}}(n)$ and $p_{\text{if}}(n)$ are measurable nuclear parameters, their corresponding factorial moments $\nu_{\text{sf},i}$ and $\nu_{\text{if},i}$ are assumed to be known.

2. The energy spectrum (hence the mean energies) of all neutrons, whether they are from spontaneous fission, (α, n) reaction or induced fission, are the same. As a result, when colliding with a ^{239}Pu nuclide, each of them induces fission with equal probability. While this assumption is more or less valid in the case of neutrons originating from the two forms of fission, the mean energy and the spectrum of neutrons from (α, n) is usually different (see Section 2.3.2). In his paper, Böhnel has outlined the process of re-deriving the equations with non-identical spectra, but the results were very complex.

3. The probability of suffering a collision is the same for every neutron regardless the position it was born and is denoted by p. This assumptions holds for samples that are dilute or small with respect to the neutron mean free path. The collision

is assumed to be induced fission on ^{239}Pu; neutron capture is neglected. As a consequence, the probability of leaving the sample is $1 - p$ for each neutron.

Using the above assumptions and notations, the following quantities are introduced to describe the three sources of neutrons:

- The amount of spontaneous fission in the sample is given by the *spontaneous fission rate*, F. Clearly, F is proportional to the ^{240}Pu-effective mass:

$$F = g_{240} \, m_{240}^{\text{eff}}, \tag{2.3}$$

  where g_{240} is the specific spontaneous fission rate of ^{240}Pu. Since this latter is a physical constant known from experiments, when F is known, the value of m_{240}^{eff} can be calculated. Note that F does not depend on the chemical form of the sample or its geometry; it is only a function of its isotopic composition and the total mass.

- Although the number of (α, n) reactions is determined by the (α, n) intensity S_α, it is more customary to introduce the so-called α-ratio, defined as

$$\alpha = \frac{S_\alpha}{\nu_{\text{sf},1} \, F}, \tag{2.4}$$

  where $\nu_{\text{sf},1}$ is the average number of neutrons generated in a spontaneous fission event. The α-ratio gives the expected fraction of neutrons generated in (α, n) reactions relative to those generated in spontaneous fission, per unit time. Unlike F, α does not only depend on the isotopic composition of the sample; it is also a strong function of its chemical form.

- The quantity used to characterize the multiplication property of the sample is called the net leakage multiplication, defined as

$$M = \frac{1 - p}{1 - p \, \nu_{\text{if},1}}, \tag{2.5}$$

  where $\nu_{\text{if},1}$ is the average number of neutrons created in an induced fission event and p is the collision probability. It gives the total number of neutrons that leave the sample per one primary source neutron. Clearly, M is a function of not only the plutonium isotopic composition and the chemical form of the sample, but also its geometry.

In order to describe the neutron emission from the sample completely, the parameters Q_{s} and $P(n)$, introduced above, need to be given in terms of the three unknowns F, α and M, characterizing the strengths of the neutron sources, as well as the physical constants $\nu_{\text{sf},i}$ and $\nu_{\text{if},i}$. Using (2.4), it is easy to see that Q_{s} can be written as

$$Q_{\text{s}} = F + S_\alpha = F(1 + \alpha \, \nu_{\text{sf},1}). \tag{2.6}$$

The probability mass function $P(n)$ is specified via its probability generating function, defined as

$$G(z) = \sum_{k=0}^{\infty} P(k) \, z^k. \tag{2.7}$$

The derivation of $G(z)$ is performed in two steps using a backward master equation formalism [26] [35]. First the generating function of the number of emitted neutrons per one initial neutron, denoted as g_1, is calculated:

$$g_1(z) = (1-p)z + p\, g_{\text{if}}[g_1(z)], \tag{2.8}$$

where g_{if} denotes the generating function of $p_{\text{if}}(n)$. It is then shown that G can be expressed with g_1 as

$$G(z) = \frac{F}{Q_{\text{s}}}\, g_{\text{sf}}[g_1(z)] + \frac{S_\alpha}{Q_{\text{s}}}\, g_1(z), \tag{2.9}$$

where g_{sf} denotes the generating function of $p_{\text{sf}}(n)$.

In the possession of the generating function G, the factorial moments of the corresponding distribution can be obtained by simple differentiation as

$$\nu_k = \left.\frac{\mathrm{d}^k G(z)}{\mathrm{d}z^k}\right|_{z=1}. \tag{2.10}$$

For the purposes of multiplicity counting, one usually uses the first three factorial moments ν_1, ν_2 and ν_3 [1] often referred to as the Böhnel moments. In order to simplify the upcoming formulas, let us introduce the following modified form of these moments [18]:

$$\tilde{\nu}_k = \nu_k(1 + \alpha\nu_{\text{sf},1}). \tag{2.11}$$

The first three of the modified Böhnel moments can be written as [18]

$$\tilde{\nu}_1 = M\,\nu_{\text{sf},1}(1+\alpha), \tag{2.12a}$$

$$\tilde{\nu}_2 = M^2\left[\nu_{\text{sf},2} + \left(\frac{M-1}{\nu_{\text{i},1}-1}\right)\nu_{\text{sf},1}(1+\alpha)\nu_{\text{i},2}\right], \tag{2.12b}$$

$$\tilde{\nu}_3 = M^3\left[\nu_{\text{sf},3} + \left(\frac{M-1}{\nu_{\text{i},1}-1}\right)\,[3\nu_{\text{sf},2}\nu_{\text{i},2} + \nu_{\text{sf},1}(1+\alpha)\nu_{\text{i},3}]\right.$$
$$\left.+3\left(\frac{M-1}{\nu_{\text{i},1}-1}\right)^2\nu_{\text{sf},1}(1+\alpha)\nu_{\text{i},2}^2\right]. \tag{2.12c}$$

Finally, let us note that the following relation holds:

$$Q_{\text{s}}\,\nu_k = F\,\tilde{\nu}_k. \tag{2.13}$$

2.3.4 Mathematical model of neutron detection – detection rates

As we have seen in the previous section, the expression (2.6) of the Q_{s} rate of the primary source events together with expression (2.12) of the factorial moments $\tilde{\nu}_i$ ($i = 1, 2, 3$) of the number of neutrons released from the sample after a primary source event form a system of algebraic equations with the three unknown parameters F, α and M. As a consequence, the determination of the parameters of an unknown sample is equivalent to determining Q_s and $\tilde{\nu}_i$ ($i = 1, 2, 3$). These factorial moments of the number of emitted neutrons are, however, not directly measurable. Therefore,

they need to be converted into a set of other quantities, which are measurable. The classical choice of measurable quantities are the singles, doubles and triples detection rates, denoted traditionally as S, D and T; these serve as the basis of the multiplicity counting method [1]. A recently suggested alternative approach uses the mean, variance and skewness of the number of detected counts [36]. In the following, the method of multiplicity counting is described.

Consider an array of detectors that detect neutrons coming from the sample. Let $\boldsymbol{n}_d$ denote the number of neutrons detected following an emission. Let us introduce the intensity of detection k neutrons from the same sample emission and denote it by C_k. By definition, $S = C_1$, $D = C_2$ and $T = C_3$. It is easy to see that C_k, in general, can be written as

$$C_k = Q_s \, \mathbb{E}\left[\binom{\boldsymbol{n}_d}{k}\right] = Q_s \, \frac{r_k}{k!}, \tag{2.14}$$

where r_k denotes the kth factorial moment of $\boldsymbol{n}_d$. Then, the singles, doubles and triples rates take the forms:

$$S = Q_s \, r_1, \tag{2.15a}$$

$$D = Q_s \, \frac{r_2}{2}, \tag{2.15b}$$

$$T = Q_s \, \frac{r_3}{6}. \tag{2.15c}$$

To arrive to the final expressions of the detection rates, one must specify the forms of the moments r_k. These are derived by Cifarelli, Dierckx and Hage [12,37] as well as by Ensslin [1]. Although the assumptions made are similar in the two cases (see below), the calculation of Cifarelli, Dierckx and Hage is based on a combinatorial model of the neutron emission, whereas Ensslin follows the generating function approach of Böhnel (see Section 2.3.3). In the following, this latter case is summarized briefly.

The following assumptions are made when calculating the expression of r_k:

1. The detection efficiency does not depend on neutron energy and is uniform over the sample volume. As a consequence, the detection probability is the same for every neutron and will be denoted by ε.

2. When a new neutron is created in the sample, it suffers a collision or leaves the sample instantly. As a consequence, neutrons leave the sample simultaneously and at the same time when the primary source event (spontaneous fission or (α, n) reaction) has occurred. This is called the superfission concept [26]. It is a realistic assumption, whenever fission chains in the sample are much shorter than the migration time of the neutrons to the detectors, which is usually the case with small samples in thermal detection systems [3].

Let $P_d(n)$ denote the probability mass function of $\boldsymbol{n}_d$. Using the first assumption above, it can be written in terms of $P(n)$ as

$$P_d(k) = \sum_{n=k}^{\infty} P(n) \binom{n}{k} \varepsilon^k (1 - \varepsilon)^{n-k}. \tag{2.16}$$

Using this expression, it is easy to show that the probability generating function $G_d(z)$ of $\boldsymbol{n}_d$ can be written as

$$G_d(z) = G[1 + \varepsilon(z - 1)]. \tag{2.17}$$

where $G(z)$ is the probability generating function of $\boldsymbol{n}$ and was given by (2.9). The factorial moments r_k can now be obtained from the derivatives of $G_d(z)$; the first three moments take the form [1, 18]

$$r_1 = \varepsilon\, \nu_1 \tag{2.18a}$$

$$r_2 = \varepsilon^2\, \nu_2 \tag{2.18b}$$

$$r_3 = \varepsilon^3\, \nu_3. \tag{2.18c}$$

In almost every practical case, neutrons travel through a moderating material before they get detected. Since the time these neutrons spend in the moderator is random, neutrons from the same emission will reach the detectors at different time instants, despite leaving the sample simultaneously. This migration time is referred to as the detector die-away time [1] and in thermal detection systems it typically has a distribution illustrated on Figure 2.5. The fact of non-simultaneous detection has an effect on the estimation of r_2 and r_3.
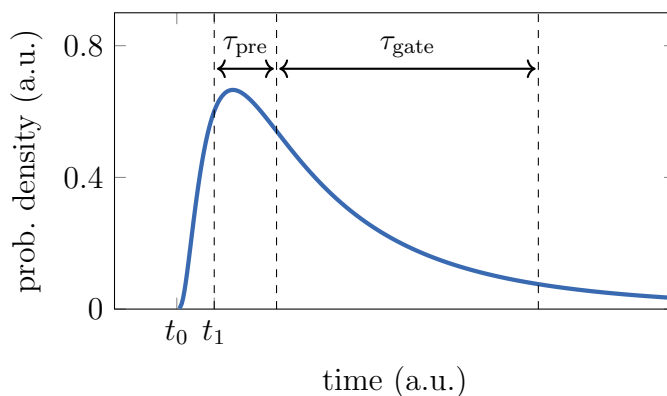
Figure 2.5: The probability density function of the detection time of neutrons after a sample emission event. The emission occurred at time t_0; t_1 denotes the detection of the first neutron in a concrete measurement. Following a short τ_{pre} time called the pre-delay, a gate of length τ_{gate} is opened during which detections are counted.

The estimation of r_1 in an experimental setup is straightforward: one needs to count every detection following an emission event. This procedure is not affected by the non-simultaneous detection of neutrons. In the case of r_2 and r_3, however, a gate is opened with a short delay by the first detection; this short delay is called the pre-delay and will be denoted by τ_{pre}. After opening the gate, detections are counted for a finite time; this time is called the gate width and will be denoted by τ_{gate}. Because the window is finite, there is a non-zero probability of missing some correlated pairs or triples, which leads to an underestimation of r_2 and r_3. This underestimation can be taken into account by introducing the so-called doubles and triples gate fraction factors, denoted as f_d and f_t. In particular, one can show that the underestimated values of r_2 and r_3 are [1]

$$r_2 = \varepsilon^2\, \nu_2\, f_d \tag{2.19a}$$

$$r_3 = \varepsilon^3\, \nu_3\, f_t. \tag{2.19b}$$

The values and mathematical forms of f_d and f_t depend on the distribution of the die-away time. Assuming an exponential distribution with a time constant θ, one can show [1] that $f_d = f$ and $f_t = f^2$, where

$$f = e^{-\tau_{\mathrm{pre}}/\theta}\left(1 - e^{-\tau_{\mathrm{gate}}/\theta}\right). \tag{2.20}$$

Now, returning to the definitions (2.15) and substituting the above expressions of r_1, r_2 and r_3, singles, doubles and triples detection rates can be written as

$$S = Q_{\mathrm{s}}\, \nu_1\, \varepsilon, \tag{2.21a}$$

$$D = Q_{\mathrm{s}}\, \nu_2\, \varepsilon^2 \frac{f_{\mathrm{d}}}{2}, \tag{2.21b}$$

$$T = Q_{\mathrm{s}}\, \nu_3\, \varepsilon^3 \frac{f_{\mathrm{t}}}{6}, \tag{2.21c}$$

or, by using the modified factorial moments (2.12), as

$$S = F\, \widetilde{\nu}_1\, \varepsilon, \tag{2.22a}$$

$$D = F\, \widetilde{\nu}_2\, \varepsilon^2 \frac{f_{\mathrm{d}}}{2}, \tag{2.22b}$$

$$T = F\, \widetilde{\nu}_3\, \varepsilon^3 \frac{f_{\mathrm{t}}}{6}. \tag{2.22c}$$

2.3.5 Recovering the plutonium effective mass from the detection rates

By inserting the modified factorial moments (2.12) into the expressions (2.22) of the detection rates, a system of algebraic equations is obtained for the three unknown sample parameters, F, M and α. If we invert this system, then the unknown parameters are expressed with the measured values of the singles, doubles and triples rates, along with some reactor physics constants and detector parameters. The inversion procedure is described in [1, 18]; here only the results are summarized.

First, the value of the sample multiplication M needs to be determined by solving the following third order equation:

$$a + b\, M + c\, M^2 + M^3 = 0, \tag{2.23}$$

where

$$a = \frac{T\, \nu_{\mathrm{sf},2}(1 - \nu_{\mathrm{if},1})}{\varepsilon^2\, f_t\, S\, (\nu_{\mathrm{sf},2}\, \nu_{\mathrm{if},3} - \nu_{\mathrm{sf},3}\, \nu_{\mathrm{if},2})}$$

$$b = \frac{2\, D\, [\nu_{\mathrm{sf},3}\, (\nu_{\mathrm{if},1} - 1) - 3\, \nu_{\mathrm{sf},2}\, \nu_{\mathrm{if},2}]}{\varepsilon\, f_d\, S\, (\nu_{\mathrm{sf},2}\, \nu_{\mathrm{if},3} - \nu_{\mathrm{sf},3}\, \nu_{\mathrm{if},2})}$$

$$c = \frac{6\, D\, \nu_{\mathrm{sf},2}\, \nu_{\mathrm{if},1}}{\varepsilon\, f_d\, S\, (\nu_{\mathrm{sf},2}\, \nu_{\mathrm{if},3} - \nu_{\mathrm{sf},3}\, \nu_{\mathrm{if},2})} - 1.$$

Once M is known, F and α can be calculated as

$$F = \frac{1}{\varepsilon\, M^2\, \nu_{\mathrm{sf},2}} \left[\frac{2D}{\varepsilon f_d} - \frac{M\,(M-1)\,\nu_{\mathrm{if},2}\, S}{\nu_{\mathrm{if},1} - 1}\right] \tag{2.25}$$

17

and

$$\alpha = \frac{S}{F \, \varepsilon \, \nu_{\mathrm{sf},1} \, M} - 1. \tag{2.26}$$

Using (2.3), the ^{240}Pu-effective mass can be obtained from F as

$$m_{240}^{\mathrm{eff}} = \frac{F}{g_{240}}. \tag{2.27}$$

2.3.6   The design of multiplicity counter devices

Depending on the characteristics (e.g. size and composition) of the measured sample as well as the measurement environment, neutron multiplicity counters come in many different shapes, forms and sizes. There are, however, four design goals that every device tries to achieve; these are:

1. Maximize the neutron detection efficiency. Because the triples rates are proportional to the third power of the detection efficiency, a large detection efficiency is required to increase its detection rate. Large detection efficiencies can be achieved by using ^{3}He detectors. A typical goal is 50–60 %.

2. Minimize dead time losses. Triples rates are extremely sensitive to dead time arising in the counting electronics. This type of dead time can be decreased by the increase of independent amplifier/discriminator units that process the signals of the detectors.

3. Minimize the die-away time. The width of the counting gate is chosen in a way that it covers the die-away time. The larger the gate is, the more emission events will be overlap within one counting gate, which increases the uncorrelated background in the counting statistics thus decreasing the precision.

4. Minimize the effect of sample placement within the cavity and the difference in the energy spectrum of neutron sources. This is important because the assumption of the theory in Section 2.3.4 was that the detection efficiency is space and energy independent.

Maximizing efficiency and minimizing die-away time are usually competing goals. Depending on which of the two is preferred, there are two classes of multiplicity counters: thermal counters as well as epithermal counters. The majority of multiplicity counters are thermal devices which, in general, provide a high detection efficiency of around 50–60 %. Since thermal neutron detectors are usually based on some type of a neutron capturing reaction, thermal counters usually have a good gamma insensitivity [3, 38]. Because they are both thermal detectors, a strong moderation is required to achieve good detection efficiency which, in turn, produces a large die-away time in the order of 10–100 µs. Most are equipped with ^{3}He gas-filled detectors. BF$_3$ gas-filled detectors are sometimes used in high gamma fields because they are less sensitive to gamma radiation then ^{3}He detectors; their efficiency is, however, a factor of 2 less. The description of several thermal multiplicity counters can be found in [1, 19, 22]. A small fraction of counters are fast or epithermal counters. Since these detectors are usually based on recoil reactions of fast neutrons, epithermal counters have a small die-away time on the

order of 10 ns [3]. On the other hand, they are generally more sensitive to gamma rays and are sometimes not as efficient as thermal counters. Such systems have been used in the past [21], but enjoy a renewed interest [23, 39–44].

The typical layout of the electronic circuit connected to the detectors of a thermal multiplicity counter with ^{3}He detectors is shown of Figure 2.6. The voltage applied to the detectors is around 1500 V so that they operate in the proportional region where the pulse amplitudes are proportional with the deposited energy [38]. Pulses in this region have a fast rise time on the order of 0.1 µs and the recovery time of the detector (the time before it can provide another pulse) is around 1–2 µs. Usually a small number of detectors are connected parallelly and attached to a common integrated circuit containing a pre-amplifier and amplifier and an integral discriminator [1]. The logic pulses produced by the discriminator are typically 50 ns wide and the effective time constant of the circuit (the time before it can create a new logic pulse) is 150 ns. Dead time losses might occur at high count rates due to the overlapping of voltage pulses, however, the probability of such losses decreases with the number of detectors connected. For this reason, multiplicity counters have typically 10–60 independent discriminator circuits, with 2–8 detectors in each [1]. Each of these circuits produce an independent stream of logic pulses which are then unified into a single stream by a derandomizer circuit. Due to its internal buffer, the derandomizer circuit can reduce dead time originating from the overlapping of logic pulses even at a very high count rate of 2 MHz. Finally, the unified pulse stream is sent through a multiplicity shift register, that determines the detection rates. The operation of the shift register will be described in Section 2.3.7.
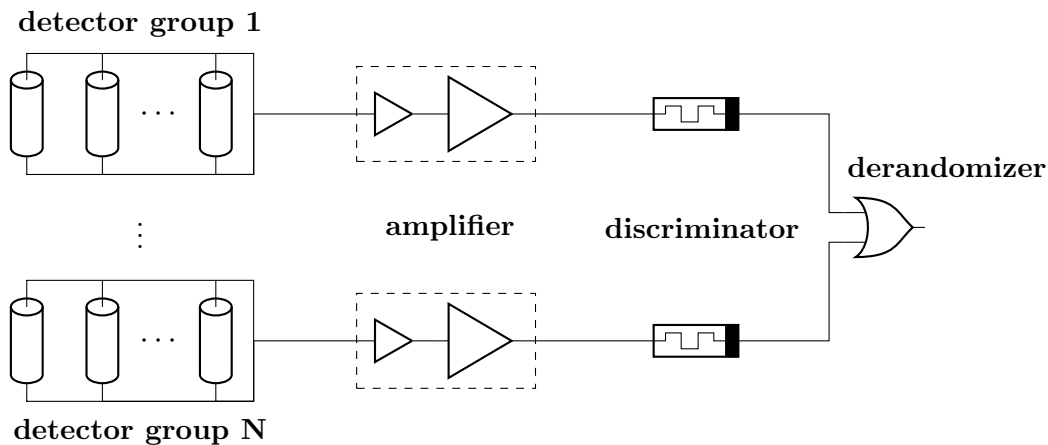
Figure 2.6: Layout of a typical electronic circuit connected to a multiplicity counter.

As an illustration, Figure 2.7 shows the Plutonium Scrap Multiplicity Counter [1,45]. The device measures impure plutonium and mixed oxide scrap materials in the mass range of a few tens of grams to several kilograms. The horizontal cross section of the device is 66 cm×66 cm and has a height of 92 cm. The design contains 80 ^{3}He detectors embedded into a polyethylene moderator in a circular arrangement; this provides a 55 % detection efficiency and a 47 µs die-away time. The signals of the detectors are processed by 19 preamplifier/discriminator circuits; the dead-time coefficient (see Section 2.3.8) is 121 ns. The device has a relatively flat axial efficiency profile.

(a) Horizontal view.   (b) Vertical view.
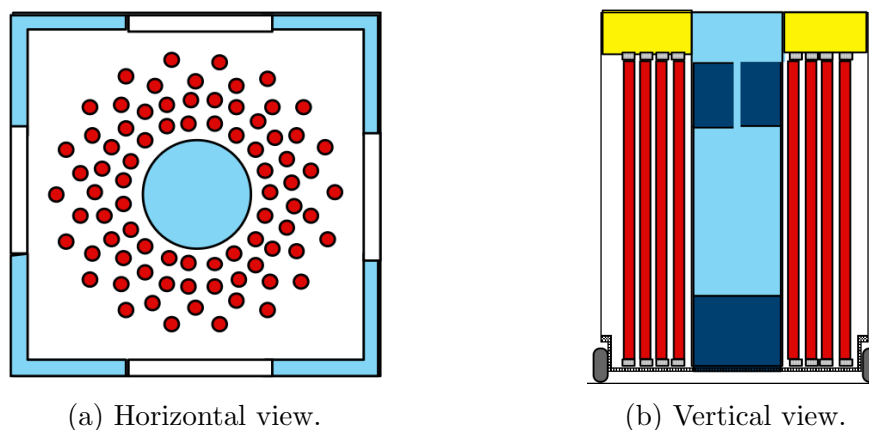
Figure 2.7: The design schematic of the Plutonium Scrap Multiplicity Counter from Reference [1]. The sample cavity is surrounded by 80 ^{3}He gas-filled neutron detectors. The space between the detectors is filled with polyethylene for moderation. Graphite plates are placed above and below the cavity to reflect escaping neutrons.

2.3.7   Estimation of the detection rates – the shift register

As we have seen in Section 2.3.4, to estimate singles, doubles and triples detection rates, one needs to count single pulses, correlated pairs and correlated triplets, respectively, that belong to the same spontaneous fission event. Figure 2.8 shows typical streams of logic pulses produced by the derandomizer circuit in two different cases. In the first case shown on Figure 2.8a, the emission intensity and the die-away time is low enough that pulses originating from subsequent emissions are far away from each other and form well separated groups. In this case, the correlated pulses can easily be identified. Most often, however, the emission intensity and the die-away time are so large, that pulses from subsequent emissions overlap as shown on Figure 2.8b. The separation of correlated pulses from uncorrelated ones in this case is possible only on a statistical basis. In multiplicity counters, this separation is performed by an integrated circuit called the multiplicity shift register. In the following, the operation of the shift register is described from a mathematical point of view.
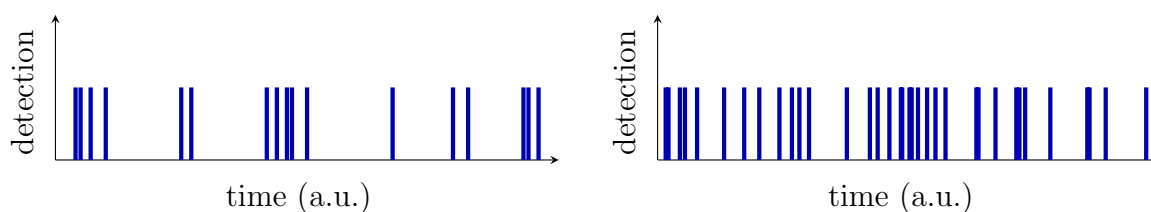
(a) Low emission intensity and die-away time: pulses from subsequent emissions are separated.

(b) Large emission intensity and die-away time: pulses from subsequent emissions overlap.

Figure 2.8: An illustration of the logic pulse stream sent to a multiplicity shift register at low and high emission intensities.

The multiplicity shift register operates as a sort of buffer and stores incoming pulses for a predetermined time interval of length τ_{gate}. Note that τ_{gate} is identical to the

gate width introduced in Section 2.3.4 and illustrated on Figure 2.5. A typical length of the gate width is $32\,\mu s$. As time passes, incoming pulses shift through the register and the whole process takes time τ_{gate}. At any time, the number of events stored in the shift register is called the multiplicity of the shift register. In order to keep track of the multiplicity at all times, the shift register has an associated up-down counter. When an event enters the register, the value of the counter is increased by one; when an event leaves the register, the value of the counter is decreased by one. The shift register is also associated with a multiplicity scaler, which registers the number of times that different multiplicities occur during a course of a measurement, i.e. the unnormalized multiplicity distribution of the register. The multiplicity scaler is an array of sub-scalers, each associated with a multiplicity $0, 1, \ldots, N$, where N is a maximal multiplicity that can be registered. When the shift register receives a trigger signal (we shall specify what a trigger signal is in the next paragraph), the multiplicity scaler reads the value of the counter and the value of the corresponding sub-scaler is increased.

In order to estimate correlated multiplicities, two shift registers are used each with a separate multiplicity scaler. The relation of the two registers is illustrated on Figure 2.9. The vertical dashed line represents the present time. Pulses on the right represent past detections, whereas pulses on the left represent future detections. The two shift registers have the same gate width τ_{gate} chosen to be close to the die-away time, however, they are separated in time. The detection events first flow through the *reals plus accidentals* (R+A) gate into which they enter after a time called *predelay*, denoted as τ_{pre}, with respect to the time of their detection, which is typically a small fraction of the die-away time. After the R+A gate, the detection events flow through a second gate called the *accidentals* (A) gate, following a time called *long delay*, denoted as τ_{long}, which is chosen to be much larger than the die-away time (and the gate width). Whenever a new event is detected, both shift registers are triggered and their multiplicity scalers get updated.
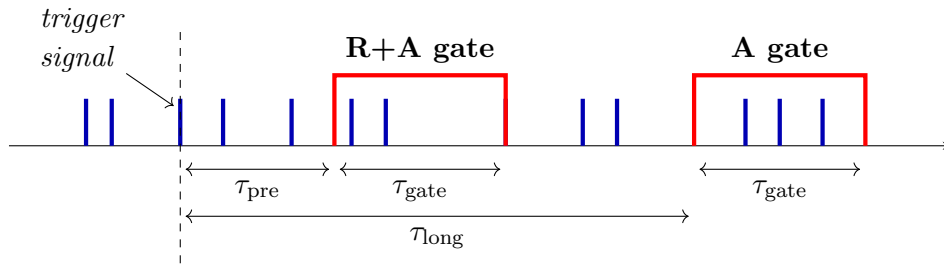
Figure 2.9: Illustration of the operation logic of the multiplicity shift register.

As an example, Figure 2.10 shows the multiplicity distribution of the $R + A$ and A gates measured with a $3.8\,\mathrm{kg}$ plutonium metal sample. One can see that although the shape of the distribution is similar in the two gates, the actual values differ. Since the predelay is much smaller than the die-away time, the $R + A$ gate will contain the multiplicities from two types of events: events that are correlated with the trigger signal because they are from the same emission (reals) and events that not correlated with the trigger signal either because they are from a different emission or because they are from an uncorrelated background (accidentals). On the other hand, since long delay is much longer than the die-away time, the A gate will contain multiplicities only from events, which are not correlated with the trigger event (accidentals).
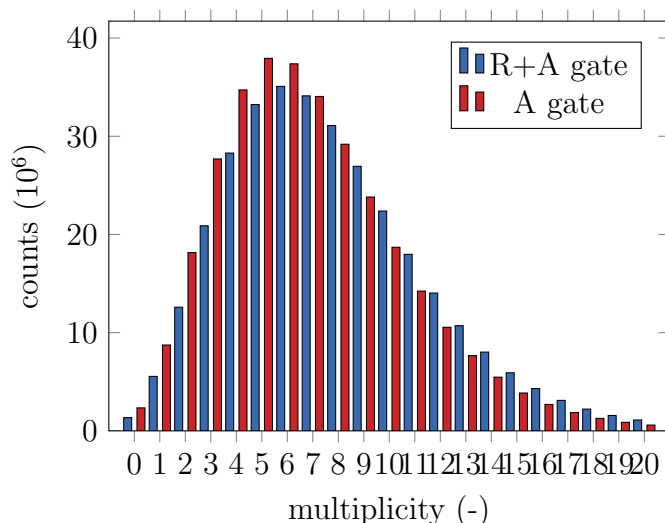
Figure 2.10: A measured multiplicity distribution of a 3.8 kg plutonium metal sample. Values are taken from [1].

The correlated detection rates can be estimated from the multiplicity distribution of the R+A and A gates. The procedure is based on the fact that because the two gates are of equal length, the number of non-correlated events (accidentals) in them are the same within statistical uncertainty. As a result, the number of real correlated events can be obtained in a form of a difference in the two multiplicity distribution. After a measurement of length T, let F_i and B_i denote the observed number of multiplicities $i = 0, \ldots, N$ in the $R + A$ gate and the A gate, respectively. The estimated values of the singles, doubles and triples rates can than be written as [46]:

$$\hat{S} = \frac{1}{T} \sum_{i=0}^{N} F_i = \frac{1}{T} \sum_{i=0}^{N} B_i, \tag{2.28a}$$

$$\hat{D} = \frac{1}{T} \sum_{i=1}^{N} i \, (F_i - B_i), \tag{2.28b}$$

$$\hat{T} = \frac{1}{T} \left[\sum_{i=2}^{N} \frac{i \, (i-1)}{2} (F_i - B_i) - \left(\sum_{i=1}^{N} i \, B_i \right) \frac{\hat{D}}{\hat{S}} \right]. \tag{2.28c}$$

Formulas for calculating the uncertainties of the above estimates can be found in [46] and will not be presented here.

2.3.8 Dead time correction of the estimated detection rates

In every detection system there is a minimum time that must separate two events so that they can be distinguished. This minimum time is called the *dead time* [38]. Dead time may arise in several parts of a detection chain for various reasons. Within a neutron detector, a dead time is posed by the charge collection time: in gas-filled detectors, a charge signal can be obtained 1–2 µs after the neutron interaction [3]. The preamplifier output pulse has a rise time of around 0.1 µs and the amplifier has a

time constant around $0.5\,\mu s$. The integral discriminator produced logic pulses of width $50\,ns$ [1]. When two events are closer than the dead time, they will be treated as one, so the information on one of the events is lost. This is called the *dead time loss*. Dead time losses can become severe especially at high counting rates. In such cases, losses must be quantified and compensated for; this process is called *dead time correction*. It should be emphasized that there is a large literature on the topic of dead time, both in general and specific to multiplicity counting. For this reason, only a brief overview is given here on the general treatment of dead time, then the most frequently used techniques applied to multiplicity counting will be discussed.

Essentially, there are two fundamental types of dead time correction techniques: empirical and theoretical. Empirical correction techniques provide ad-hoc formulas, which contain dead time parameters that can be determined from a given system with reference measurements. Theoretical correction techniques, on the other hand, derive formulas for the detection rates based on a stochastic model of the dead time process. There are two common models of dead time: paralyzable (or updating) and non-paralyzable (or non-updating) [38]; they are illustrated on Figure 2.11. A fixed dead time τ is assumed. In both models a registered true event starts a dead time period of length τ and any further event that occurs during the dead period is lost. The difference in the models is how the lost true events affect the dead period. In the non-paralyzable model, lost events have no effect on the dead period; in the paralyzable model, however, these effects (although lost), prolong the dead period by τ again. It is important to emphasize that these two models are idealizations. The dead time in real detection systems can be described by one of them, by a mix of them, or by none of them. For example, the pulse formation in an ionization chamber creates a paralyzable dead time, because when the detector is ionized, a new detected particle will cause additional ionization; in a coincidence circuit, however, incoming logic pulses create non-paralyzable dead time.

From a mathematical point of view, the fundamental difficulty with developing dead time correction techniques is that the detection process will not be Markovian in the presence of dead time, since a detection event in the present time will affect detection events in a future time [47].
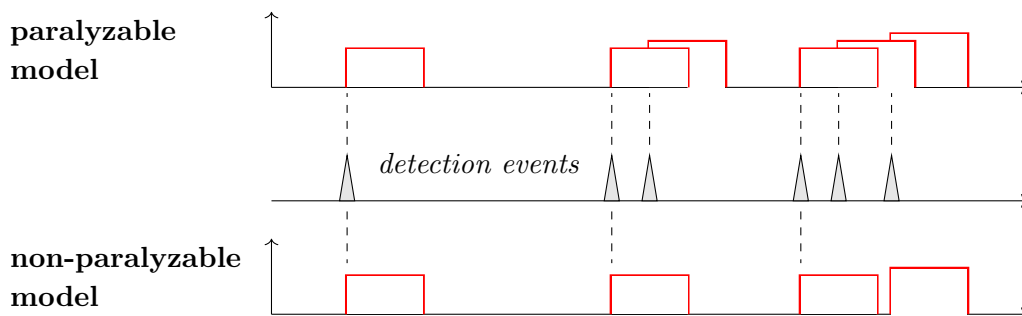
Figure 2.11: Illustration of the paralyzable and non-paralyzable model of dead time.

In multiplicity counting, the most dominant source of dead time losses could be integral discriminator, that serves many detectors [3]. This source of the dead time is, however, greatly reduced by applying many independent pulse processing circuits each of which serves only a small number of detectors (see Section 2.3.6). Nevertheless, at large count rates other dead time sources might become so dominant that the esti-

mated detection rates become smaller than that given by the expressions (2.28), hence corrections become necessary.

The most frequently used empirical correction technique provides formulas for the singles and doubles rates only. In particular, the corrected detection rates are written as [1, 48, 49]:

$$S = \hat{S} e^{\delta \hat{S}/4} \tag{2.29}$$

$$D = \hat{D} e^{\delta \hat{S}}, \tag{2.30}$$

where $\hat{S}$ and $\hat{D}$ are the detection rates estimated by the shift register according to (2.28). Above, $\delta = A + B\hat{S}$, where A and B are dead-time parameters. Their values depend on the actual multiplicity counter. The standard method to determine A and B is to perform measurements with several ^{252}Cf sources of different strengths and adjust A and B in a way that the corrected D/S ratio is constant for all strengths [3, 49]. Since no such empirical formula exists for the triples rate, usually a theoretical formula shown below is used [1, 50].

The most widespread theoretical correction method is that derived by Dytlewski [46]. This approach calculates the corrected detection rates from the multiplicity distributions registered in the R+A and A gates (see Section 2.3.7):

$$S = e^{\delta \hat{S}} \hat{S}, \tag{2.31a}$$

$$D = e^{\delta \hat{S}} \frac{1}{T} \sum_{i=1}^{N} \alpha_i (F_i - B_i), \tag{2.31b}$$

$$T = e^{\delta \hat{S}} \frac{1}{T} \left[\sum_{i=2}^{N} \beta_i (F_i - B_i) - \left(\sum_{i=1}^{N} \alpha_i B_i \right) \frac{\hat{D}}{\hat{S}} \right] \tag{2.31c}$$

where

$$\alpha_1 = 1 \quad \text{and} \quad \alpha_i = 1 + \sum_{k=0}^{i-2} \binom{i-1}{k+1} \frac{(k+1)^k \phi^k}{[1-(k+1)\phi]^{k+2}} \quad \text{for } i \geq 2 \tag{2.32}$$

and

$$\beta_2 = \alpha_2 - 1 \quad \text{and} \quad \beta_i = 1 + \sum_{k=0}^{i-3} \binom{i-1}{k+2} \frac{(k+1)(k+2)^k \phi^k}{[1-(k+2)\phi]^{k+3}} \quad \text{for } i \geq 3. \tag{2.33}$$

where ϕ is a dead time parameter. The above set of formulas were recently extended to the correction of quads [51].

The fundamental assumption of the above model is that the incoming detection form a Poisson process, i.e the inter-event times are independent and identically distributed exponential variables. This is certainly not the case with multiplicity counting, where the goal is exactly to characterize the correlation between detection events. Dead time models, that take into account the non-Poissonian character of the detection process have been published [47, 52–57].

2.4 The improvement of traditional multiplicity counting

Although multiplicity counting is used to measure un-irradiated samples (fresh fuel assemblies, nuclear warheads, laboratory items), most of the plutonium can be found in spent reactor fuel [3]. The assay of spent fuel poses two major challenges that make the quantification of plutonium difficult [58–60]: a large gamma background created primarily by the fission fragments, and an extremely large neutron "background" originating from the spontaneous fission of certain transuranic elements (mainly ^{242}Cm and ^{244}Cm). Two standard techniques to manage the gamma background are the application of gamma shielding materials as well as the use of detectors with low gamma sensitivity (e.g. fission chambers) [60]. To separate the neutron signature of plutonium from that of the transuranic elements, two measurement techniques have been introduced [61]: the passive neutron reactivity technique [62–64] and the differential die-away self-interrogation technique [65]. Both of these are close relatives of multiplicity counting, because they rely on determining the doubles and triples detection rates.

Due to the high overall neutron (typically 10^7–10^8 n/s [58]) and gamma emission rate of irradiated fuels, the estimation of singles rate and, especially, the estimation of the doubles and triples rates is difficult with the standard approach of pulse counting using ^{3}He detectors. One possibility to overcome this problem is to adopt a practice used in on-line flux measurement of reactors: the analysis of the continuous signals of fission chambers operated in Campbelling or current mode. This option is elaborated in the following.

2.4.1 The operation modes of detectors

Consider a neutron detector subject to a permanent neutron radiation. Let us assume, that the observed detection rate is S and the time evolution of each voltage pulse induced by a detection is described by the function $f(t)$. Clearly, the fluctuating voltage signal observed at the output of the detector is an aggregate of the individual pulses; let us denote it by $y(t)$.

Depending on how information on the detection process is extracted from the voltage signal $y(t)$, we distinguish between three modes of operation: *pulse mode*, *Cambelling mode* and *current mode*; these are illustrated on Figure 2.12. The appropriate mode of operation in a given practical situation will be determined primarily by the value of the detection rate S.

At low detection rates, the average time between two consecutive detections is large (compared to the duration of pulses) and adjacent pulses are well separated from each other. In this case, the most appropriate mode of operation is the pulse mode. In pulse mode operation, the signal is sent through an integral discriminator which selects every pulse that crosses a given threshold value and creates a stream of logic pulses. These can then be counted allowing to estimate the detection rates S. Since pulses induced by gamma particles are smaller compared to neutron induced pulses in most detectors, the gamma background is effectively suppressed by pulse amplitude discrimination.

As the detection rate increases, the average time between two consecutive detection

events becomes shorter and adjacent pulses tend to overlap each other. Since such overlapping pulses cannot be distinguished by an integral discriminator effectively, loss of counts (dead time losses) occurs during pulse mode operation. Dead time correction can be applied to compensate for these losses until a certain point. At extremely large detection rates, however, none of the pulses will be separated from the others, hence pulse mode operation becomes impossible. In this case, the value of the detection rate S can be indirectly deduced by analyzing the characteristics of the continuous signal $\boldsymbol{y}(t)$. This procedure is based on the Campbell theorem, [66], which states that the mean value and the variance of the detector signal are proportional to the detection rate S, when the detections follow a Poisson process. In this case:

$$\langle \boldsymbol{y} \rangle = \mathbb{E}[\boldsymbol{y}(t)] = S \int_0^\infty f(t)\,\mathrm{d}t,$$
$$\mathbb{E}[\boldsymbol{y}(t) - \langle \boldsymbol{y} \rangle]^2 = S \int_0^\infty f^2(t)\,\mathrm{d}t. \tag{2.34}$$

The original theorem of Campbell has been extended to higher order statistic in the form of the high-order Campbell theorem [66–69]:

$$\mathbb{E}[\boldsymbol{y}(t) - \langle \boldsymbol{y} \rangle]^n = S \int_0^\infty f^n(t)\,\mathrm{d}t \qquad n > 2. \tag{2.35}$$
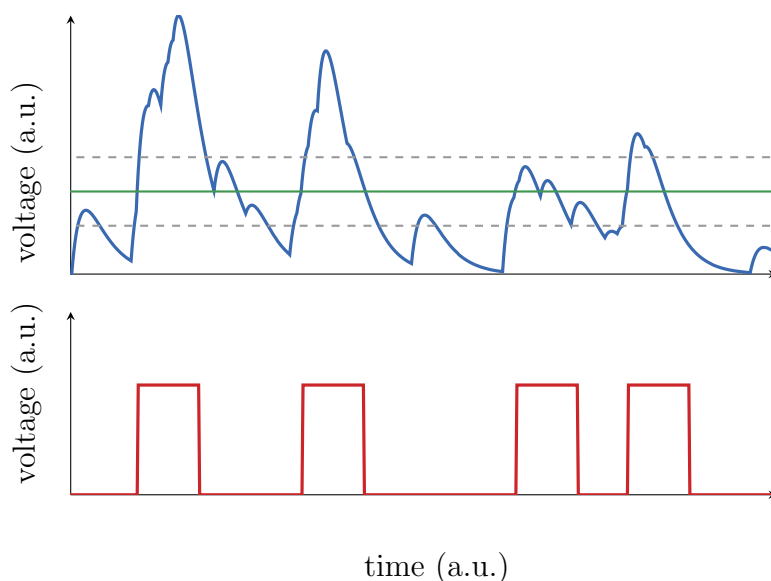
Figure 2.12: Illustration of the operation mode of detectors.

In current mode, the mean value of the signal is measured and detection rate is retrieved using the first part of the above theorem. In this mode of operation, the gamma background can be discriminated by the joint use of two almost identical detectors, one of which does not contain the neutron-sensitive material and is therefore sensitive only to gamma radiation. In Campbelling mode, the variance (or higher order central moments) of the signal is estimated. In this case, the gamma pulses are inherently suppressed because the pulse shape $f(t)$ is raised to a higher power, hence larger neutron pulses are emphasized.

2.4.2 Fission chambers

Fission chambers, just like ³He detectors, belong to the type of gas-filled detectors [38]. The schematic design of a fission chamber is shown on Figure 2.13. The detector usually has two coaxial electrodes. The outer electrode, namely the cathode, can have an outer diameter as small as 3 mm for miniature chambers. A thin layer of fissile material (from a few micrograms to a few grams) is deposited on at least one of the electrodes, usually only on the anode. The most typical coating material is ²³⁵U. The space between the electrodes is filled with pressurized gas (e.g., argon at 1.5 bar). When a neutron reaches the fissile deposit, it is likely to induce a fission that generates two heavily charged ions. The two fission fragments are oppositely directed, hence one of them gets absorbed in the coating while the other will likely enter the filling gas. This latter fission fragment will ionize the filling gas on its trajectory. Given that a high voltage of a few hundred volts is applied between the electrodes, the electrons and positive ions get separated and drift across the gas, generating a current signal that can be amplified and processed. In most applications, the voltage value is chosen to be high enough to collect all the charges, but low enough to prevent the production of secondary ionization pairs. In this case, the neutron-induced current signal is proportional to the fission rate and nearly insensitive to the voltage. In this case, the fission chamber is said to work in the saturation regime.
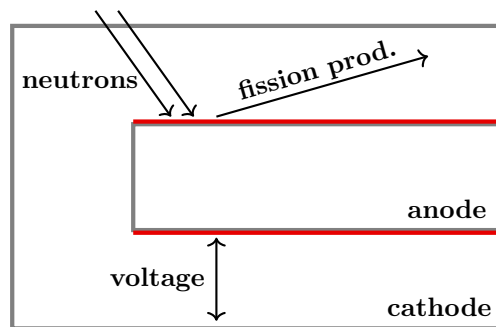
Figure 2.13: A schematic illustration of the design of a fission chamber.

One outstanding characteristic of fission chambers compared to other types of neutron detectors is the large amount of energy released during detection [38]. In ²³⁵U coated fission chambers, for example, the average total energy released per fission is 200 MeV of which 160 MeV appears as the kinetic energy of the two fission fragments. Given that usually one of the two fission fragments enter the filling gas, on average 80 MeV energy is used for ionization per detection. In comparison, in ³He detectors the total kinetic energy released in the ³He(n,p) reaction is 764 keV [38]. As a consequence, in fission chambers pulses induced by neutrons are much larger in magnitude than pulses generated by any other particles. Due to this inherent gamma suppressing property, fission chambers can be effectively operated in all three modes of operation mentioned in Section 2.4.1, unlike other detector types which are usually used in one operation mode only. For this reason fission chambers are routinely used as in-core neutron detectors for the on-line monitoring of the neutron flux, where this one detector is able to serve measurement data over a wide range of reactor power (and corresponding detection rates) [70–73].

The major disadvantage of fission chambers is their low detection efficiency, especially compared to ^{3}He detectors: while ^{3}He detectors can provide a $90\,\%$ detection efficiency, the efficiency of fission chambers is typically $1\,\%$. This is primarily due to two factors: *a)* while in ^{3}He detectors, the target material is mixed with the filling gas in large amounts, fission chambers have a very thin fissile layer; *b)* the cross-section of neutron induced fission in ^{235}U is generally smaller by about 1 order of magnitude than the cross section of the ^{3}He(n,p) reaction. This low detection efficiency is especially problematic in safeguards applications, where low emission intensities are often encountered. Therefore, in most cases ^{3}He detectors operated in pulse mode are preferred [3]. However, as noted in the beginning of Section 2.4, the large neutron and gamma intensities encountered at spent fuel measurements make the use of ^{3}He detectors difficult. In these cases the analysis of the continuous signals of fission chambers operated in the Campbelling or current mode can be a viable option.

2.4.3 Extending the traditional Campbell theorem

As we have seen, the analysis of the continuous voltage signal of neutron detectors (especially fission chambers) is based on the Campbell theorem. However, the primary assumption behind this theorem is that the detections follow a homogeneous Poisson process. Strictly speaking, however, this assumption does not hold, when neutrons are detected from a fission chain, which is the case when measuring the flux in a reactor or the mass of a fissile sample. In order to establish the possibility to investigate the properties of continuous detector signals generated by correlated detection events, a new formalism has been developed recently by Pál and Pázsit for the mathematical formulation of the signals (primarily that of fission chambers) [5]. In the following, this formalism is described briefly.

Consider a fission chamber and let us assume that it detects a neutron at time $t = 0$. As a result of the detection, a voltage pulse is induced at the detector output; a possible representation of the pulse is shown on Figure 2.14a). In general, the observed properties of the pulse (e.g. its height, length or shape) are influenced by a number of factors, including the energy and direction of the incident neutron, the point of entry into the detector, or the processes of charge generation and collection in the sensitive volume; these have been investigated analytically, experimentally as well as with simulations [74–78]. Due to its random characteristics, the time evolution of a pulse can a described as a stochastic process, which will be denoted as $\boldsymbol{x}(t)$. According to the model described in Reference [5], each pulse has a fixed deterministic shape given by the function $f(t)$, but they have a random amplitude $\boldsymbol{a}$, which is characterized by a probability density function denoted as $w(a)$[1]. With these assumptions $\boldsymbol{x}(t)$ takes the form $\boldsymbol{x}(t) = \boldsymbol{a}\,f(t)$. It is shown that the probability density function of $\boldsymbol{x}(t)$ can be written as

$$h(x,t) = \int_0^\infty \delta[x - a\,f(t)]\,w(a)\,\mathrm{d}a. \tag{2.36}$$

Consider now the case when the detector is subject to a permanent neutron radiation. Clearly, each detection induces a pulse $\boldsymbol{x}(t)$, which are assumed to be independent

---

[1]This probability density can be experimentally estimated from a measurement of the pulse height spectrum.

of each other. As the aggregate effect of the individual pulses, a fluctuating voltage signal, denoted as $\boldsymbol{y}(t)$, is formed at the detector output. A possible realization of this signal can be seen on Figure 2.14b. In order to formalize the statistics of the observed voltage signal in a particular case, the discrete process of the detection events must be described and combined with the above model of a single voltage pulse. Since, however, the continuous signal of the detector is not a Markovian process, it can only be formulated using a backward type Kolmogorov equation. In the simplest case, for example, when the detection events arrive in a Poisson process with rate S, the following backward equation can be written for the probability density function of the signal:

$$p(y,t) = \mathrm{e}^{-St}\,\delta(y) + \int_0^t \mathrm{e}^{-St'} h(y',t-t')\,p(y-y',t-t')\mathrm{d}t'. \tag{2.37}$$

Starting from this equation, the expressions of the original as well as the higher-order Campbell theorems, given in (2.34) and (2.35), have been re-derived in an exceptionally simple manner [5].
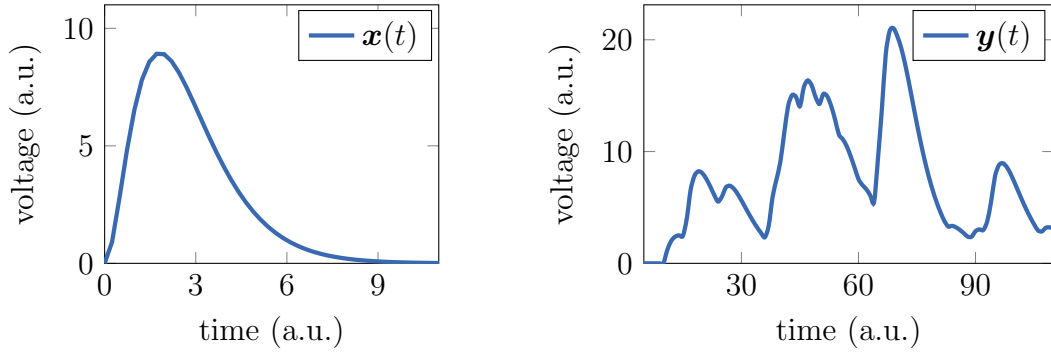
(a) A voltage pulse induced by a single detection.

(b) A voltage signal induced by a series of detections.

Figure 2.14: Illustration of the voltage signal of a neutron detector after a single detection event (left) and after a series of detection events (right).

Besides reproducing these results corresponding to detections in a homogeneous Poisson process, formulas have been derived for detections in a non-homogeneous Poisson process [5] as well as for detections from a multiplying chain [79]. Recently, even alternative versions [79–81] of the traditional Feynman-alpha and Rossi-alpha methods [82–85] have been proposed for determining the prompt neutron decay constant in nuclear reactors.

The aim of the research presented in this thesis is, by continuing on the above line, to develop a new, alternative version of neutron multiplicity counting based on the Campbelling-type analysis of the continuous voltage signals of neutron detectors. By carrying the favourable properties of the original Campbell technique, it might be a practical tool for measuring nuclear materials, especially in the form of high intensity spent nuclear fuel. The description and investigation of this new version of neutron multiplicity counting is the topic of the reminder of the thesis.

Chapter 3

Multiplicity counting with continuous detector signals

3.1 Basic principles

As we have seen in Section 2.3, the aim of a multiplicity counting measurement is to estimate the three sample parameters, the spontaneous fission intensity F, the alpha-ratio α and the net leakage multiplication M. According to Böhnel's theory of superfission, determining the sample parameters is equivalent to determining the Q_s intensity of the sample emission events and the ν_i $(i = 1, 2, 3)$ factorial moments of the number of emitted neutrons per event. Since, however, these factorial moments are not themselves measurable, one had to identify three other quantities, which are directly measurable and which form a mathematical relationship with Q_s and ν_i $(i = 1, 2, 3)$. In the traditional form of multiplicity counting the three measurable quantities are the singles, doubles and triples detection rates which are the rates of the first three factorial moments of the number of detections observed a finite time window. Recall that the practical applicability of the method is provided by the fact that the detection rates are able to quantify (on a statistical basis) the number of correlated detection events caused by neutrons that originate from the same spontaneous fission event.

Compared to this traditional approach, extracting sample parameters from the continuous signals of fission chambers poses two key difficulties. First, the mathematical formulation of the continuous valued process representing the detector signal is more complicated than describing the discrete counting process observed in a detector. Second, contrary to pulse counting, no individual detection events are identified when analyzing the continuous signals of the detectors. For this reason, the presence of correlated detection events must be inferred indirectly from the correlated changes in the signal value. An obvious choice of measurable quantities that reflect such correlations are the moments of the signals.

To derive expressions for these moments, the point model of the neutron emission and detection processes in Sections 2.3.3 and 2.3.4 will be combined with the new formalism, described in Section 2.4.3, for characterizing fission chamber signals. Accordingly, neutrons are emitted at a rate Q_s from the sample, and the probability mass function of the number of emitted neutrons is $P(n)$, whose first three factorial moments are denoted as ν_1, ν_2 and ν_3. We shall assume that every neutron is detected with the

same probability by any of the detectors and this probability for each specific detector is denoted by ε. Note that ε here has a somewhat different meaning than in the previous chapter where it represented the overall detection probability of the whole array of detectors. Each neutron detection produces a stochastic pulse $\boldsymbol{x}(t) = \boldsymbol{a}\, f(t)$ with shape $f(t)$ and a random amplitude $\boldsymbol{a}$ whose density function is $w(a)$. For the sake of simplicity, we shall assume that $f(t)$ and $w(a)$ is the same for every detector. As a result of the consecutive emission (and subsequent detection) of neutrons, each detector produces a fluctuating continuous signal. In particular, we shall focus on the correlated signals of three detector at a time; these will be denoted as $\boldsymbol{y}_1(t), \boldsymbol{y}_2(t)$ and $\boldsymbol{y}_3(t)$. A possible realization of the signals is shown on Figure 3.1.
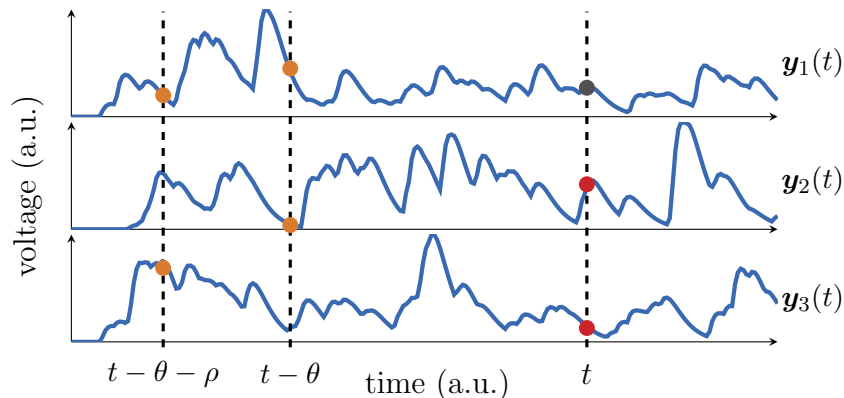
Figure 3.1: A possible realization of the voltage signals of three detectors in a multiplicity counting measurement. The dashed lines select three different points in time $(t, t - \theta$ and $t - \theta - \rho)$ whereas the dots highlight the signal amplitudes at these time instants. Together they illustrate the moments of the signals we wish to determine.

Our goal in the following is to pick at least three moments of the signals and express them as functions of the sample emission rate Q_s and the factorial moments ν_i ($i = 1, 2, 3$) of the number of emitted neutrons per one emission event. Although in principle we can choose from an infinite number of moments, we are interested in those with an order up to three; this restriction is not independent from the fact that ν_3 is the highest order factorial moment we wish to obtain. The selected set of moments will be the cumulants corresponding either to the distribution of one signal, or to the joint distribution of two or three signals.

Depending on the way the moments describe the information on the correlated detection events in the continuous signals, the theory presented in this chapter has gone through three major stages, each being extensions of the preceding one. The key concept of the three stages can be summarized as follows:

1. In the first stage, we shall make the rather idealistic assumption that every neutron is detected instantly following its emission. An important consequence of this assumption is that neutrons originating from the same emission are detected simultaneously. The identification of correlated detections, in this case, will be based on the fact that pulses induced by these detections perfectly overlap in time. At this stage we shall derive expressions for six of the so-called *one-point moments* which characterize the distribution of the signals at a single point in

time (see Figure 3.1); such moments include the *mean* or the *covariance*. As we shall see, by assuming instant detection the one-point moments are capable of recovering the factorial moments ν_i.

2. In the second stage, we shall drop the idealistic assumption of instant detection by assuming that each neutron is detected with a random time delay following its emission. The consequence of this assumption is that neutrons originating from the same emission are detected at different times, hence the pulses they induce will not necessarily overlap in time. In this stage, the same set of one-point moments are calculated as in the first stage. We shall see that the first factorial moment ν_1 can still be recovered, however, the information on the second and third moment ν_2 and ν_3 is lost in the most anticipated practical scenarios.

3. A solution to this problem is provided in stage three. Here, we maintain the realistic assumption that neutrons are detected after a random time delay, however, we extend the set of moments to consider. Beyond the one-point moments, we start to investigate the so-called *two- and three point moments* as well (see Figure 3.1); such moments include the *covariance function* or the *bicovariance function*. By characterizing the distribution of the signals in more than one points in time, they are able to identify the correlation between detection events that are temporally separated from each other. As we shall see, the two- and three point moments allow us to recover the second and third moment, ν_2 and ν_3, even in cases where one-point moments cannot.

At this point it should be emphasized that the first of the above three stages has been completed by the time the author has joined the research project. The second and third stages, however, have been elaborated by the author. Nevertheless, because they form a logical chain, all three stages are described separately in Sections 3.2–3.4. Each section will be divided into two parts. While the first part only concerns the derivation of the moment expressions, the second part is devoted to the interpretation of the results. Note, however, that the calculation of the moments is rather extensive and complicated. Therefore, for the sake of transparency and compactness, every calculation in the main text will be given schematically, focusing mainly on the final results. The details of the calculations can be found in the Appendix.

Once the expressions of the moments are available, it might be desirable to invert them, and express the sample parameters F, α and M with the (measurable) moments. The same inversion procedure with the traditional detection rates has been described in Section 2.3.5. However, we shall see that the moments of the continuous signals are very closely related to the singles, doubles and triples rates of the traditional multiplicity counting. For this reason, in Section 3.5, we chose to derive equations that express the traditional detection rates with the moments of the signal. Once, the values of the detection rates are determined, the same inversion procedure described in Section 2.3.5 can be used to recover the three sample parameters.

3.2 One-point distribution with instant detection

We start by investigating the one-point moments of the detector signals, which characterize their distribution at a single point in time, say t (see Figure 3.1). We have also said that in doing so we shall make the assumption that neutrons are detected instantly following their emission. As stated earlier, from all the possible moments we are primarily interested in the cumulants up to the order of three. Regarding the signal of one detector, say $\boldsymbol{y}_1(t)$, there are three moments meeting this criteria: the (stationary) *mean*, *variance* and *skewness*. They are defined as

$$\kappa_1 = \lim_{t\to\infty} \mathbb{E}\left[\boldsymbol{y}_1(t)\right], \tag{3.1a}$$

$$\kappa_2 = \lim_{t\to\infty} \mathbb{E}\left\{[\boldsymbol{y}_1(t) - \langle\boldsymbol{y}_1\rangle]^2\right\}, \tag{3.1b}$$

$$\kappa_3 = \lim_{t\to\infty} \mathbb{E}\left\{[\boldsymbol{y}_1(t) - \langle\boldsymbol{y}_1\rangle]^3\right\}. \tag{3.1c}$$

Regarding the signals of two detectors, say $\boldsymbol{y}_1(t)$ and $\boldsymbol{y}_2(t)$, there are two cumulants to consider: the (stationary) *covariance* and *another moment without a special name*. They are defined as

$$\kappa_{1,1} = \lim_{t\to\infty} \mathbb{E}\left\{[\boldsymbol{y}_1(t) - \langle\boldsymbol{y}_1\rangle]\,[\boldsymbol{y}_2(t) - \langle\boldsymbol{y}_2\rangle]\right\}, \tag{3.2a}$$

$$\kappa_{2,1} = \lim_{t\to\infty} \mathbb{E}\left\{[\boldsymbol{y}_1(t) - \langle\boldsymbol{y}_1\rangle]^2\,[\boldsymbol{y}_2(t) - \langle\boldsymbol{y}_2\rangle]\right\}, \tag{3.2b}$$

Regarding the signals of three detectors, $\boldsymbol{y}_1(t)$, $\boldsymbol{y}_2(t)$ and $\boldsymbol{y}_3(t)$, there is only one suitable cumulant: the (stationary) *bicovariance*. It is defined as

$$\kappa_{1,1,1} = \lim_{t\to\infty} \mathbb{E}\left\{[\boldsymbol{y}_1(t) - \langle\boldsymbol{y}_1\rangle]\,[\boldsymbol{y}_2(t) - \langle\boldsymbol{y}_2\rangle]\,[\boldsymbol{y}_3(t) - \langle\boldsymbol{y}_3\rangle]\right\}. \tag{3.3}$$

3.2.1 Derivation of the moment expressions

The fundamental building block in calculating the expressions of any of the above cumulants are the quantities related to the distribution of a single pulse. Therefore we start by characterizing this latter, and continue with the former after that.

Distribution of a single pulse

Consider a neutron emitted at time $t = 0$ and detected instantly. According to our model, the detection induces a random impulse $\boldsymbol{x}(t) = \boldsymbol{a}\,f(t)$ with respect to the time of emission (which is also the time of detection), where $f(t)$ is a fixed shape and $\boldsymbol{a}$ is a random amplitude with a density function $w(a)$.

In order to characterize the statistical properties of the pulse, we start by specifying its one-point cumulative distribution function, $H_1(x,t)$, which equals the probability that the observed value of the pulse at time t does not exceed x. Formally, H_1 can be written as $H_1(x,t) = \mathbb{P}[\boldsymbol{x}(t) \leq x] = \mathbb{P}[\boldsymbol{a}\,f(t) \leq x]$. A more concrete form of H_1 is obtained if we notice that the right hand side equals the probability that $\boldsymbol{a}$ takes a value a such that at time t the relation $a\,f(t) \leq x$ holds. With this in mind one can write

$$H_1(x,t) = \int_0^\infty \Delta[x - af(t)]\,w(a)\,\mathrm{d}a, \tag{3.4}$$

where Δ stands for the Heaviside step function defined as

$$\Delta(x) = \begin{cases} 0, & \text{for } x < 0 \\ 1, & \text{for } x \geq 0. \end{cases} \tag{3.5}$$

Three quantities, in particular, related to the distribution of the pulse will appear in the derivations later; all of them can be derived starting from one-point cumulative distribution function H_1. The first of these quantities is the density function of the pulse, which is defined as the derivative of H_1 with respect to x and takes the form

$$h_1(x, t) = \frac{\partial H_1(x, t)}{\partial x} = \int_0^\infty \delta[x - af(t)] \, w(a) \, \mathrm{d}a. \tag{3.6}$$

Here, we have accounted for the fact that the derivative of the Heaviside step function is the Dirac delta function, denoted as δ. The second quantity of interest is the characteristic function of the pulse, which is defined as the Fourier transform of the density function with respect to x and takes the form

$$\chi_1(\omega, t) = \int_{-\infty}^\infty \mathrm{e}^{\imath \omega x} \, h_1(x, t) \, \mathrm{d}x = \int_0^\infty \mathrm{e}^{\imath \omega a f(t)} \, w(a) \, \mathrm{d}a. \tag{3.7}$$

The third quantity is the raw moment of order k of the pulse, which is obtained from the characteristic function as

$$\mu_k(t) = \frac{1}{\imath^k} \left. \frac{\partial^k \chi_1(\omega, t)}{\partial \omega^k} \right|_{\omega=0} = \langle a^k \rangle \, f^k(t). \tag{3.8}$$

Here f^k is the kth power of the shape, whereas $\langle a^k \rangle$ denotes the moment of order k of the amplitude and is defined as

$$\langle a^k \rangle = \int_0^\infty a^k \, w(a) \, \mathrm{d}a. \tag{3.9}$$

Distribution of one detector signal

The one-point distribution of the signal of one detector, say that labeled with 1, concerns the random variable $\{\boldsymbol{y}_1(t)\}$, which is characterized by the cumulative distribution function

$$F_1(y, t) = \mathbb{P}[\boldsymbol{y}_1(t) \leq y].$$

The procedure of calculating the cumulants (3.1) of the signal takes four steps:

- In the first step we start by writing a backward Kolmogorov equation for the density function of the distribution, defined as

$$p_1(y, t) = \frac{\partial F_1(y, t)}{\partial y}. \tag{3.10}$$

This equation is formulated by considering the probabilities of all events that change the value of the signal.

- Since the above equation cannot be solved analytically, in the second step we transform it to an equation for the characteristic function, defined as

$$\pi_1(\omega, t) = \int_{-\infty}^{\infty} e^{\imath \omega y} \, p_1(y, t) \, \mathrm{d}y. \tag{3.11}$$

This equation can easily be solved analytically.

- In the third step, using the solution of the characteristic function, we calculate an expression for the stationary cumulant-generating function, defined as

$$\gamma_1(\omega) = \lim_{t \to \infty} \ln[\pi_1(\omega, t)]. \tag{3.12}$$

- In the fourth step, the cumulant of order k is obtained by differentiating the cumulant-generating function:

$$\kappa_k = \frac{1}{\imath^k} \left. \frac{\partial^k \gamma_1(\omega)}{\partial \omega^k} \right|_{\omega=0}. \tag{3.13}$$

These four steps are described in great detail in Section A.1.1. Here, only certain parts will be reproduced.

As noted above, we start by formulating an expression for the density function p_1 of the signal. Recalling that the detection process starts at time $t = 0$, it is clear that value of the signal at earlier times is zero. As a consequence, for $t < 0$, the density function takes the form

$$p_1(y, t) = \delta(y). \tag{3.14}$$

On the other hand, as we shall explain below, for $t \geq 0$ it obeys the following Kolmogorov backward integral equation:

$$
\begin{aligned}
p_1(y, t) = e^{-Q_s t} \, \delta(y) + \int_0^t Q_s \, e^{-Q_s t'} \sum_{n=0}^{\infty} P(n) \sum_{k=0}^{n} \binom{n}{k} \varepsilon^k \, (1 - \varepsilon)^{n-k} \\
\times \int_0^y U_k^{(1)}(y', t - t') \, p_1(y - y', t - t') \, \mathrm{d}y' \mathrm{d}t'.
\end{aligned}
\tag{3.15}
$$

Here Q_s and $P(n)$ denote the intensity and multiplicity of the source and were defined earlier in Section 2.3.3; ε denotes the detection efficiency (more precisely: the probability of detecting a neutron) and was introduced in Section 3.1; finally the function $U_k^{(1)}$ is defined as

$$U_k^{(1)}(y, t) = \int_0^{\infty} \cdots \int_0^{\infty} h_1(y_1, t) \cdots h_1(y_k, t) \, \mathrm{d}y_k \cdots \mathrm{d}y_1, \tag{3.16}$$
$$\scriptstyle y_1 + \cdots + y_k = y$$

where h_1 denotes the one-point density function of a single pulse and was defined in (3.6).

Before interpreting the Kolmogorov equation (3.15), we should consider the physical meaning of the the function $U_k^{(1)}$ given by (3.16). One can recognize that it is essentially

the density function of k pulses induced by k neutrons originating from the same emission at time $t = 0$. As a k-fold convolution of h_1, it reflects the fact that pulses induced by more that one neutrons are independent and add up linearly. With these in mind, Equation (3.15) can be interpreted in the following way. As an application of the law of total probability, the probability density of having a signal value y at time t (left-hand side) is expressed with the probabilities (or probability densities) of events, that cause it (right-hand side). The two terms on the right-hand side correspond to two mutually exclusive events. The first term represents the event when no source emission occurs until time t with probability $e^{-Q_s t}$, in which case the signal value at time t remains zero with probability density $\delta(y)$. The second term represents the event when there was at least one source emission until time t. In fact, its is a sum (or integral) over the probabilities (or probability densities) of a set of mutually exclusive events, each of which can be described as follows. The first emission occurs at time t' with probability density $Q_s e^{-Q_s t'}$; during the emission n neutrons are released with probability $P(n)$; from the n neutrons k are detected and $n - k$ escape with probability $\binom{n}{k} \varepsilon^k (1 - \varepsilon)^{n-k}$; the k pulses induced in the detector contribute by y' to the signal at time t with probability density $U_k^{(1)}(y', t - t')$; pulses from subsequent emissions contribute to it by $y - y'$ with probability density $p_1(y - y', t - t')$.

After lengthy calculations, detailed in Section A.1.1, we find that the characteristic function takes the form

$$\pi_1(\omega, t) = \exp\left(Q_s \int_0^t \left(G\left\{ c_1\left[\chi_1(\omega, t') \right] \right\} - 1 \right) \mathrm{d}t' \right), \tag{3.17}$$

where χ_1, the characteristic function of a single pulse, is given by (3.7), whereas c_1 is defined as

$$c_1(x) = 1 + \varepsilon (x - 1). \tag{3.18}$$

Finally, using (3.12), the following expression is obtained for the stationary cumulant-generating function:

$$\gamma_1(\omega) = Q_s \int_0^\infty \left(G\left\{ c_1\left[\chi_1(\omega, t) \right] \right\} - 1 \right) \mathrm{d}t. \tag{3.19}$$

By substituting the above expression into (3.13), we are able to calculate κ_k, the stationary cumulant of order k. As noted in the beginning of Section 3.2, we are interested in three moments of the signal of one detector: its mean value κ_1, its variance κ_2 and its skewness κ_3. If we account for the definitions (2.22) of the detection rates, these take the forms

$$\kappa_1 = S \int_0^\infty \mu_1(t) \, \mathrm{d}t, \tag{3.20a}$$

$$\kappa_2 = S \int_0^\infty \mu_2(t) \, \mathrm{d}t + 2 D \int_0^\infty \mu_1^2(t) \, \mathrm{d}t, \tag{3.20b}$$

$$\kappa_3 = S \int_0^\infty \mu_3(t) \, \mathrm{d}t + 6 D \int_0^\infty \mu_2(t) \, \mu_1(t) \, \mathrm{d}t + 6 T \int_0^\infty \mu_1^3(t) \, \mathrm{d}t. \tag{3.20c}$$

At this point it might worth to take a look at the physical meaning of the above expressions of the moments. The κ_1 mean value (first order moment) of the signal

originates from one "source": the first moment μ_1 of one pulse (single). The κ_2 variance (second order moment) of the signal, on the other hand, originates from two "sources": the second moment μ_2 of one pulse (single) or the joint second moment μ_1^2 of two distinct pulses (doubles). Finally, the κ_3 skewness (third order moment) of the signal originates from three "sources": the third moment μ_3 of one pulse (single), the joint third moment $\mu_2 \, \mu_1$ of two distinct pulses (doubles) or the joint third moment μ_1^3 of three distinct pulses (triples).

Finally, when we insert the explicit form of the moments (3.8) of the pulse into Equation (3.20) then, by introducing the notation

$$I_n = \int_0^\infty f^n(t) \, \mathrm{d}t, \tag{3.21}$$

the cumulants of the signal take the particularly compact forms

$$\kappa_1 = S \, \langle a \rangle \, I_1, \tag{3.22a}$$

$$\kappa_2 = \left[S \, \langle a^2 \rangle + 2 \, D \, \langle a \rangle^2 \right] I_2, \tag{3.22b}$$

$$\kappa_3 = \left[S \, \langle a^3 \rangle + 6 \, D \, \langle a^2 \rangle \langle a \rangle + 6 \, T \langle a \rangle^3 \right] I_3. \tag{3.22c}$$

Distribution of two detector signals

The one-point distribution of the signal of two detectors, say those labeled with 1 and 2, concerns the random variable $\{\boldsymbol{y}_1(t), \boldsymbol{y}_2(t)\}$, which is characterized by the cumulative distribution function

$$F_{1,1}(y_1, y_2, t) = \mathbb{P}[\boldsymbol{y}_1(t) \leq y_1, \boldsymbol{y}_2(t) \leq y_2].$$

The procedure of calculating the corresponding cumulants (3.2) follows the same steps as in the previous case of one signal. The details of this calculation can be found in Section A.1.2. Here only the final results are presented, which take the form:

$$\kappa_{1,1} = 2 \, D \int_0^\infty \mu_1^2(t) \, \mathrm{d}t, \tag{3.23a}$$

$$\kappa_{2,1} = 2 \, D \int_0^\infty \mu_2(t) \, \mu_1(t) \, \mathrm{d}t + 6 \, T \int_0^\infty \mu_1^3(t) \, \mathrm{d}t, \tag{3.23b}$$

The interpretation of the above equations is analogous to that of (3.20). The $\kappa_{1,1}$ covariance (second order moment) of two signals originates from one "source": the joint second moment $\mu_1^2(t)$ of two distinct pulses (doubles) each from a different detector. $\kappa_{2,1}$ (third order moment) originates from two "sources": the joint third moment $\mu_2 \, \mu_1$ of two distinct pulses (doubles) each from a different detector and the joint third moment μ_1^3 of three distinct pulses (triples) of which two comes from one detector and one comes from the other.

Again, when we use the explicit form of the moments (3.8) of the pulse furthermore we account for (3.21), the expressions can be rewritten into the compact form

$$\kappa_{1,1} = 2 \, D \, \langle a \rangle^2 \, I_2, \tag{3.24a}$$

$$\kappa_{2,1} = \left[2 \, D \, \langle a^2 \rangle \langle a \rangle + 6 \, T \, \langle a \rangle^3 \right] I_3. \tag{3.24b}$$

Distribution of three detector signals

The one-point distribution of the signal of three detectors, those labeled with 1, 2 and 3, concerns the random variable $\{\boldsymbol{y}_1(t), \boldsymbol{y}_2(t), \boldsymbol{y}_3(t)\}$, which is characterized by the cumulative distribution function

$$F_{1,1,1}(y_1, y_2, y_3, t) = \mathbb{P}[\boldsymbol{y}_1(t) \leq y_1, \boldsymbol{y}_2(t) \leq y_2, \boldsymbol{y}_3(t) \leq y_3].$$

With the derivation presented in Section A.1.3, the following expression is obtained for the cumulant $\kappa_{1,1,1}$ defined in (3.3):

$$\kappa_{1,1,1} = 6\,T\,\langle a \rangle^3 \int_0^\infty \mu_1^3(t)\,\mathrm{d}t. \tag{3.25}$$

The interpretation of this equation is analogous to that of (3.20) and (3.23). Again, when we use the explicit form of the moments (3.8) of the pulse and account for (3.21), the expression can be rewritten into the compact form

$$\kappa_{1,1,1} = 6T\,\langle a \rangle^3 I_3. \tag{3.26}$$

3.2.2 Interpretation of the results

In order to give a comprehensive overview of moment expressions derived in this section, let us collect them into one place below. For the mean, variance and skewness of one detector signal we obtained

$$\kappa_1 = S\,\langle a \rangle\,I_1, \tag{3.27a}$$
$$\kappa_2 = \left[S\,\langle a^2 \rangle + 2\,D\,\langle a \rangle^2 \right] I_2, \tag{3.27b}$$
$$\kappa_3 = \left[S\,\langle a^3 \rangle + 6\,D\,\langle a \rangle \langle a^2 \rangle + 6\,T\,\langle a \rangle^3 \right] I_3. \tag{3.27c}$$

The cross-covariance and the cumulant $\kappa_{2,1}$ of two detector signals read as

$$\kappa_{1,1} = 2\,D\,\langle a \rangle^2\,I_2 \tag{3.27d}$$
$$\kappa_{2,1} = \left[2\,D\,\langle a \rangle \langle a^2 \rangle + 6\,T\,\langle a \rangle^3 \right]\,I_3. \tag{3.27e}$$

The bicovariance of three detectors took the form

$$\kappa_{1,1,1} = 6\,T\,\langle a \rangle^3\,I_3. \tag{3.27f}$$

The quantities I_n and $\langle a^n \rangle$ were defined in Equations (3.21) and (3.9).

Equation (3.27a) shows that the mean value of the signal of a detector is proportional to the singles rate; the proportionality factor is the product $\langle a \rangle I_1$. Since, in general, I_n and $\langle a^n \rangle$ are solely properties of the pulses produced by the detector, they can be determined in a calibration step using a large sample of individual recorded pulses. Consequently, the singles rate can be retrieved from the mean value of the continuous detector signal. Moreover, Equation (3.27a) reveals a big advantage of the new approach over the traditional one: the singles rate can be obtained at arbitrarily large count rates from the continuous signal. This is because when, for example, two pulses completely

overlap, their amplitude together will be twice as large as the amplitude of each, hence their presence is reflected in the mean value.

An inspection of Equations (3.27b) and (3.27c) reveals a way of determining S and D from the variance and skewness. The procedure goes as follows. In the possession of S from the mean, D can be obtained from the variance using (3.27b). Then, with the known values of S and D, T can be obtained from the skewness using (3.27c). These formulas reveal two additional favourable quality of the new method. The first one is that, unlike in the traditional case, the doubles and triples rates can be obtained from the signal of only one detector. The explanation is the same as in the case of the mean: the amplitudes of the pulses generated by coincident events add together, which is reflected in the variance and the skewness. The second one is that these higher order moments suppress the contribution of minority signal components (e.g. noise, gamma pulses, alpha pulses, etc.), similarly to the application of the higher order Campbelling methods (see Section 2.4.1). This is explained with the presence of I_2 and I_3 in the formulas, which contain the second and third power of the pulse.

Although the variance and the skewness allow us to estimate the dobles and the triples rates from one signal, the method has certain disadvantages. Namely, when we calculate D from the variance (3.27b), we propagate the uncertainty of the estimate of S. Similarly, when we calculate T from the skewness (3.27c), we propagate the uncertainties of S and D. This problem can be bypassed by accounting for the cross moments (3.27d)–(3.27f). Taking a look at the covariance (3.27d) of two signals, we see that it is identical to the second term of the variance (3.27b), that is, it is directly proportional to the doubles rate. This means that using the covariance, D can be obtained without using S, hence avoiding the propagation of its uncertainty. Using the moment (3.27e) of two signals, we can obtain T without requiring S, however, we still need to use D while propagating its uncertainty. The triples rate can most conveniently obtained from the bicovariance (3.27f) of three signals without needing to use either S or D.

To conclude, Equations (3.27) form a system of (overdetermined) linear algebraic equations between the singles, doubles and triples detection rates and certain moments of the signal. By measuring the moments, the values of the detection rates can be determined by inverting this system of equations. Alternatively, if one selects three of the moments, the κ_1 mean of one signal (3.27a), the $\kappa_{1,1}$ covariance of two signals (3.27d), as well as the $\kappa_{1,1,1}$ bicovariance of three signals (3.27f), then each of these can be used to determine one of the detection rates. Finally, we note that this ability of the moments to recover the detection rates of traditional pulse counting relies on the fact that neutrons from the same spontaneous fission are detected simultaneously, hence the pulses they induce alter the value of the detector signal simultaneously as well.

3.3 One point moments with delayed detection

Contrary to the assumption of the previous section, neutrons emitted from the sample are not detected instantly. Instead, they arrive to the detectors with a time delay which, in addition, is random in nature. This randomness has two sources: the random velocity of the emitted neutrons (i.e. their energy spectrum) as well as the slowing down in the intermediate medium. In a fast detection system, where neutrons

travel mostly through air without moderation, the distribution of the time delay is primarily determined by the neutron spectrum. As an illustration, in Chapter B an explicit formula is derived for the density function of the delay in the case when the initial neutron energy follows the Watt spectrum. In a thermal detection system, on the other hand, where neutrons travel through a moderating material, the information on the initial energy is lost hence the time delay will mostly be determined by the properties (size, composition) of the moderator. The distribution of the time delay, in this case, is often approximated by the exponential distribution [1]. The time scale-parameter of this distribution (which gives the average time delay) is traditionally referred to as the *detector die-away time* [1].

As a formal representation of the delay, we introduce the random variable $\boldsymbol{\tau}$, which denotes the arrival time of a neutron to the detector with respect to the time of its emission. In the following, we shall assume, that $\boldsymbol{\tau}$ is independent and identically distributed for every detector and every detected neutron (including those originating from the same emission and that this distribution is characterized by the probability density function $u(\tau)$. As we have mentioned above, the form of $u(\tau)$ is a function of the parameters of the sample and the moderating material.

The primary objective of this section is to investigate the impact of the random time delay on the moments of the signals. For this reason, in Section 3.3.1 we shall derive formulas for the same set of moments as in the previous section. In doing so, no explicit form of the delay will be assumed in order to maintain generality. A specific expression for $u(\tau)$ will be considered only in Section 3.3.2 where we assess how certain properties of delay affect the values of the moments and their ability to recover the detection rates.

3.3.1 Derivation of the moment expressions

Let us begin by highlighting a simple (but important) observation that will make the recalculation of the moment expressions extremely easy. Consider a neutron emitted at time $t = 0$. Detecting this neutron with a time delay $\boldsymbol{\tau}$ means that it induces a pulse characterized by a time dependence $\boldsymbol{x}(t)$ with respect to the time of the detection. From a mathematical point of view, however, this is the same as if the neutron got detected instantly (that is, at time $t = 0$) and induces the same pulse but with a time dependence $\boldsymbol{x}(t - \boldsymbol{\tau})$ with respect to the time of emission.

The above observation allows us to base the calculation of the moments in the case of delayed detection on the grounds of the earlier described case of instant detection. This is due to the fact, that the only elements that change in the derivations are the expressions of the statistical properties of a single pulse (its density function, characteristic function and raw moments) which, however, appear only symbolically until until a very late point in the derivations. In particular, equations have been derived in the previous section, which express the moments of the signal in terms of the raw moments of the pulse.

For this reason, we begin with deriving the updated form of the moments of a single pulse by assuming a delay in the detections. After that, we obtain new expressions for the moments of the signal by inserting the updated pulse moments into the general expressions derived in Section 3.2.1.

Distribution of a single pulse

Consider a neutron emitted at time $t = 0$ and detected after a time delay $\boldsymbol{\tau}$, where this latter is distributed according the density function $u(\tau)$. Based on what we have said above, this detection induces a random pulse $\boldsymbol{x}(t) = \boldsymbol{a}\, f(t - \boldsymbol{\tau})$ with respect to the time of emission (which, in this case, is not the time of detection), where, again, $f(t)$ is a fixed shape and $\boldsymbol{a}$ is a random amplitude with a density function $w(a)$.

Just as in the case of instant detection in Section 3.2.1, the characterization of the statistical properties of the pulse starts by specifying its one-point cumulative distribution function, $H_1(x, t)$. In an analogy with Equation (3.4), it can be written as

$$H_1(x, t) = \int_0^\infty \int_0^\infty \Delta[x - af(t - \tau)]\, w(a)\, u(\tau)\, \mathrm{d}a\mathrm{d}\tau, \tag{3.28}$$

where Δ stands for the Heaviside step function again and was defined in (3.5).

The expressions of the density function, the characteristic function as well as the kth raw moment of the pulse can be derived from the above expression of H_1. The density function takes the form

$$h_1(x, t) = \frac{\partial H_1(x, t)}{\partial x} = \int_0^\infty \int_0^\infty \delta[y - af(t - \tau)]\, w(a)\, u(\tau)\, \mathrm{d}a\mathrm{d}\tau. \tag{3.29}$$

The characteristic function reads as

$$\chi_1(\omega, t) = \int_{-\infty}^\infty \mathrm{e}^{\imath\omega y}\, h_1(y, t)\, \mathrm{d}y = \int_0^\infty \int_0^\infty \mathrm{e}^{\imath\omega af(t-\tau)}\, w(a)\, u(\tau)\, \mathrm{d}a\mathrm{d}\tau. \tag{3.30}$$

For the kth raw moment, we get

$$\mu_k(t) = \frac{1}{\imath^k}\left.\frac{\partial^k \chi_1(\omega, t)}{\partial\omega^k}\right|_{\omega=0} = \langle a^k\rangle \int_0^\infty f^k(t - \tau)\, u(\tau)\, \mathrm{d}\tau, \tag{3.31}$$

where $\langle a^k\rangle$ again denotes the moment of order k of the pulse amplitude and was defined in (3.9).

Note that by assuming $u(\tau) = \delta(\tau)$, which represents the case of instant detection, all the above expressions revert back to their forms derived in the previous section – as one would expect naturally.

Distribution of one detector signal

By substituting (3.31) into the general expressions (3.20 of the moments, and performing simplifications detailed in Section A.2.1, we obtain

$$\kappa_1 = S\,\langle a\rangle\, I_1, \tag{3.32a}$$

$$\kappa_2 = \left[S\,\langle a^2\rangle + 2\,D\,\langle a\rangle^2\,\xi_{1,1}\right]\, I_2, \tag{3.32b}$$

$$\kappa_3 = \left[S\,\langle a^3\rangle + 6\,D\,\langle a\rangle\langle a^2\rangle\,\xi_{1,2} + 6\,T\,\langle a\rangle^3\,\xi_{1,1,1}\right]\, I_3. \tag{3.32c}$$

Here, the quantities denoted by ξ are defined as

$$\xi_{1,1} = \frac{1}{I_2}\int_0^\infty I_1^2(t)\,\mathrm{d}t, \quad \xi_{1,2} = \frac{1}{I_3}\int_0^\infty I_1(t)\,I_2(t)\,\mathrm{d}t, \quad \xi_{1,1,1} = \frac{1}{I_3}\int_0^\infty I_1^3(t)\,\mathrm{d}t, \tag{3.33}$$

where I_n is the same as (3.21) and we have introduced the function

$$I_n(t) = \int_0^\infty f^n(t - \tau)\, u(\tau)\, \mathrm{d}\tau. \tag{3.34}$$

Distribution of two detector signals

By substituting (3.31) into the general expressions (3.23, then, after simplifications, we obtain

$$\kappa_{1,1} = 2\,D\,\langle a \rangle^2\,\xi_{1,1}\,I_2, \tag{3.35a}$$

$$\kappa_{2,1} = \left[2\,D\,\langle a \rangle\langle a^2 \rangle\,\xi_{1,2} + 6\,T\,\langle a \rangle^3\,\xi_{1,1,1}\right]\,I_3. \tag{3.35b}$$

Distribution of three detector signals

By substituting (3.31) into the general expression (3.25), after simplifications, we obtain

$$\kappa_{1,1,1} = 6\,T\,\langle a \rangle^3\,\xi_{1,1,1}\,I_3. \tag{3.36}$$

3.3.2 Interpretation of the results

Again, let us collect the expressions of the moments derived in this section into one place below. For the mean, variance and skewness of one detector signal we obtained

$$\kappa_1 = S\,\langle a \rangle\,I_1, \tag{3.37a}$$

$$\kappa_2 = \left[S\,\langle a^2 \rangle + 2\,D\,\langle a \rangle^2\,\xi_{1,1}\right]\,I_2, \tag{3.37b}$$

$$\kappa_3 = \left[S\,\langle a^3 \rangle + 6\,D\,\langle a \rangle\langle a^2 \rangle\,\xi_{1,2} + 6\,T\,\langle a \rangle^3\,\xi_{1,1,1}\right]\,I_3. \tag{3.37c}$$

The cross-covariance and the cumulant $\kappa_{2,1}$ of two detector signals read as

$$\kappa_{1,1} = 2\,D\,\langle a \rangle^2\,\xi_{1,1}\,I_2, \tag{3.37d}$$

$$\kappa_{2,1} = \left[2\,D\,\langle a \rangle\langle a^2 \rangle\,\xi_{1,2} + 6\,T\,\langle a \rangle^3\,\xi_{1,1,1}\right]\,I_3. \tag{3.37e}$$

The cross-bicovariance of three detector signals took the form

$$\kappa_{1,1,1} = 6\,T\,\langle a \rangle^3\,\xi_{1,1,1}\,I_3. \tag{3.37f}$$

Here, the quantities $\langle a^n \rangle$ and I_n are the same as in the case of instant detection and were defined in (3.9) and (3.21), respectively. The ξ's were defined in (3.33).

Observe that the moment expressions (3.37) are nearly identical to those in (3.27) obtained by assuming an instant detection. The only difference is the presence of the ξ's as multiplying factors in certain terms of the moments. According to their definitions (3.33), these factors are functions of the pulse shape $f(t)$ and the delay density $u(\tau)$. This shows that unlike $\langle a \rangle^n$ and I_n, the ξ factors are not only properties of the detection system: through $u(\tau)$ they depend on the sample and the measurement geometry as well.[1] Notice that when neutrons are detected with a constant τ_0 time delay (that is, when $u(\tau) = \delta(\tau - \tau_0)$), all three ξ's equal 1. In this case, the moments are the same as if neutrons were detected instantly. In every other case, the ξ's differ from unity and the moments will not be the same as with instant detection. In general, one might

---

[1] In order to determine the values of the ξ factors in a given measurement setup, one needs the pulse shape $f(t)$ and delay density $u(\tau)$. While the former can easily be obtained from the inspection of the recorded pulses, the latter is difficult to measure. One can either obtain an estimate of $u(\tau)$ from simulations, or assume a concrete analytic form.

conclude that when the ξ factors are known, the detection rates can be recovered the same way as described in Section (3.2.2) for the case of instant detection – at least in principle. In order to see how much this is true in practice, let us investigate the content and the typical magnitude of the ξ's.

An inspection of the definitions (3.33) of the ξ factors as well as their positions in (3.37) reveal that they are analogous to the doubles and triples gate fraction factors (denoted as f_d and f_t) appearing in the expressions (2.21) and (2.22) of the traditional detection rates. As a matter of fact, the analogy stands from two aspects. First, just as f_d and f_t, the ξ's multiply the doubles and the triples rates but not the singles rates. As a consequence, the κ_1 mean value of a signal remained the same as in the previous section. Second, through their dependence on the delay density $u(\tau)$, the ξ's account for the temporal separation of neutrons (the fact that simultaneously emitted neutrons are detected at different times), similarly to f_d and f_t. For these reasons, we shall refer to the ξ's as *continuous gate fraction factors*, despite having no gates when analyzing continuous detector signals. There is, however, an important difference between the traditional and the continuous gate fractions: while the former were introduced empirically (see Section 2.3.4), the latter appear directly from the theory.

In order to estimate the typical values of the continuous gate fraction factors as well as their dependence on the pulse shape and the distribution of the delay, we consider simple analytic forms of $f(t)$ and $u(\tau)$. In particular, let us assume that pulses have an exponentially decaying shape with a characteristic decay time $\theta_{\text{pulse}} > 0$, that is

$$f(t) = f(t; \theta_{\text{pulse}}) = \begin{cases} \mathrm{e}^{-t/\theta_{\text{pulse}}}, & \text{for } t \geq 0 \\ 0, & \text{otherwise.} \end{cases} \tag{3.38}$$

Although real pulses rarely have this form [38], it describes one of their key properties: their "length" which, in this case, is quantified by the parameter θ_{pulse}. A larger θ_{pulse} value means a longer pulse. Let us further assume that neutrons arrive to the detector with an exponentially distributed time delay characterized by a scale parameter $\theta_{\text{delay}} > 0$ (which equals the mean as well as the standard deviation), that is

$$u(\tau) = u(\tau; \theta_{\text{delay}}) = \begin{cases} \theta_{\text{delay}}^{-1}\, \mathrm{e}^{-\tau/\theta_{\text{delay}}}, & \text{for } \tau \geq 0 \\ 0, & \text{otherwise.} \end{cases} \tag{3.39}$$

As we have noted at the beginning of this section, the exponential distribution describes the time delay in a thermal detection system very well. Although in some cases the distribution might differ from the exponential, even the above form captures the most important property of a delay distribution: its "spread" which, in this case, is quantified by the parameter θ_{delay}. A larger θ_{delay} value means a larger spread, hence a bigger difference in the arrival times of neutrons from the same emission.

By inserting (3.38) and (3.39) into the definitions (3.33) of the continuous gate fraction factors, we find that they take the following forms:

$$\xi_{1,1}(\eta) = \frac{1}{1+\eta}, \quad \xi_{1,2}(\eta) = \frac{2+3\eta}{2+6\eta+4\eta^2}, \quad \xi_{1,1,1}(\eta) = \frac{2}{2+5\eta+2\eta^2}, \tag{3.40a}$$

where $\eta = \theta_{\text{delay}}/\theta_{\text{pulse}}$ is the fraction of the delay spread and the pulse length. Recalling the physical meaning of θ_{pulse} and θ_{delay}, it is clear that η is a measure of the pulse

dispersion, that is, how little pulses from the same emission overlap in time. When η is close the zero, the spread of the delay is small compared to the pulse length, hence pulses overlap largely (small dispersion). As η increases, the spread of the delay becomes larger compared to the pulse size, hence pulses tend to overlap less frequently (large dispersion). For this reason, we shall refer to η as the *pulse dispersion factor*. It is important to emphasize that the value of the pulse dispersion is not a matter of the delay spread alone: rather it is a matter of how the delay spread compares to the pulse length.

To make the analysis easier, functions (3.40) are plotted on Figure 3.2. One can observe that all three gate fraction factors are quick monotonically decreasing functions of the dispersion factor η. What is more, the higher the order of the gate fraction (for example, $\xi_{2,1}$ has a higher order than $\xi_{1,1}$), the quicker it decays. When the dispersion is small, the values of all three gate fractions are close to 1. In this case, the doubles and the triples rates in the moment expressions (3.37) have approximately the same weight as the singles rate. As a consequence, all three detection rates can be recovered from the measured one-point moments of the signals. On the other hand, even at a moderately large values of the dispersion factor, the values of the gate fractions approach zero. In this case, the doubles and the triples rates in the moment expressions (3.37) appear with a negligible weight compared to the singles rate. As a consequence, the moments will contain information only on the singles rates; the doubles and the triples rates cannot be recovered.
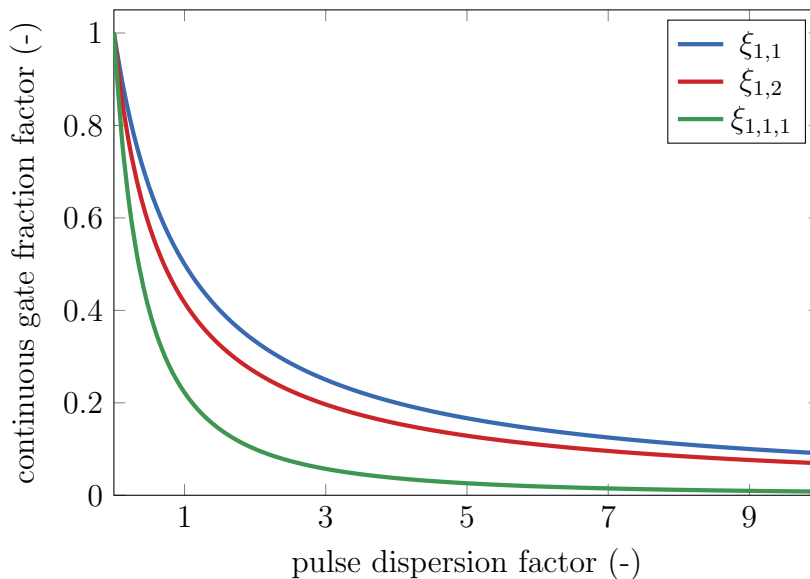
Figure 3.2: The value of the gate fractions (3.33) as a function of the pulse dispersion factor $\eta = \theta_{\text{delay}}/\theta_{\text{pulse}}$ assuming an exponential pulse shape with decay time θ_{pulse} and an exponentially distributed time delay with scale parameter θ_{delay}.

These last findings have a rather illustrative explanation. Recall that the quantification of coincident detection events (measured by the doubles and triples rates) with the analysis of continuous detector signals is based on identifying the correlated changes they make to the values of the signals. This changes are well captured by the one-point moments, when the pulse dispersion is small and pulses induced by correlated

detections overlap in time. However, when the pulse dispersion is large, pulses from correlated detections contribute to the signal at different times, hence their joint effect does not appear in the moments.

To conclude, estimation of the detection rates using the one-point moments of continuous detector signals is feasible only when the observed pulse dispersion is small. The questions is, what this means in practice. The typical length of fission chamber pulses is in the range of $10\,\text{ns}$–$10\,\mu\text{s}$ [38]. In a fast measurement configuration, the time delay is on the order of $10\,\text{ns}$–$100\,\text{ns}$ (see Chapter B). In such circumstances the values of the gate fraction factors might be large enough to allow to recover the detections rates from the signal moments. In a thermal configuration, however, the time delay is usually in the order of $1\,\mu\text{s}$–$100\,\text{ms}$ [1]. In this case, the values of the gate fraction factors are expected to be negligible. This suggests that in the most frequently used thermal systems the doubles and the triples detection rates cannot be recovered from the one-point moments of continuous detector signals.

3.4   Two- and three-point moments with delayed detection

In order to retrieve all three detection rates from the continuous detector signals even with the large delay times encountered in thermal detection systems, one must find a way to quantify the correlations between distant points of the signal. This can be achieved with the use of the multipoint moments of the signal, which characterize its distribution at more than one point in time. In particular, we shall consider at most three points in time: besides time t, a second time instant $t - \theta$ is chosen to describe the so-called *two-point distribution*s, whereas an additional third time instant $t - \theta - \rho$ is selected for the *three-point distribution*s (see Figure 3.1). In the following we shall assume that θ and ρ are both non-negative, that is, $\theta, \rho \geq 0$.

As in the case of the one-point distributions, we can choose from an infinite number of two- and three-point distributions as well. However, for the same reason as before, we will be interested only in moments up to the order of three. In fact, it is reasonable to examine the two- and three-point analogies of the one-point moments given in Equations (3.1)–(3.3). Regarding the signal of one detector, say $\boldsymbol{y}_1(t)$, we shall consider its (stationary) *auto-covariance function* and *auto-bicovariance function*, defined as

$$\text{Cov}_2(\theta) = \lim_{t \to \infty} \mathbb{E}\left\{ [\boldsymbol{y}_1(t) - \langle \boldsymbol{y}_1 \rangle] [\boldsymbol{y}_1(t - \theta) - \langle \boldsymbol{y}_1 \rangle] \right\}, \tag{3.41a}$$

$$\text{Cov}_3(\theta, \rho) = \lim_{t \to \infty} \mathbb{E}\left\{ [\boldsymbol{y}_1(t) - \langle \boldsymbol{y}_1 \rangle] [\boldsymbol{y}_1(t - \theta) - \langle \boldsymbol{y}_1 \rangle] [\boldsymbol{y}_1(t - \theta - \rho) - \langle \boldsymbol{y}_1 \rangle] \right\}. \tag{3.41b}$$

Note that these moments are generalizations of the variance and skewness in (3.1): for $\theta = \rho = 0$, when the distinct time instants coincide, they become identical. Regarding the signals of two detectors, say $\boldsymbol{y}_1(t)$ and $\boldsymbol{y}_2(t)$, we shall consider their (stationary) *cross-covariance function*

$$\text{Cov}_{1,1}(\theta) = \lim_{t \to \infty} \mathbb{E}\left\{ [\boldsymbol{y}_1(t) - \langle \boldsymbol{y}_1 \rangle] [\boldsymbol{y}_2(t - \theta) - \langle \boldsymbol{y}_2 \rangle] \right\}, \tag{3.42}$$

which is the generalization of the covariance in (3.2); note that we are not considering the generalized version of the unnamed moment $\kappa_{2,1}$. Finally, regarding the signal

of three detectors, $\boldsymbol{y}_1(t)$, $\boldsymbol{y}_2(t)$ and $\boldsymbol{y}_3(t)$, we shall consider the (statioanry) *cross-bicovariance function*

$$\mathrm{Cov}_{1,1,1}(\theta, \rho) = \lim_{t \to \infty} \mathbb{E}\left\{[\boldsymbol{y}_1(t) - \langle \boldsymbol{y}_1 \rangle][\boldsymbol{y}_2(t - \theta) - \langle \boldsymbol{y}_2 \rangle][\boldsymbol{y}_3(t - \theta - \rho) - \langle \boldsymbol{y}_3 \rangle]\right\}, \quad (3.43)$$

the generalization of the cross-bicovariance in (3.3).

The above moments are able to quantify the correlations between pulses at specific distances in time. In multiplicity counting, however, we are interested only in the total amount of the correlations regardless of their distance. For this reason, it is not the moments themselves we shall use for recovering the detection rates, rather their integrals with respect to their arguments. That is, our aim is to determine the following quantities:

$$\mathrm{Cov}_2 = \int_0^\infty \mathrm{Cov}_2(\theta)\, \mathrm{d}\theta \qquad \mathrm{Cov}_{1,1} = \int_0^\infty \mathrm{Cov}_{1,1}(\theta)\, \mathrm{d}\theta, \qquad (3.44)$$

and

$$\mathrm{Cov}_3 = \int_0^\infty \int_0^\infty \mathrm{Cov}_3(\theta, \rho)\, \mathrm{d}\rho \mathrm{d}\theta \qquad \mathrm{Cov}_{1,1,1} = \int_0^\infty \int_0^\infty \mathrm{Cov}_{1,1,1}(\theta, \rho)\, \mathrm{d}\rho \mathrm{d}\theta. \qquad (3.45)$$

Continuing the practice of earlier sections, we divide the rest of this section into two parts. In Section 3.4.1, expressions are derived for the moments (3.41)–(3.43) and their respective integrals are calculated. Then in Section 3.4.2, we provide a comprehensive interpretation of the results.

3.4.1 Derivation of the moment expressions

Before turning to the calculation of the moments, we begin by characterizing the two- and three point distribution of a single pulse.

Two- and three-point distributions of a single pulse

Consider a neutron emitted at time $t = 0$, which is detected after a time delay $\boldsymbol{\tau}$ distributed according the density function $u(\tau)$. As before, this detection induces a pulse $\boldsymbol{x}(t) = \boldsymbol{a}\, f(t - \boldsymbol{\tau})$ with respect to the time of emission, where $f(t)$ is a fixed shape and $\boldsymbol{a}$ is a random amplitude with a density function $w(a)$.

The two-point distribution of the pulse is characterized by the two-point cumulative distribution function $H_2(x_1, x_2, t, \theta)$, which equals the probability that the observed value of the pulse does not exceed x_1 at time t, whereas it does not exceed x_2 at time $t - \theta$. In an analogy with the one-point distribution function H_1 in (3.28), H_2 can be written as

$$H_2(x_1, x_2, t, \theta) = \int_0^\infty \int_0^\infty \Delta[x_1 - af(t - \tau)]\, \Delta[x_2 - af(t - \tau - \theta)]\, w(a)\, u(\tau)\, \mathrm{d}a \mathrm{d}\tau,$$

where the Heaviside step function Δ was defined in Equation (3.5). As in the one-point case, the expressions of the two point versions of the density function, the characteristic

function as well as the raw moment can be calculated from H_2. In particular, the two-point density function is defined as the derivative of H_2 with respect to x_1 and x_2 and takes the form

$$h_2(x_1, x_2, t, \theta) = \frac{\partial^2 H_2(x_1, x_2, t, \theta)}{\partial x_1 \, \partial x_2} = \int_0^\infty \int_0^\infty \delta[x_1 - af(t - \tau)]$$
$$\times \, \delta[x_2 - af(t - \tau - \theta)] \, w(a) \, u(\tau) \, \mathrm{d}a \mathrm{d}\tau.$$

(3.46)

The two-point characteristic function is defined as the two-dimensional Fourier transform of the two-point density function with respect to x_1 and x_2:

$$\chi_2(\omega_1, \omega_2, t, \theta) = \int_{-\infty}^\infty \int_{-\infty}^\infty e^{\imath(\omega_1 x_1 + \omega_2 x_2)} \, h_2(x_1, x_2, t, \theta) \, \mathrm{d}x_1 \mathrm{d}x_2$$
$$= \int_0^\infty \int_0^\infty e^{\imath \omega_1 af(t-\tau)} \, e^{\imath \omega_2 af(t-\tau-\theta)} \, w(a) \, u(\tau) \, \mathrm{d}a \mathrm{d}\tau.$$

(3.47)

The two-point raw moment of order (m, n) is obtained from the two-point characteristic function as:

$$\mu_{m,n}(t, \theta) = \imath^{-(m+n)} \left. \frac{\partial^{(m+n)} \chi_2(\omega_1, \omega_2, t, \theta)}{\partial \omega_1^m \, \partial \omega_2^n} \right|_{\omega_1 = \omega_2 = 0}$$
$$= \langle a^{(m+n)} \rangle \int_0^\infty f^m(t - \tau) \, f^n(t - \tau - \theta) \, u(\tau) \, \mathrm{d}\tau.$$

(3.48)

In a completely analogous way, we can introduce the corresponding three-point characteristics of the pulse. Without any further commentary, they take the forms:

$$H_3(x_1, x_2, x_3, t, \theta, \rho) = \int_0^\infty \int_0^\infty \Delta[x_1 - af(t - \tau)] \, \Delta[x_2 - af(t - \tau - \theta)]$$
$$\times \Delta[x_3 - af(t - \tau - \theta - \rho)] \, w(a) \, u(\tau) \, \mathrm{d}a \mathrm{d}\tau,$$

$$h_3(x_1, x_2, x_3, t, \theta, \rho) = \frac{\partial^3 H_3(x_1, x_2, x_3, t, \theta, \rho)}{\partial x_1 \, \partial x_2 \, \partial x_3}$$
$$= \int_0^\infty \int_0^\infty \delta[x_1 - af(t - \tau)] \, \delta[x_2 - af(t - \tau - \theta)]$$
$$\times \delta[x_3 - af(t - \tau - \theta - \rho)] \, w(a) \, u(\tau) \, \mathrm{d}a \mathrm{d}\tau,$$

(3.49)

$$\chi_3(\omega_1, \omega_2, \omega_3, t, \theta, \rho) = \int_{-\infty}^\infty \int_{-\infty}^\infty \int_{-\infty}^\infty e^{\imath(\omega_1 x_1 + \omega_2 x_2 + \omega_3 x_3)}$$
$$\times h_3(x_1, x_2, x_3, t, \theta, \rho) \, \mathrm{d}x_1 \mathrm{d}x_2 \mathrm{d}x_3$$
$$= \int_0^\infty \int_0^\infty e^{\imath \omega_1 af(t-\tau)} \, e^{\imath \omega_2 af(t-\theta-\tau)}$$
$$\times e^{\imath \omega_3 af(t-\theta-\rho-\tau)} \, w(a) \, u(\tau) \, \mathrm{d}a \, \mathrm{d}\tau$$

(3.50)

and

$$\mu_{k,m,n}(t, \theta, \rho) = \imath^{-(k+m+n)} \left. \frac{\partial^{(k+m+n)} \chi_3(\omega_1, \omega_2, \omega_3, t, \theta, \rho)}{\partial \omega_1^k \, \partial \omega_2^m \, \partial \omega_3^n} \right|_{\omega_1 = \omega_2 = \omega_3 = 0}$$
$$= \langle a^{(k+m+n)} \rangle \int_0^\infty f^k(t - \tau) \, f^m(t - \tau - \theta)$$
$$\times f^n(t - \tau - \theta - \rho) \, u(\tau) \, \mathrm{d}\tau.$$

(3.51)

Two-point distribution of one detector signal

The two-point distribution of the signal of one detector, say that labeled with 1, concerns the random variable $\{\boldsymbol{y}_1(t), \boldsymbol{y}_1(t-\theta)\}$, which is characterized by the cumulative distribution function

$$F_2(y_1, y_2, t, \theta) = \mathbb{P}\left[\boldsymbol{y}_1(t) \le y_1, \boldsymbol{y}_1(t - \theta) \le y_2\right].$$

The calculation of the two-point moments of the detector signal follows the same four steps as the calculation of the one-point moments discussed in Sections 3.2: starting from a Kolmogorov backward integral equation for the density function we arrive to an expression of the stationary cumulant-generating function from which the desired moments can be obtained by differentiation. Again, the details of the derivation can be found in the Appendix in Section A.3.1.

After lengthy calculations, the following expression is obtained for the auto-covariance function $\text{Cov}_2(\theta)$ of the signal:

$$\text{Cov}_2(\theta) = S \int_\theta^\infty \mu_{1,1}(t, \theta)\, \mathrm{d}t + 2\,D \int_\theta^\infty \mu_1(t)\, \mu_1(t - \theta)\, \mathrm{d}t. \tag{3.52}$$

Here, μ_1 denotes the same one-point moment of the pulse, which appeared in the earlier derivations and which was given in (3.31); $\mu_{1,1}$ is the newly introduced two point moment, given by (3.48). The physical content of the above equation can be stated as follows: the first term corresponds to the $\mu_{1,1}$ "auto-covariance function" of one pulse (single), whereas the second term describes the $\mu_1\,\mu_1$ "cross-covariance function" of two distinct pulses (doubles).

As noted earlier, we are mostly interested in the integral Cov_2 of the auto-covariance function, as defined in (3.44). By substituting the explicit forms of μ_1 and $\mu_{1,1}$ into (3.52) and performing the necessary simplifications, we obtain

$$\text{Cov}_2 = \frac{1}{2}\left[S\,\langle a^2\rangle + 2\,D\,\langle a\rangle^2\right]\,I_1^2, \tag{3.53}$$

where I_1 is the same as (3.21).

Two-point distribution of two detector signals

The two-point distribution of the signal of two detectors, say those labeled with 1 and 2, concerns the random variable $\{\boldsymbol{y}_1(t), \boldsymbol{y}_2(t - \theta)\}$, which is characterized by the cumulative distribution function

$$F_{1,1}(y_1, y_2, t, \theta) = \mathbb{P}\left[\boldsymbol{y}_1(t) \le y_1, \boldsymbol{y}_2(t - \theta) \le y_2\right].$$

After the derivation, described in Section A.3.2, the following expression is obtained for the cross-covariance function $\text{Cov}_{1,1}(\theta)$, defined in (3.42):

$$\text{Cov}_{1,1}(\theta) = 2\,D \int_\theta^\infty \mu_1(t)\, \mu_1(t - \theta)\, \mathrm{d}t,$$

where μ_1 is the one-point moment of the pulse and was given in (3.31). The interpretation of this equation is analogous to that of (3.52): its only term corresponds to the

$\mu_1 \mu_1$ "cross-covariance function" of two distinct pulses (doubles) each from a different detector. The integral of this moment, as defined by (3.44), takes the form

$$\text{Cov}_{1,1} = D \langle a \rangle^2 I_1^2, \tag{3.54}$$

where I_1 is the same as (3.21).

Three-point distribution of one detector signal

The three-point distribution of the signal of one detector, say that labeled with 1, concerns the random variable $\{\boldsymbol{y}_1(t), \boldsymbol{y}_1(t - \theta)\}, \boldsymbol{y}_1(t - \theta - \rho)\}$, which is characterized by the cumulative distribution function

$$F_3(y_1, y_2, y_3, t, \theta, \rho) = \mathbb{P}\left[\boldsymbol{y}_1(t) \leq y_1, \boldsymbol{y}_1(t - \theta) \leq y_2, \boldsymbol{y}_1(t - \theta - \rho) \leq y_3\right].$$

After the derivations described in Section A.3.3, the following expression is obtained for the auto-bicovariance function $\text{Cov}_3(\theta, \rho)$, defined in (3.41b):

$$\begin{aligned}
\text{Cov}_3(\theta, \rho) = {}& S \int_{\theta+\rho}^{\infty} \mu_{1,1,1}(t, \theta, \rho) \, \mathrm{d}t \\
& + 2\, D \int_{\theta+\rho}^{\infty} [\mu_1(t)\, \mu_{1,1}(t, \rho) \\
& + \mu_1(t - \theta)\, \mu_{1,1}(t, \theta + \rho) + \mu_1(t - \theta - \rho)\, \mu_{1,1}(t, \theta)] \, \mathrm{d}t \\
& + 6\, T \int_{\theta+\rho}^{\infty} \mu_1(t)\, \mu_1(t - \theta)\, \mu_1(t - \theta - \rho) \, \mathrm{d}t,
\end{aligned}$$

where μ_1, $\mu_{1,1}$ and $\mu_{1,1,1}$ are the moments of the pulse and were defined in (3.31), (3.48) and (3.51), respectively. The auto-bicovariance function of the signal has three components: the "auto-bicovariance function" $\mu_{1,1,1}$ of one pulse (single), the "cross-bicovariance function" $\mu_1 \mu_{1,1}$ of two distinct pulses (doubles) and the "cross-bicovariance function" $\mu_1 \mu_1 \mu_1$ of three distinct pulses (triples).

The integral Cov_3 of the above auto-bicovariance function, as defined in (3.45), takes the form

$$\text{Cov}_3 = \frac{1}{6} \left[S \langle a^3 \rangle + 2\, D \langle a \rangle \langle a^2 \rangle (\xi_A + \xi_B + \xi_C) + 6\, T \langle a \rangle^3 \right] I_1^3, \tag{3.55}$$

where

$$\xi_A = \frac{6}{I_1^3} \int_0^{\infty} \int_0^{\infty} \int_0^{\infty} I_1(t)\, I_{1,1}(t - \theta, t - \theta - \rho) \, \mathrm{d}t\mathrm{d}\theta\mathrm{d}\rho, \tag{3.56a}$$

$$\xi_B = \frac{6}{I_1^3} \int_0^{\infty} \int_0^{\infty} \int_0^{\infty} I_1(t - \theta)\, I_{1,1}(t, t - \theta - \rho) \, \mathrm{d}t\mathrm{d}\theta\mathrm{d}\rho, \tag{3.56b}$$

$$\xi_C = \frac{6}{I_1^3} \int_0^{\infty} \int_0^{\infty} \int_0^{\infty} I_1(t - \theta - \rho)\, I_{1,1}(t, t - \theta) \, \mathrm{d}t\mathrm{d}\theta\mathrm{d}\rho. \tag{3.56c}$$

Here I_1 and $I_1(t)$ are the same as in (3.21) and (3.34), respectively, whereas $I_{m,n}(t, s)$ is defined as

$$I_{m,n}(t, s) = \int_0^{\infty} f^m(t - \tau)\, f^n(s - \tau)\, u(\tau) \, \mathrm{d}\tau. \tag{3.57}$$

Three-point distribution of three detector signals

The three-point distribution of the signal of three detectors, those labeled with 1, 2 and 3, concerns the random variable $\{\boldsymbol{y}_1(t), \boldsymbol{y}_2(t - \theta)\}, \boldsymbol{y}_3(t - \theta - \rho)\}$, which is characterized by the cumulative distribution function

$$F_{1,1,1}(y_1, y_2, y_3, t, \theta, \rho) = \mathbb{P}\left[\boldsymbol{y}_1(t) \le y_1, \boldsymbol{y}_2(t - \theta) \le y_2, \boldsymbol{y}_3(t - \theta - \rho) \le y_3\right].$$

The cross-bicovariance function of three signals, defined in (3.43), takes the form

$$\mathrm{Cov}_{1,1,1}(\theta, \rho) = 6\,T \int_{\theta+\rho}^{\infty} \mu_1(t)\,\mu_1(t - \theta)\,\mu_1(t - \theta - \rho)\,\mathrm{d}t.$$

The integral $\mathrm{Cov}_{1,1,1}$ of this function, defined in (3.45), reads as

$$\mathrm{Cov}_{1,1,1} = T\,\langle a \rangle^3\,I_1^3. \tag{3.58}$$

3.4.2 Interpretation of the results

As in the two preceding sections, we collect the expressions of all the two- and three-point moments in order to give a comprehensive overview of them. For the integrals of the auto-covariance function and the auto-bicovariance function of one detector signal we obtained

$$\mathrm{Cov}_2 = \frac{1}{2}\left[S\,\langle a^2 \rangle + 2\,D\,\langle a \rangle^2\right] I_1^2, \tag{3.59a}$$

$$\mathrm{Cov}_3 = \frac{1}{6}\left[S\,\langle a^3 \rangle + 2\,D\,\langle a \rangle \langle a^2 \rangle\,(\xi_A + \xi_B + \xi_C) + 6\,T\,\langle a \rangle^3\right] I_1^3, \tag{3.59b}$$

The integral of the cross-covariance function of two detector signals reads as

$$\mathrm{Cov}_{1,1} = D\,\langle a \rangle^2\,I_1^2. \tag{3.59c}$$

Finally, the integral of the cross-bicovariance function of three detector signals took the form

$$\mathrm{Cov}_{1,1,1} = T\,\langle a \rangle^3\,I_1^3. \tag{3.59d}$$

The quantities $\langle a^n \rangle$ and I_n are the same as in the case of instant detection, and were defined in (3.9) and (3.21), respectively. The ξ's were defined in (3.56).

Let us compare the two- and three point moments in (3.59) with their one-point versions (3.37) obtained by assuming a delayed detections. The most apparent difference is that, except for Cov_3, none of the two- or three point moments contain continuous gate fractions. To investigate the characteristics of the gate fractions appearing in the second term of Cov_3, the same analytical form of the pulse shape and the delay density are assumed as in Section 3.3.2 for the gate fractions of the one-point moments. This gives the results

$$\xi_A(\eta) = \frac{2 + 18\eta + 58\eta^2 + 63\eta^3 + 18\eta^4}{6 + 36\eta + 78\eta^2 + 72\eta^3 + 24\eta^4}, \tag{3.60a}$$

$$\xi_B(\eta) = \frac{1 + 3\eta + 3\eta^2}{1 + 3\eta + 2\eta^2}, \tag{3.60b}$$

$$\xi_C(\eta) = \frac{1 + 3\eta}{1 + 3\eta + 2\eta^2}, \tag{3.60c}$$

where $\eta = \theta_{\text{delay}}/\theta_{\text{pulse}}$ is, again, the pulse dispersion factor. Inspecting the plotted values of these gate factors on Figure 3.3, one can observe that their sum converges asymptotically to a value near 3 and, in general, changes slowly with the pulse dispersion factor η. This last property makes it possible to estimate the value of $\xi_A + \xi_B + \xi_C$ in a measurement with a relatively good accuracy.
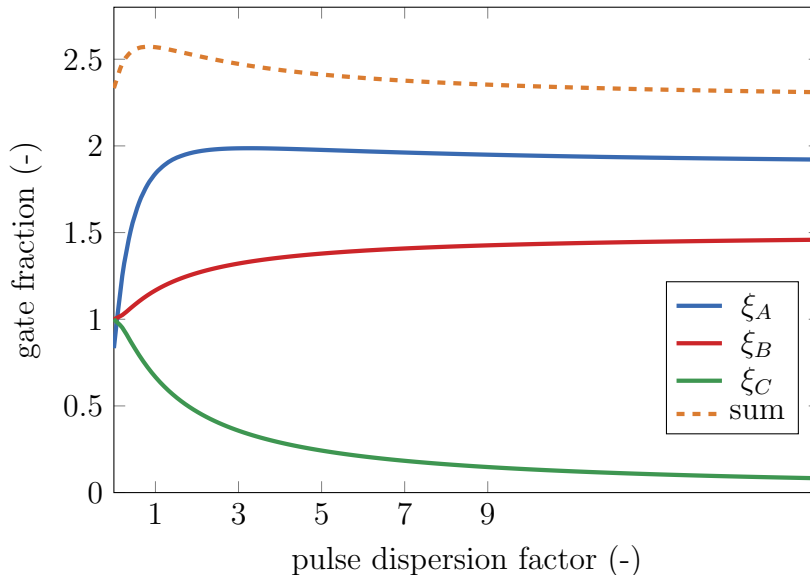
Figure 3.3: The value of the gate fractions (3.56) as a function of the pulse dispersion factor $\eta = \theta_{\text{delay}}/\theta_{\text{pulse}}$ assuming an exponential pulse shape with decay time θ_{pulse} and an exponentially distributed time delay with scale parameter θ_{delay}.

The above results show that the values of the integrals of the two- and three point moments is independent – or, in one case, depends weakly – of the time delay density. As a consequence, the singles, doubles and triples detection rates can be recovered from them even in a thermal system. In this sense, they show a close similarity to the one-point moments (3.27) obtained by assuming instant detection. This finding has a very illustrative explanation. The integral operations performed on the two- and three point moments essentially shift the pulses in time which, at some point, become fully overlapped. In a formal sense, this operation restores the original idealistic assumption of an instant detection.

3.5 Recovering the detection rates from the moments of signals

In the proceeding sections, expressions have been derived for several moments of the continuous signals. The moments concerned the signals of up to three detectors at a time, and the derivations were performed by assuming, that the detectors are identical, that is, they were characterized by the same detection efficiency, pulse shape and pulse amplitude distribution. The moments have been expressed with the traditional detection rates and a careful investigation showed that some of them are particularly useful

for recovering the detection rates in both fast and thermal detection systems. They are listed in Table 3.1 along with the detection rates they contain information on.

Table 3.1: The list of moments that can be used to recover the traditional detection rates.

description	symbol	detection rate
mean value of one signal	κ_1	S
integral of the auto covariance function of one signal	Cov_2	S, D
integral of the cross covariance function of two signals	$\text{Cov}_{1,1}$	D
integral of the auto bicovariance function of one signal	Cov_3	S, D, T
integral of the cross bicovariance function of two signals	$\text{Cov}_{1,1,1}$	T

In the following, we consider a measurement performed with $N \geq 3$ fission chambers. Moreover, we shall no longer assume that the detectors are identical. The ith detector will be characterized by a detection efficiency ε_i, by a mean amplitude $\langle a \rangle_i$ as well as by the area I_i under the pulse amplitude. The detection efficiency of the system is

$$\varepsilon = \sum_{i=1}^{N} \varepsilon_i. \tag{3.61}$$

We shall provide expressions for the singles, doubles and triples detection rates in terms of the moments obtained from all relevant combinations of the detector signals. For this purpose, the following moments will be used only:

- the mean value of the signal of detector i, denoted by κ_i and given by the expression

$$\kappa_i = Q \, \nu_1 \, \varepsilon_i \, \langle a \rangle_i \, I_i. \tag{3.62}$$

- the integral of the covariance function of the signals of detector i and j ($i \neq j$), denoted by $\text{Cov}_{i,j}$ and given by the expression:

$$\text{Cov}_{i,j} = \frac{Q \, \nu_2}{2} \, \varepsilon_i \, \varepsilon_j \, \langle a \rangle_i \, \langle a \rangle_j \, I_i \, I_j. \tag{3.63}$$

- the integral of the bicovariance function of the signals of detectors i, j and j ($i \neq j \neq k$), denoted by $\text{Cov}_{i,j,k}$ and given by the expression:

$$\text{Cov}_{i,j,k} = \frac{Q \, \nu_3}{6} \, \varepsilon_i \, \varepsilon_j \, \varepsilon_k \, \langle a \rangle_i \, \langle a \rangle_j \, \langle a \rangle_k \, I_i \, I_j \, I_k. \tag{3.64}$$

3.5.1 Recovering the singles rate

Inserting (3.61) into its definition in (2.21), the singles rate measured in the system can be written as

$$S = Q_s \, \nu_1 \sum_{i=1}^{N} \varepsilon_i = \sum_{i=1}^{N} S_i \tag{3.65}$$

where

$$S_i = Q_s \, \nu_1 \, \varepsilon_i. \tag{3.66}$$

One can see that the total singles rate S is the sum of singles rates S_i measured by the individual detectors. Notice that S_i can be expressed with κ_i as

$$S_i = \frac{\kappa_i}{\langle a \rangle_i \, I_i}. \tag{3.67}$$

As a result, the singles rates can be obtained from the mean values of the signals in the following way:

$$S = \sum_{i=1}^{N} \frac{1}{\langle a \rangle_i \, I_i} \kappa_i. \tag{3.68}$$

3.5.2 Recovering the doubles rate

Inserting (3.61) into its definition in (2.21), the doubles rate measured in the system can be written as

$$D = Q_s \frac{\nu_2}{2} \left(\sum_{i=1}^{N} \varepsilon_i \right)^2 = \sum_{i=1}^{N} D_i + 2 \sum_{i=1}^{N} \sum_{j=i+1}^{N} D_{i,j}. \tag{3.69}$$

where

$$D_i = \frac{Q_s \, \nu_2}{2} \varepsilon_i^2 \qquad\qquad D_{i,j} = \frac{Q_s \, \nu_2}{2} \, \varepsilon_i \, \varepsilon_j. \tag{3.70}$$

One can see that the total doubles rate comes from the doubles rate D_i observed in the individual detectors and the doubles rate $D_{i,j}$ observed in pairs of detectors. Notice that $D_{i,j}$ can be expressed with $\mathrm{Cov}_{i,j}$ as

$$D_{i,j} = \frac{1}{\langle a \rangle_i \, \langle a \rangle_j \, I_i \, I_j} \, \mathrm{Cov}_{i,j}. \tag{3.71}$$

Further note that D_i can be expressed $\mathrm{Cov}_{i,j}$ for all $j \neq i$ as

$$D_i = \frac{1}{\langle a \rangle_i^2 \, I_i^2} \frac{\kappa_i}{\kappa_j} \, \mathrm{Cov}_{i,j} \qquad \forall \, j \neq i, \tag{3.72}$$

or, when taking an average over all j:

$$D_i = \frac{\kappa_i}{\langle a \rangle_i^2 \, I_i^2} \frac{1}{N-1} \sum_{\substack{j=1 \\ j \neq i}}^{N} \frac{1}{\kappa_j} \, \mathrm{Cov}_{i,j}. \tag{3.73}$$

The total doubles rate can then be written as:

$$D = \sum_{i=1}^{N} \frac{\kappa_i}{\langle a \rangle_i^2 \, I_i^2} \left(\frac{1}{N-1} \sum_{\substack{j=1 \\ j \neq i}}^{N} \frac{1}{\kappa_j} \, \mathrm{Cov}_{i,j}. \right) + 2 \sum_{i=1}^{N} \sum_{j=i+1}^{N} \frac{1}{\langle a \rangle_i \, \langle a \rangle_j \, I_i \, I_j} \, \mathrm{Cov}_{i,j}. \tag{3.74}$$

3.5.3   Recovering the triples rate

Inserting (3.61) into its definition in (2.21), the doubles rate measured in the system can be written as

$$T = Q_s \frac{\nu_3}{6} \left(\sum_{i=1}^{N} \varepsilon_i \right)^3 = \sum_{i=1}^{N} T_i + 3 \sum_{i=1}^{N} \sum_{j=1, j\neq i}^{N} T_{i,j} + 6 \sum_{i=1}^{N} \sum_{j=i+1}^{N} \sum_{k=j+1}^{N} T_{i,j,k}. \qquad (3.75)$$

where

$$T_i = \frac{Q_s\,\nu_3}{6}\,\varepsilon_i^3 \qquad T_{i,j} = \frac{Q_s\,\nu_3}{6}\varepsilon_i^2\,\varepsilon_j \qquad T_{i,j,k} = \frac{Q_s\,\nu_3}{6}\,\varepsilon_i\,\varepsilon_j\,\varepsilon_k. \qquad (3.76)$$

One can see that the total triples rate comes from triples rates observed in one detector, two detectors or three detectors. In a similar was than before, one can show that the following expressions hold:

$$T_{i,j,k} = \frac{1}{\langle a \rangle_i \, \langle a \rangle_j \, \langle a \rangle_k \, I_i \, I_j \, I_k} \, \text{Cov}_{i,j,k}. \qquad (3.77)$$

$$T_{i,j} = \frac{\kappa_i}{\langle a \rangle_i^2 \, I_i^2 \, \langle a \rangle_j \, I_j} \frac{1}{N-2} \sum_{\substack{k=1 \\ k \neq i \neq j}}^{N} \frac{1}{\kappa_k} \, \text{Cov}_{i,j,k} \qquad (3.78)$$

and

$$T_i = \frac{\kappa_i^2}{\langle a \rangle_i^3 \, I_i^3} \frac{1}{(N-1)\,(N-2)} \sum_{\substack{j=1 \\ j \neq k \neq i}}^{N} \sum_{k=1}^{N} \frac{1}{\kappa_j\,\kappa_k} \, \text{Cov}_{i,j,k}. \qquad (3.79)$$

As a result, the total triples rates can be written as:

$$
\begin{aligned}
T = \sum_{i=1}^{N} \frac{\kappa_i^2}{\langle a \rangle_i^3 \, I_i^3} & \left(\frac{1}{(N-1)\,(N-2)} \sum_{\substack{j=1 \\ j \neq k \neq i}}^{N} \sum_{k=1}^{N} \frac{1}{\kappa_j \kappa_k} \, \text{Cov}_{i,j,k} \right) \\
+ 3 \sum_{i=1}^{N} \sum_{j=1, j\neq i}^{N} \frac{\kappa_i}{\langle a \rangle_i^2 \, I_i^2 \, \langle a \rangle_j \, I_j} & \left(\frac{1}{N-2} \sum_{\substack{k=1 \\ k \neq i \neq j}}^{N} \frac{1}{\kappa_k} \, \text{Cov}_{i,j,k} \right) \\
+ 6 \sum_{i=1}^{N} \sum_{j=i+1}^{N} \sum_{k=j+1}^{N} & \frac{1}{\langle a \rangle_i \, \langle a \rangle_j \, \langle a \rangle_k \, I_i \, I_j \, I_k} \, \text{Cov}_{i,j,k}.
\end{aligned}
\qquad (3.80)
$$

Chapter 4

Computational investigations and analysis methods

In Chapter 3, the theory of an alternative version of neutron multiplicity counting has been laid down, which permits the extraction of the singles, doubles and triples rates from appropriately chosen moments of continuous detector signals. Many important characteristics of the method have been revealed and discussed on an analytical basis. However, certain phenomena that might affect the practical use of the method were not addressed in the preceding chapter. Among others, these include: the time resolution by which the signal is recorded, the duration of the measurement, the actual shape of the pulse, the distribution of the pulse amplitude, the distribution of the time delay (in spite of not appearing explicitly in the final formulas), the presence of electronic noise in the signal as well as the presence of non-neutron sources (alpha or gamma background).

Some of these phenomena could have been investigated within the framework of the theory. For example, when deriving the high-order Campbell formulae, Lux and Baranyai have included non-neutron signal components into their model [67]; nevertheless, they were entirely omitted from the model presented in Chapter 3. In certain cases, however, the analytical treatment is either not possible or can only be made at the cost of severe simplifications. One possibility to overcome these limitations is to perform a computational study on simulated measurement data. With the use of simulations, even very complex phenomena can easily be accounted for in the detector signals in a controllable way. Then by analyzing the simulated signals as if they were measured, conclusions can be drawn on the impact of various phenomena on the practical use of the newly proposed method. The description and analysis of such a computational investigation is the topic of this chapter.

4.1 Computational tools

This section describes the programs that were used in the computational study presented in later parts of this Chapter. First the data structures used to store detector signals are introduced in Section 4.1.1. Then a program for simulating detector signals in a multiplicity counting measurement is described in Section 4.1.2. Finally, in Section 4.1.3, a tool that can be used to analyze detector signals (simulated and measured

ones as well) and estimating their moments is presented.

4.1.1 The file representation of signals

From a data representation point of view, there are two forms of a signal recorded by the data acquisition system connected to a neutron detector. The form in use is normally determined by the operation mode of the acquisition system. In campbelling mode the amplitude of the voltage signal is sampled with some time resolution Δt; this produces a data sequence $y_1, y_2, \ldots$, where y_i represents the observed amplitude at time $i \Delta t$. In pulse counting mode the times of individual detections – more precisely, the times when the voltage signal crosses a predefined threshold value – are determined; this produces a data sequence $t_1, t_2, \ldots$, where t_i represents the time of the ith detection.

In order to store detector signals (whether they are simulated or measured) of any of these two forms on a computer, two file formats have been defined: the `time resolved signal format` encodes a signal recorded in campbelling mode as a sequence of amplitudes; the `time stamped signal format` is a container for a signal recorded in pulse counting mode as sequence of detection times.

Figure 4.1: The structure of the `time stamped signal format`.

These formats are used by all the programs presented in this chapter and by the data acquisition used in the experiments described in Chapter 5.
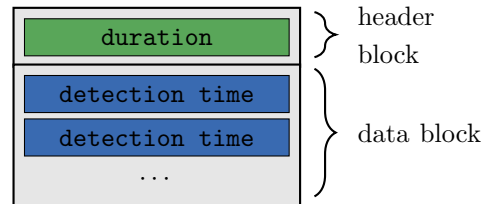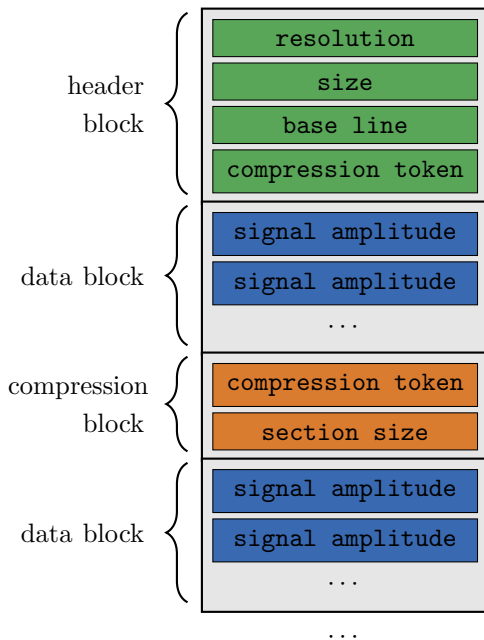
Figure 4.2: The structure of the `time resolved signal format`.

The structure of the file formats is shown on Figures 4.1 and 4.2. Both files start with a header block containing metadata used by the programs that operate on them. The header block is then followed by one or more types of data blocks which encode the actual recorded data sequence.

As it is seen from Figure 4.1, the structure of the `time stamped signal format` is extremely simple. Its header block contains one item, `duration`, which holds the total length of the signal in time. This is followed by a single data block, which contains an arbitrary number of `detection time` items, each holding the time of a detection.

The `time resolved signal format` has a slightly more complex structure, as seen from Figure 4.2. Its header block contains four items: `resolution` holds the time resolution used to sample the signal; `size` holds the number of samples recorded (including compressed sections – see a bit later); `base line` holds the signal amplitude observed when there is no incoming detection – it serves to represent any constant offset that might be present

in an experimental data acquisition system; `compression token` holds an amplitude value which is outside the range of the possible amplitude values and which indicates the beginning of a compression block – see a bit later.

The header block is followed by an arbitrary number of blocks, each of which is from one of two types: `data block` or `compression block`. A `data block` might contain an arbitrary number of `signal amplitude` items, each holding a sampled amplitude value. The `compression block` encodes a section of the signal, where there were no detected pulses. In such sections the value of the signal either equals the `base line` or – more likely in practice – fluctuates around it. As a consequence, there is no need to store the individual amplitudes; they can well be represented by the constant value of the `base line`. The `compression block` has two items: `compression token` indicates the start of the block and `section size` holds the size of the compressed section.

4.1.2   Tool for simulating signals

The simulation of the continuous voltage signals of detectors is performed in two steps using a pair of programs. Because the generation of the signal files requires large amounts of I/O operations, the programs were implemented in the C++ language to ensure good performance. The complete process, including the programs involved and the data formats they use, is shown on Figure 4.3. In the following, the two steps of the process are described briefly, which are based on the mathematical model presented in Section 3.1.
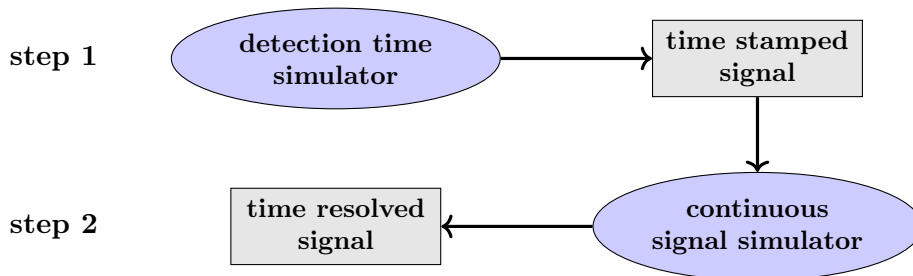
Figure 4.3: The two step process of simulating continuous signals.

In the first step, the times of detections are determined for an array of detectors by the program `detection time simulator`. The detection times of each detector are written to a separate file in the `time stamped signal` format. The user of the program can define a neutron emitting sample and a detector array containing an arbitrary number of detectors. The emission intensity and the multiplicity distribution of the sample can be specified. Each detector can be associated with its own detection efficiency and time delay distribution. The distribution of the time delay can either be selected from a predefined set (including the gamma, exponential, uniform or constant distributions), or its probability density function can be provided in a tabulated form.

In the second step, the amplitude values of the fluctuating continuous signal of a detector are determined with some time resolution and are written to a file in the `time resolved signal` format by the program `continuous signal simulator`. The user can specify the time resolution of the signal, as well as the shape and amplitude distribution of the pulses generated by the individual detections. The shape of the pulses

can either be selected from a predefined set (including the rectangular, exponential or double exponential shapes) or can be provided in a tabulated form. In a similar way, the amplitude distribution can also be selected from a predefined set (exponential, gamma, log-normal or constant distribution) or it can be given in a tabulated form. By providing a set of detection times (in the `time stamped signal` format) as input, a (finite) pulse is generated at each detection and the cumulative value of all the pulses is calculated for each time instant. The program offers two features, which go beyond the mathematical model in the previous chapter. First, electronic noise can be superimposed on the signal in the form of Gaussian white noise [86]; the standard deviation of noise amplitude can be specified by the user. Second, multi-component signals can also be generated, meaning that an arbitrary number of detection time sets can be specified each with their own pulse characteristics (shape and amplitude distribution). Using this feature, one can simulate a neutron signal with parasitic pulses generated by the gamma background (or by the alpha-background in the case of a fission chamber).

4.1.3 Tool for analysing signals

An application named `continuous signal analyser` has been created for the (off-line) analysis of continuous detector signals. To ensure a good performance, the program has been implemented in the C++ language. The signals chosen for analysis are expected to be the `time resolved signal` format and might either be simulated or recorded in a real measurement. Depending on the type of the analysis, the program takes one, two or three signals at a time. The source code of the application has a modular nature: a basic structure for passing through signals and generating outputs is established, and the different analysis types are defined on this structure as independent modules. As a result, the application can easily be extended with a new type of analysis, when required. Table 4.1 shows a list of currently available types of analyses with a short description for each. Regarding the topic of this thesis, three of them are particularly relevant: *mean value analysis, covariance function integral analysis* and *bicovariance function integral analysis*. In the following, the details of these three analyses are described.

The objective of the mean value analysis is to estimate the mean value of one detector signal, as defined by Equation (3.1a). Similarly, the objectives of the covariance function integral analysis and bicovariance function integral analysis is to estimate the integrals of the covariance and bicovariance functions of one, two or three signals, as defined by Equations (3.44) and (3.45). In the following let q denote any of these three quantities. In order to give an estimation of their value and variance in the measurement, the signal(s) are divided into segments of equal size, and q is calculated for each segment independently. Assuming that there are M segments in total, let q_i denote the value of the quantity q determined on segment i. The unbiased estimator of the value of q is the sample mean

$$\mu_q = \frac{1}{M} \sum_{i=1}^{M} q_i. \tag{4.1}$$

Table 4.1: A list of analysis types available in the program `continuous signal analyser` and their description.

analysis	description
mean value	Estimates the mean value of a signal, as defined by Equation (3.1a).
covariance function integral	Estimates the *integral of the covariance function* of one or two signals, as defined by Equation (3.44).
bicovariance function integral	Estimates the *integral of the bicovariance function* of one or two signals, as defined by Equation (3.45).
covariance function	Estimates the *covariance function* of one or two signals, as defined by Equations (3.41a) and (3.42).
bicovariance function	Estimates the *bicovariance function* of one or three signals, as defined by Equations (3.41b) and (3.43).
spectrum	Estimates the power spectrum of one or two signals, defined as the Fourier-transform of their covariance function.
bispectrum	Estimates the power bispectrum of one or three signals, defined as the two-dimensional Fourier-transform of their bicovariance function.
pulse height distribution	Given a threshold value, estimates the distribution of maximum values of continuous sections of the signal which are above the threshold.

The error of this estimator is

$$\sigma_q = \sqrt{\frac{s_q^2}{M}}, \tag{4.2}$$

where s_q^2 is the unbiased estimator of the sample variance, defined as

$$s_q^2 = \frac{1}{M-1} \sum_{i=1}^{M} (q_i - \mu_q)^2 = \frac{1}{M(M-1)} \left[M \sum_{i=1}^{M} q_i^2 - \left(\sum_{i=1}^{M} q_i \right)^2 \right]. \tag{4.3}$$

Let us now specify q_i in the case of the above three analysis types. Consider three detector signals recorded in the same measurement (real or simulated) with a time resolution Δt. The three signals will be labeled with a, b and c. Suppose that all the signals are divided into segments of size N. Clearly, the length of the segments in time is $T = N \cdot \Delta t$. Within the ith segment, let $y_{k,1}, y_{k,2}, \ldots, y_{k,n}$ denote the samples of the signal of detector k ($k = a, b, c$). This is illustrated on Figure 4.4. Let us now define the quantity

$$I_k(x) = \Delta t \sum_{i=1}^{N} (y_{k,i} - x), \tag{4.4}$$

which is a numerical approximation of the area under signal k, after it has been shifted downwards by a constant value x.
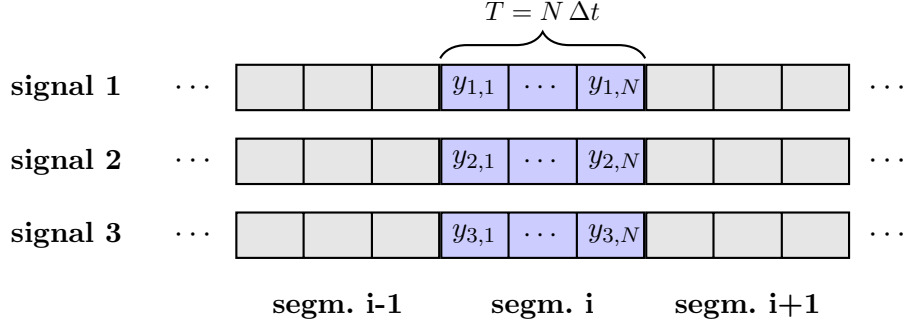
Figure 4.4: An illustration of how the signals are divided into segments during analysis.

For clarity, instead of q, we shall use the notations κ, Cov and Bicov in the case of the mean value, the integral of the covariance function and the integral of the bicovariance function, respectively. With the above notations, when estimating the mean value of one signal (say that of k), $\kappa_{k,i}$ has the form:

$$\kappa_{k,i} = \frac{1}{T} I_k(0) = \frac{1}{N} \sum_{j=1}^{N} y_{k,j}. \tag{4.5}$$

When estimating the integral of the covariance functions of two signals (say that of 1 and 2), Cov$_i$ has the form:

$$\text{Cov}_i = \frac{1}{T} I_1(\mu_{\kappa,1}) I_2(\mu_{\kappa,2}) = \frac{\Delta t}{N} \left(\sum_{i=1}^{N} y_{1,i} - \mu_{\kappa,1} \right) \left(\sum_{i=1}^{N} y_{2,i} - \mu_{\kappa,2} \right), \tag{4.6}$$

where $\mu_{\kappa,1}$ and $\mu_{\kappa,2}$ denote the estimate of the mean value of signals 1 and 2. Similarly, when estimating the integral of the bicovariance functions of signals 1, 2 and 3, Bicov_i has the form:

$$
\begin{aligned}
\mathrm{Bicov}_i &= \frac{1}{T} I_1(\mu_{\kappa,1}) \, I_2(\mu_{\kappa,2}) \, I_3(\mu_{\kappa,3}) \\
&= \frac{\Delta t^2}{N} \left(\sum_{i=1}^{N} y_{1,i} - \mu_{\kappa,1} \right) \left(\sum_{i=1}^{N} y_{2,i} - \mu_{\kappa,2} \right) \left(\sum_{i=1}^{N} y_{3,i} - \mu_{\kappa,3} \right).
\end{aligned}
\tag{4.7}
$$

The above three formulas can be derived from the definitions (3.1a), (3.44) and (3.45).

4.1.4 Verification of the analysis tools

In order to verify the correct behaviour of the programs described in Sections 4.1.2 and 4.1.3, three test signals have been created by simulating a measurement, then their mean values, the integrals of their covariance functions and the integral of their bicovariance function were estimated. Since every parameter of the simulated system is known, the true analytical values of the quantities could be calculated and compared with the results of the estimations. Because the aim at this point is to inspect the programs and not the theory behind them, the parameters of the simulated system were chosen to be mostly simple and not necessarily physically reasonable. The numerical validation of the theory with realistic parameters is the topic of the following two sections.

The emission rate of the simulated sample was $Q = 10\,000\,\mathrm{s}^{-1}$. The multiplicity distribution of the number of emitted neutrons is

$$
P(n) = 1/5 \qquad \text{for} \qquad 0 \leq n \leq 4;
\tag{4.8}
$$

the first three factorial moments of this distribution are $\nu_1 = 2$, $\nu_2 = 4$ and $\nu_3 = 6$. The emitted neutrons were detected by three detectors which had identical parameters. The detection efficiency of each detector was $30\,\%$; this gives a total detection efficiency of $90\,\%$ for the entire system. The neutrons arrived to the detectors with an exponentially distributed time delay, characterized by the probability density function

$$
u(\tau) = \theta_{\mathrm{delay}}^{-1} \mathrm{e}^{-\tau/\theta_{\mathrm{delay}}} \qquad \text{for} \qquad t \geq 0;
\tag{4.9}
$$

the value of the time constant was $\theta_{\mathrm{delay}} = 50\,\mu\mathrm{s}$. The pulses induced by the neutron detectors had an exponentially decaying shape given by

$$
f(t) = \mathrm{e}^{-t/\theta_{\mathrm{pulse}}} \qquad \text{for} \qquad t \geq 0,
\tag{4.10}
$$

with a time constant $\theta_{\mathrm{pulse}} = 1\,\mu\mathrm{s}$. The pulses had a constant amplitude of $a = 1\,\mathrm{V}$.

With these parameters, a $100\,000\,\mathrm{s}$ long measurement was simulated and the signals were recorded with a time resolution of $\Delta t = 0.1\,\mu\mathrm{s}$. The mean value of each signal, the integrals of the covariance functions of each signal pair and the integral of the bicovariance function of the three signals were estimated by dividing the signals into segments of length $T = 20\,\mathrm{ms}$; this produced $500\,000$ segments in case of each signal. The reference values of the quantities were calculated using the general expressions

(3.62)–(3.64) and the results are summarized in Table 4.2. One can see that in the case of the mean value and the integral of the covariance function, the estimated values agree with the analytical references within $1\,\sigma$ statistical uncertainty. The integral of the bicovariance function, on the other hand, is slightly underestimated, but the result still agrees with the reference value within $2\,\sigma$ uncertainty. Using these estimated moments, the singles, doubles and triples detection rates have been calculated using expressions in Section 3.5; the results are shown in Table 4.3. The estimated values of the singles and doubles detection rates agree with the theoretical expectations within $1\,\sigma$ statistical uncertainty. The triples rate, however, are slightly underestimated, as a consequence of underestimating the integral of the bicovariance function.

Overall, the results indicate that the programs created for the simulation and analysis of detector signal work as expected.

Table 4.2: Estimated values of the mean, the integral of the covariance function and the integral of the bicovariance function from test signals and their comparison with reference values.

quantity	detector	value	
		reference	estimated
mean value (V)	A		$(5.9984 \pm 0.0098) \cdot 10^{-3}$
	B	$5.9994 \cdot 10^{-3}$	$(5.9993 \pm 0.0098) \cdot 10^{-3}$
	C		$(5.9993 \pm 0.0098) \cdot 10^{-3}$
integral of the covariance function (V^{2}s)	A–B		$(3.582 \pm 0.015) \cdot 10^{-9}$
	A–C	$3.599 \cdot 10^{-9}$	$(3.597 \pm 0.015) \cdot 10^{-9}$
	B–C		$(3.608 \pm 0.015) \cdot 10^{-9}$
integral of the bicovariance function (V^{3}s^2)	A–B–C	$2.16 \cdot 10^{-15}$	$(1.70 \pm 0.28) \cdot 10^{-15}$

Table 4.3: Estimated values of the singles, doubles and triples detection rates from test signals and their comparison with reference values.

quantity	value (s^{-1})	
	reference	estimated
singles rate	18000	17998.5 ± 1.7
doubles rate	16200	16183.4 ± 19.9
triples rate	7290	5739.2 ± 341.6

4.2 Investigation of the performance of the method

The determination of the singles, doubles and triples detection rates from the moments of continuous detector signals is based on the formulae in Equations (3.68), (3.74)

and (3.80). In Section 4.1.4, the validity of these formulae has been verified by a simple numerical test without the intention of reproducing a realistic measurement scenario. As a result, this test did not investigate the extent to which the detection rates can be obtained from the continuous signals in various measurement circumstances. For this reason a couple of phenomena and measurement parameters are selected in this section and their impact on the quality of the estimation is assessed. The parameters we consider are: the duration of the measurement, the efficiency of neutron detection, the scale of the electronic noise as well as the presence of parasitic pulses from non-neutron sources (e.g. alpha or gamma background). As a quantitative measure of the quality of the estimation, the relative error of the estimated detection rates is chosen; the absolute values of the estimations will be considered only in some cases.

4.2.1   Parameters of the simulated system

For the sake of simplicity, we shall consider a small sample of pure ^{240}Pu in metallic form. In this case neutron loss due to capture as well as neutron production due to (α, n) reactions or induced fission can be neglected. As a result, the multiplicity of the emitted neutrons (per emission event) is independent of the sample mass (as long as the sample can be considered small) and is identical to the multiplicity of the spontaneous fission ^{240}Pu. The corresponding distribution is shown in Table 4.4; its first three factorial moments are $\nu_1 = 2.153$, $\nu_2 = 3.808$ and $\nu_3 = 5.274$. The emission intensity of the sample is $Q = 10\,000\,\mathrm{s}^{-1}$ unless stated otherwise.

Table 4.4: Multiplicity distribution of emitted neutrons (per emission event) of the simulated sample. The values are taken from Reference [3].

n	0	1	2	3	4	5	6
$P(n)$	0.066	0.232	0.329	0.251	0.102	0.018	0.002

The parameters of the detection system were chosen to represent a typical thermal multiplicity counter equipped with ^{3}He gas filled detectors [1, 3]. Although such a counter normally contains dozens of neutron detectors, to simplify the simulation process, we have unified them into three "large" detectors with identical characteristics. With one exception, the detection efficiency of the entire system was $50\,\%$ which gives an efficiency of around $\varepsilon = 16.66\,\%$ per detector. As in the verification step described in Section 4.1.4, the neutrons arrive with an exponentially distributed time delay characterized by the probability density function (4.9). The time parameter of the distribution is again $\theta_{\mathrm{delay}} = 50\,\mu\mathrm{s}$, which is a typical value for a thermal multiplicity counter.

Instead of the simple exponential shape used in the verification step in Section 4.1.4, a more realistic pulse shape is considered given by the function

$$f(t) = \frac{1}{c} \left(\mathrm{e}^{-t/\theta_{\mathrm{pulse},1}} - \mathrm{e}^{-t/\theta_{\mathrm{pulse},2}} \right) \qquad \text{for} \qquad t \geq 0, \tag{4.11}$$

where the normalization constant c is defined as

$$c = \left(\frac{\theta_{\mathrm{pulse},2}}{\theta_{\mathrm{pulse},1}} \right)^{\frac{\theta_{\mathrm{pulse},2}}{\theta_{\mathrm{pulse},1} - \theta_{\mathrm{pulse},2}}} - \left(\frac{\theta_{\mathrm{pulse},2}}{\theta_{\mathrm{pulse},1}} \right)^{\frac{\theta_{\mathrm{pulse},1}}{\theta_{\mathrm{pulse},1} - \theta_{\mathrm{pulse},2}}}. \tag{4.12}$$

The values chosen for the time constants are $\theta_{\text{pulse},1} = 1\,\mu\text{s}$ and $\theta_{\text{pulse},2} = 0.9\,\mu\text{s}$; this gives a characteristic pulse length of around $10\,\mu\text{s}$ which is a typical value for thermal neutron detectors [3] and is close to the length of the pulses recorded in the measurements discussed in Chapter 5. The pulse shape with the selected parameters is shown on Figure 4.5a. To model the random variation of the pulse amplitudes, the gamma distribution was chosen with the probability density function

$$w(a) = \frac{1}{\Gamma(k)\,\theta_{\text{amplitude}}^k}\, a^{k-1}\, e^{a/\theta_{\text{amplitude}}}, \tag{4.13}$$

where Γ denotes the gamma-function. The value $k = 5$ was selected for the shape parameter, and $\theta_{\text{amplitude}} = 20\,\text{mV}$ for the scale parameter; this gives a mean amplitude $\langle a \rangle = k\,\theta_{\text{amplitude}} = 100\,\text{mV}$ which is a realistic value for pre-amplified signals. The probability density function of the pulse amplitudes is shown on Figure 4.5b.
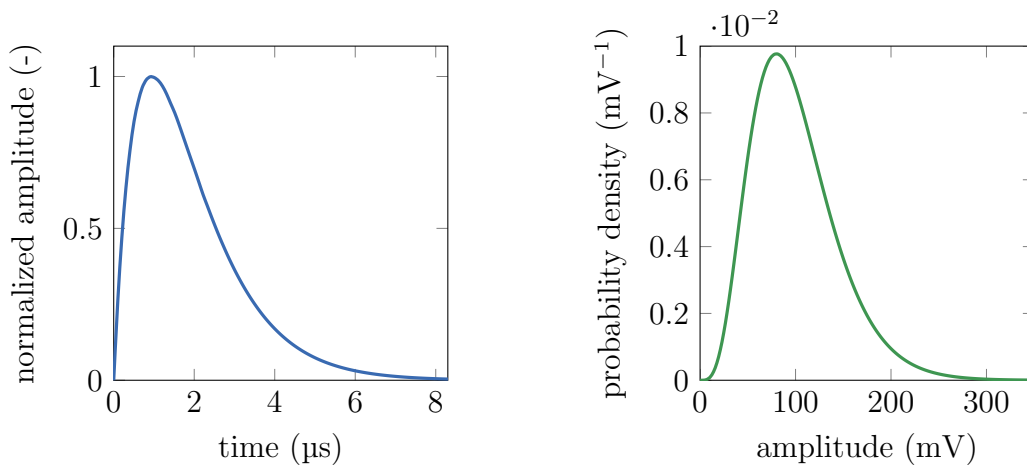
(a) The time evolution of the pulse shape.

(b) Probability density function of the pulse amplitude.

Figure 4.5: The characteristics of simulated pulses.

The signals generated with the above parameters were recorded with a time resolution of $\Delta t = 0.05\,\mu\text{s}$, which was chosen to be large enough to properly resolve individual pulses. With one exception, the length of the generated signals was $1000\,\text{s}$ which can be regarded as a typical measurement time in multiplicity counting measurements [1]. In every case, the singles, doubles and triples detection rates were calculated using Equations (3.68), (3.74) and (3.80), for which the moments of the signals were estimated as described in Section 4.1.3. During analysis, the signals were divided into $20\,\text{ms}$ long segments.

4.2.2 The impact of the measurement time

According to Equation 4.2, the error of the estimated values of the moments of the detector signals are inversely proportional to the square root of the measurement time. From Equations (3.68), (3.74) and (3.80), one can conclude that the same is true for the estimated values of the singles, doubles and triples detection rates. In order to

investigate the impact of the measurement time on the precision of the estimated detection rates, a long measurement, lasting 30 000 s which is equivalent to about 8.3 hours, has been simulated and the values of the three detection rates were determined several times along the entire measurement. Figure 4.6 shows the relative errors of the estimated detection rates.
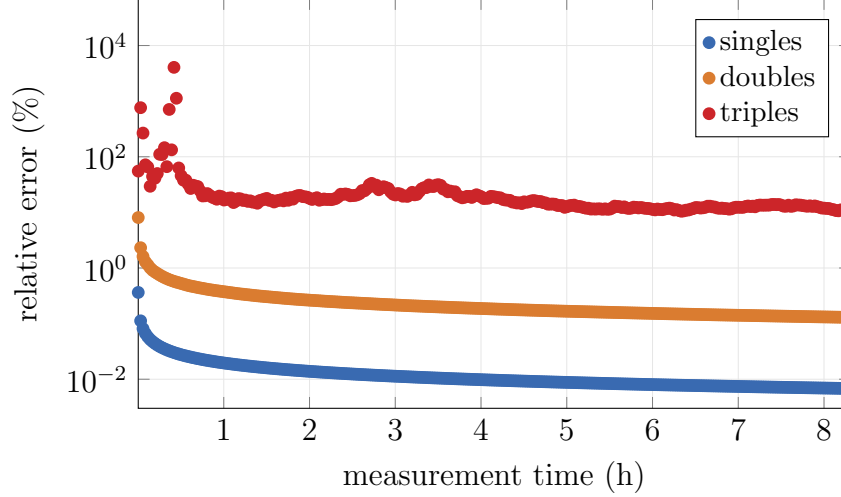

Figure 4.6: Relative errors of estimates of the singles, doubles and triples rates as a function of the measurement time.

As one would expect, the singles rate estimation provides the lowest relative error, while the triples rate estimation provides the largest. In the case of the singles rate, the relative uncertainty does not go above 1 % even for short measurement times; it reaches 0.1 % in a couple of minutes and 0.01 % in about 3 hours. The error of the doubles rate estimate reaches 1 % quickly and approaches 0.1 % after more than 8 hours. Compared with the singles and doubles rates, the estimate of the triples rate shows a much worse quality. On the time scale of minutes, relative errors as large as 1000 % can be observed; after 1 hour, the uncertainty approaches 10 % and does not decrease much by 8 hours. Moreover, unlike in the case of the other two detection rates, the relative uncertainty of the triples rates does not always decrease monotonically with the measurement time.

The observed differences in the relative errors of the three detection rates can be explained by the extent to which the information available in the signals is utilized. This question has somewhat been addressed in Section 3.5. Recall that, according to Equation (3.65), the overall singles rate in the system is the sum of singles rates observed in each detector. Expression (3.68) shows that the information on these individual singles rates is directly extracted from the mean values of the detector signals. On the other hand, the total doubles rate, as seen from Equation (3.69), comes from pairs detected either in the same detector or in two different detectors. However, expression (3.74) shows that the integral of the covariance function gives direct information only on doubles observed in two different detectors; the doubles rate measured in the individual detectors is deduced indirectly from the previous ones. Essentially, the ratio of number of terms containing direct (original) or indirect (deduced) information in (3.74) is 3 : 6. This suggests that only half of the total information available on the doubles rate is utilized. The other half, as we have seen in Section 3.4.1, can be found in the integral

of the autocovariance function of a signal, however, mixed with information on the
singles rates which might be difficult to separate. With similar considerations, one
finds that the ratio of the original and deduced information when determining the
triples rate using Equation (3.80) is $1\!:\!9$ which can easily explain the high uncertainties
and unstable convergence observed in Figure 4.6.

Due to the large number of simulation cases considered in the forthcoming sections,
only $1000\,\mathrm{s}$ long measurements were simulated which is equivalent to around $16\,\mathrm{minutes}$.
Because the uncertainty of the triples estimate in such a short time is extremely large, it
was not possible to draw clear conclusions on this rate. For this reason, in the reminder
of this chapter results will be presented only for the singles and doubles detection rates.
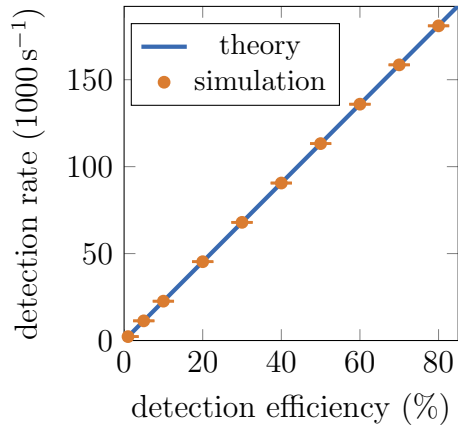
4.2.3   The impact of the detection efficiency

Of all the parameters, the detection efficiency has most likely the largest influence
on the performance of a measurement system. This is especially true for measurements
involving coincident detection events like multiplicity counting. As seen from Equa-
tions (3.65), (3.75) and (3.75), while the singles rate depends linearly on the detection
efficiency, the doubles and triples rates are proportional to its second and third powers.
For this reason, the goal in every multiplicity counting system is to achiewe as high
detection efficiency as possible. As we have mentioned in Chapter 2, ^{3}He gas-filled
detectors, which are used in most measurements of this type, can typically provide a
$40\,\%$–$60\,\%$ efficiency for thermal neutrons [1]. In the minority of cases, when other types
of detectors – for example thermal fission chambers, or some fast neutron detectors –
are used, the detection efficiency can be as low as $1\,\%$.

To illustrate the effect of the detection efficiency on the estimated values of the
detection rates and their precision, the efficiency was varied in the range of $1\,\%$–$80\,\%$.
Figure 4.7 shows the absolute values of the estimated singles and doubles rates along
with the theoretical expectation. In general, the simulations show a good agreement
with the theory. The relative uncertainties of the estimation can be seen in Figure 4.8.
In both cases, they show a fast exponential-like decrease with increasing detection
efficiency. The pace of the decrease is faster in the case of the doubles rate.

4.2.4   The impact of electronic noise

Electronic noise is the undesired fluctuation which is superimposed on a signal
recorded by an electrical measurement system. There is an extensive literature on
electronic noise; the discussion presented here is limited to few important aspects,
based on [38]. In a radiation measurement, the most significant sources of electronic
noise are located in beginning of the detection chain: the detector itself, as well as
the pre-amplifier and its input stage. Since noise forming on these elements undergo
the same amplification process as the signal, it can seriously degrade the information
carried by pulses induced by detected particles. From a practical point of view, the
two most important characteristics of the electronic noise are its power spectral density
and amplitude distribution, since these will often determine the set of techniques that
can be used to reduce it. A recent study investigating the measured signals of thermal
fission chambers showed that the power spectral density of the noise is pink (inversely

(a) Singles rate.
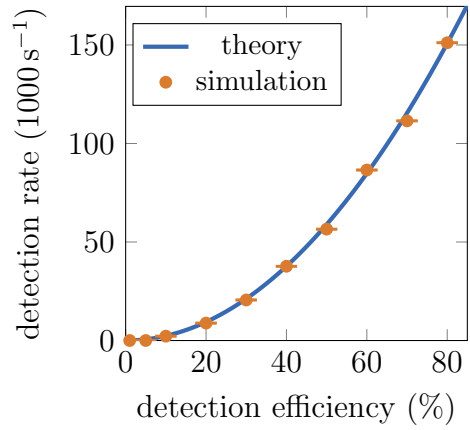
(b) Doubles rate.

Figure 4.7: The value of the singles and doubles detection rates estimated from simulated voltage signals as a function of the detection efficiency.

(a) Singles rate.

(b) Doubles rate.

Figure 4.8: The relative error of the singles and doubles detection rates estimated from simulated voltage signals as a function of the detection efficiency.

proportional to the frequency) and its amplitude distribution is close to normal [87]. For simple analytical or numerical investigations it is often assumed that the power spectral density is white (constant in frequency) and the amplitude distribution is normal with zero mean. In the following we shall make this assumption as well.

In order to investigate the effect of the electronic noise on the estimated values of the detection rates, Gaussian white noise has been superimposed on the simulated signals. The mean value of the noise was kept zero, while its standard deviation varied in the range 0 mV–50 mV; the upper limit corresponds to half of the mean amplitude of neutron pulses. Figure 4.9 shows the estimated values of the singles and doubles rates as a function of the standard deviation of the noise; the horizontal lines correspond to the value expected with no noise being present. The estimated values seem to be scattered along the horizontal line, which means that the presence of the noise does not change the value of the detection rates. This result can be explained on a theoretical basis as well: since the noise has a zero mean amplitude, it does not contribute to the mean value of the signal; furthermore, since the noise present in two different signals is independent (in fact, even within one signal the samples of a white noise at two distinct time instants are independent), its covariance function is zero. Despite leaving the values of the estimated rates unchanged, one would expect that the presence of the noise increases the statistical uncertainty of the estimation. Looking at the graphs on Figure 4.10 which show the relative errors of the detection rates, once can conclude that although the uncertainties increase with increasing amplitudes of the noise, this effect is practically negligible even at large noise amplitudes. These results suggest that the method is rather insensitive to the presence of electronic noise.
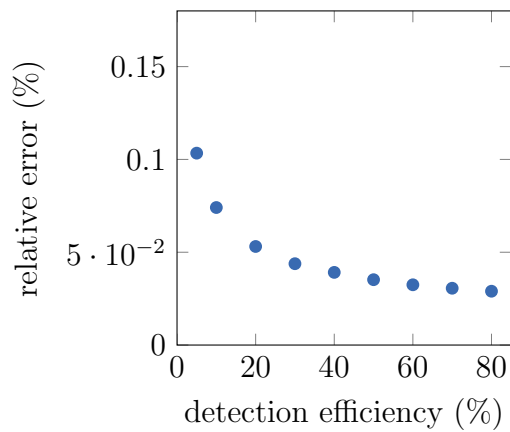

(a) Singles rate.   (b) Doubles rate.
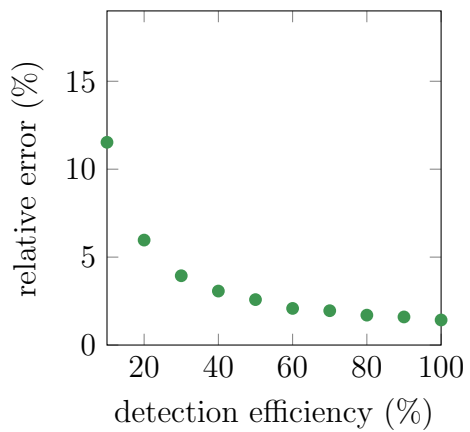
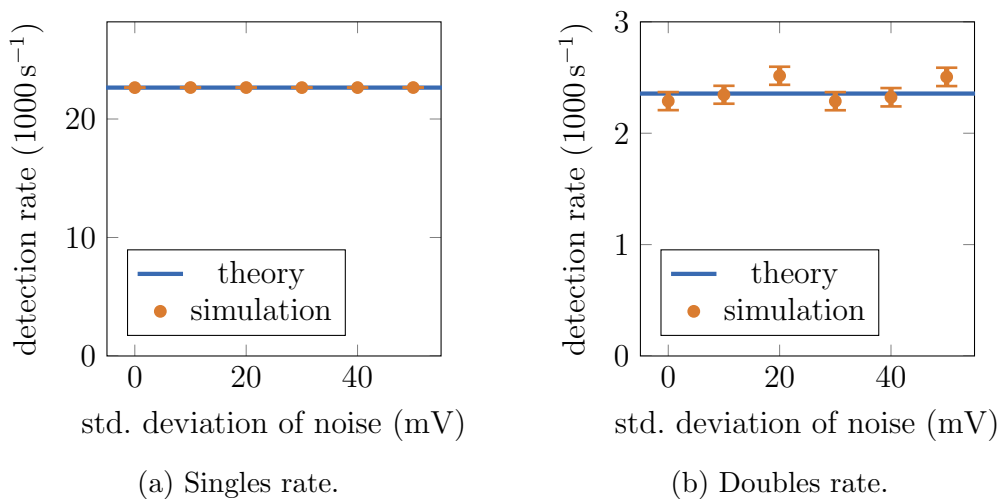Figure 4.9: The value of the singles and doubles detection rates estimated from simulated voltage signals as a function of the standard deviation of the superimposed Gaussian white noise.

4.2.5   The impact of non-neutron pulses

Every detector designed for measuring neutron radiation will also be sensitive to some degree to the particles of other radiation types as well. For example, ^{3}He-gas

(a) Singles rate. (b) Doubles rate.

Figure 4.10: The relative error of the singles and doubles detection rates estimated from simulated voltage signals as a function of the standard deviation of the superimposed Gaussian white noise.

filled detectors are known to have a relatively high detection efficiency for gamma particles [3, 38]. Although fission chambers are less sensitive to gamma radiation, they can have a high alpha background due to the α-decay of the heavy isotopes in the fissile deposit [38]. Most of the time, the pulses induced by these secondary sources have a smaller amplitude than neutron induced pulses which allows to differentiate against them. For example, alpha-particle induced pulses in a fission chamber are typically 10 times smaller than neutron pulses [38]. When a detector is operated in pulse counting mode, smaller pulses can be filtered out by differentiation on an amplitude basis. In Campbelling mode, the contribution of secondary pulses is decreased by raising the signal amplitude to a higher power [67].

In order to investigate the effect of such minority signal components, a secondary particle source is assumed besides the fissile sample. We shall assume, that the secondary source is independent from the first one and its particles arrive in a homogeneous Poisson process with intensity $Q_{\text{non-neutron}}$. This simple model describes well the inherent α background of a fission chamber or a gamma background produced by activation and fission products. No attempt is made to simulate a correlated secondary source, such as prompt fission gamma radiation in the fissile sample; this issue will be addressed in future research. For the sake of simplicity, we shall assume that pulses induced by the secondary particles have the exactly the same shape as neutron induced pulses and almost the same amplitude distribution (see Section 4.2.1). The only difference is that the scale parameter of the amplitude distribution is $2\,\text{mV}$; as a result, the mean amplitude of secondary pulses will be $10\,\text{mV}$, which is 10 times smaller than the amplitude of neutron pulses. Because the strength of the secondary source can vary in a wide range depending on the measurement conditions, its intensity varied between $Q_{\text{non-neutron}}=0\,\text{s}^{-1}$–$15\,000\,\text{s}^{-1}$ in the simulations; in its upper range, the secondary source is 1.5 times stronger in emission intensity than the neutron source.

Figure 4.9 shows the estimated values of the singles and doubles rates as a function of the intensity of the secondary source; the horizontal lines correspond to the value

expected when no secondary source is being present. Two sets of simulated values are presented for the singles rates. The first was obtained by applying Equation (3.68) to the estimated mean value by disregarding the bias introduced by the secondary source, i.e. the integral of the neutron pulses was simply inserted into (3.68). As one would expect, the singles rates obtained with this approach increase linearly with the secondary source intensity, since its contribution to the mean value of the signal is proportional to the intensity. The second set of values was obtained by correcting for the secondary source: the mean value of secondary signal component was estimated, by analyzing a signal generated without the primary neutron source. In fact, a similar approach can be applied in practice to obtain the correct singles detection rates: one can perform a background measurement and register a signal when no neutron source is present. The doubles rate appears to be insensitive to the presence of the background. This is expected on a theoretical basis, since the contribution of the secondary source to two different signals is independent due to its Poissonian nature, hence its cross-covariance is zero. Figure 4.12 shows the relative error of the estimates. In none of the cases has the non-neutron source a significant effect on the accuracy of the estimation.
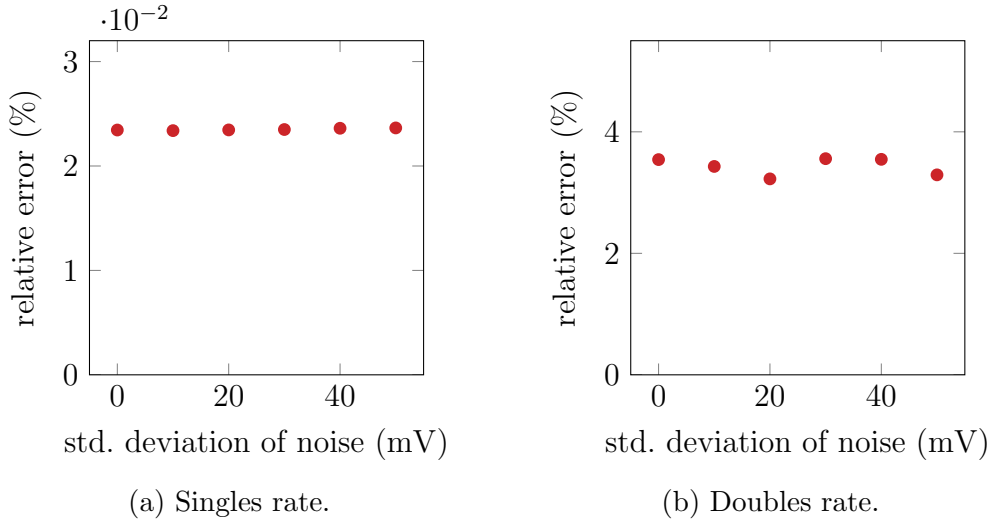

(a) Singles rate.

(b) Doubles rate.
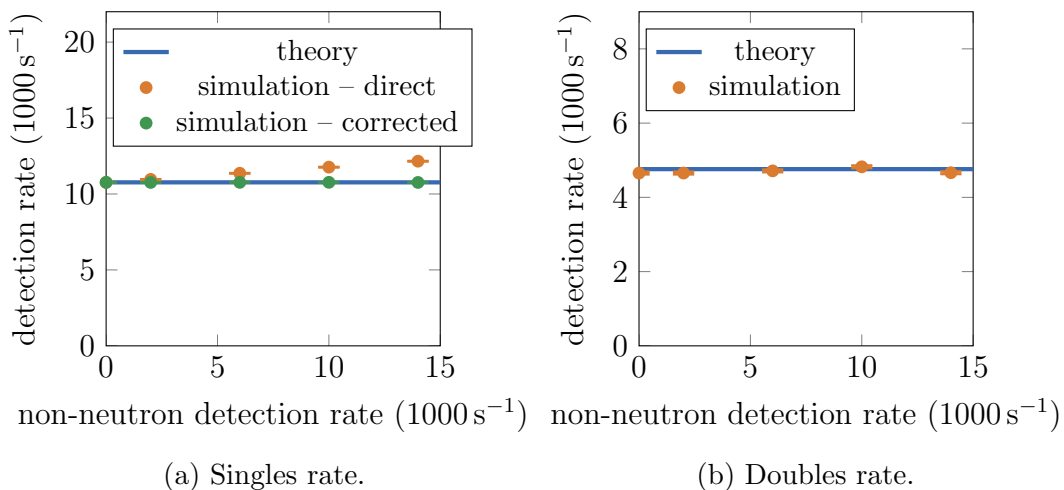
Figure 4.11: The values of the singles and doubles detection rates estimated from simulated voltage signals as a function of the intensity of a secondary non-neutron source.

4.2.6 Concluding remarks

In this section the impact of a number of different parameters on the accuracy of the proposed method of neutron multiplicity counting has been investigated by simulations. Most statements concern the singles and doubles detection rates, since the triples rates could not be recovered with acceptable accuracy. From all the parameters that were taken into account, the detection efficiency appears to have the most significant influence of the precision of the method: with increasing detection efficiency, the relative error of the estimation decreases rapidly. This suggests that maximizing the detection efficiency should be a priority in practical applications.

The second most important parameter has been the measurement time. Although

(a) Singles rate.   (b) Doubles rate.
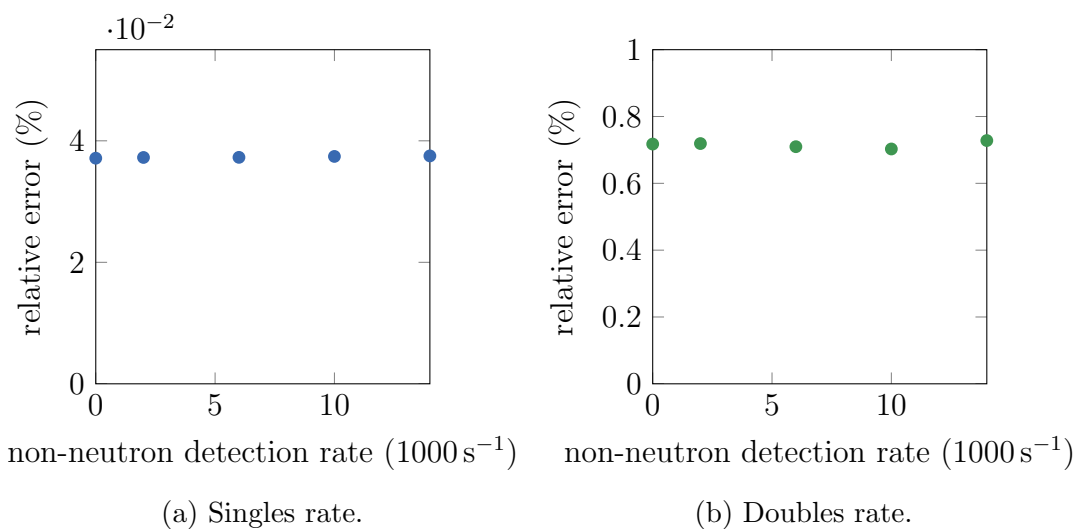
Figure 4.12: The relative error of the singles and doubles detection rates estimates a function of the intensity of the non-neutron source.

the singles estimate reach a low uncertainty rapidly, the convergence of the doubles rate seemed slow compared to the traditional method, and the triples rate did not reach an acceptable level of uncertainty even at very long measurement times. As it has been pointed out in Section 4.2.2 this behaviour is most like related to the fraction of the extracted and available information in the signals. This topic will addressed in future research.

Other parameters investigated have either small or negligible influence on the performance of the method. Among these, the only considerable bias is that introduced by non-neutron pulses to the singles rate estimate. Nevertheless, this effect can easily be compensated for by a simple background measurement, as suggested in Section 4.2.5. No such compensation is required for the doubles rates as it is not affected by the presence of non-neutron pulses. Both the singles and doubles rates appear to be insensitive to a Gaussian white noise present in the signal.

Overall, the doubles rate estimate is more sensitive to the detection efficiency than the singles estimate and provides a less accurate estimate in the same measurement time. On the other hand, the doubles rate estimate seems to be more robust against parasitic components in the signal. Partly this is due to the high-order nature of the moment which favours the neutron response by raising the signal to the second power; and partly it is a consequence of the covariance-nature of the moment, which discriminates against uncorrelated events. This suggests that the proposed method might be a viable choice for measuring spent nuclear fuel with large gamma background (see Section 2.4).

4.3   Comparison of the traditional and the new method

In Section 4.2, the performance of the newly proposed method of multiplicity counting has been assessed on its own, with no reference to the performance of the traditional approach. There are several aspects by which the two methods can be compared. Here only one parameter, possibly the most important one, is selected: the fission source in-

tensity. In Section 2.4 it has been pointed out that one factor limiting the applicability of traditional multiplicity counting is the considerable amount of dead time losses in the counting electronics caused by the large neutron counting rate. It has also been stated that one of the most appealing characteristic of the newly proposed method is its insensitivity to this type of dead time. Another set of simulations have been performed in order to illustrate the behaviour of the two version of multiplicity counting in high counting rate environments.

Measurements have been simulated using the exact same parameters, as described in Section 4.2.1. The emission rates varied in the range of 1000–100000 s^{-1}. The singles doubles and triples detection rates have been estimated from the moments of the signal the same was as in the previous section, using the equations presented in Section 3.5. In order to obtain the detection rates based on the traditional pulse counting approach, another software program has been created which emulates the behaviour of the signal processing chain of multiplicity counters (see Section 2.3.6). The program includes a simple integral discriminator model which determines the times when the signal crosses a predefined threshold value. This time data is then fed to a model of a multiplicity shift register, which provides estimates for the detection rates using the formulas presented in Section 2.3.7. The values of the detection rates are output without applying any dead time correction to them; however, correction with the gate fraction factors (see Section 2.3.4) has been included.

The singles and the doubles rates estimated with the two approaches are shown on Figure 4.13. It is seen that throughout the considered range of the emission rate, the values obtained from the new method shown an excellent agreement with the theoretical expectations. At low emission rates, when pulses rarely overlap, the agreement is also good with the values obtained from pulse counting. However, as the emission rate increases, and pulse overlapping becomes more frequent, the traditional singles and doubles estimates underestimate the real values.
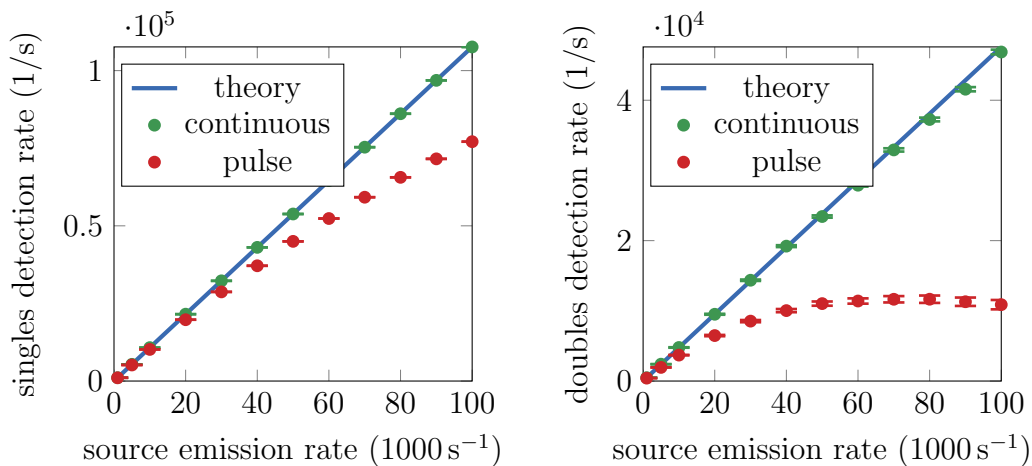
Figure 4.13: Simulated detection rates.

It should emphasize that the above presented study does not reflect the absolute performance of the two methods. The purpose here was to illustrate the conceptual difference between them and not to quantify the range of their applicability. For this reason (and because it made the simulation easier) the performance of the traditional

approach has been made worse by increasing its sensitivity to dead time. In real applications, the traditional approach is much more resistant to dead time for at least two reasons. First, as noted in Section 2.3.6, dead time is greatly reduced by using many (10–60) independent signal processing chains, whereas here all the pulses went through three chains. Second, voltage pulses go through many stages before they get counted by an integral discriminator and the discriminator itself is a complicated device [38]; on the other hand in this study a very simple technique was chosen to count based on simple level crossing detection. Nevertheless, the insensitivity of the new method to counting dead times is well shown on Figure 4.13.

Chapter 5

Experimental demonstration

5.1 The aim and background of the experiment

An experiment has been designed and executed in order to demonstrate the practical use of the method discussed in the previous two chapters by measuring a ^{252}Cf sample. The activity was carried out in a collaboration between the Budapest University of Technology and Economics, Chalmers University and the Kyoto University and took place at the Kyoto University Critical Assembly (KUCA) facility in Osaka, Japan.

Our aim was to build a measurement set-up in which the detection rate is low enough to not cause overlapping pulses very often. This allowed us to measure the detection rates not only from the continuous signals, but – to serve as a reference – also with the pulse counting procedure. The goal of the measurement was to show that the newly proposed method is able to provide the same detection rate values as the traditional multiplicity counting.

Although the general purpose of multiplicity counting is to determine the fissile mass of sample (see Chapter 2), no estimation of the mass was given in this measurement for two main reasons. First, as discussed in Section 2.3.5, in order to apply the inversion procedure that produces the mass estimate, one needs to know the values of *a)* certain nuclear physical constants of the fissile isotopes, *b)* the detection efficiency and *c)* the gate fraction factors (at least when using detection rates obtained from pulse counting). While the physical constants are generally known, the other two parameters are usually determined with the careful calibration of the multiplicity counter device (see Reference [1]). We had no option to perform such a calibration. The second, and more important, reason is that the inversion procedure requires the knowledge of all three detection rates. However, as we shall see later, it was not possible to estimate the triples detection rate in our measurement set-up.

Finally, it should be mentioned that the author of the thesis took active part only in the design and the analysis of the measurements. The set-up was built and the measurements were executed by Gergely Klujber and dr. Máté Szieberth from the Budapest University of Technology and Economics as well as by dr. Yasunori Kitamura and prof. Tsuyoshi Misawa from the Kyoto University.

5.2 The measurement set-up

The Kyoto University Critical Assembly (KUCA) facility is a multi-core facility comprising of two solid-moderated cores (A and B core) and a light-water moderated core (C core) [88]. The basis of the A core is a rectangular aluminum grid into which assemblies can be loaded. Each assembly consists of a rectangular aluminum frame into which plates of different materials (uranium, polyethylene, graphite, etc.) and thicknesses can be loaded horizontally (see Figure 5.4) similarly to how pellets are loaded into a fuel rod. This modular nature of the assemblies makes it possible to construct a large variety of measurement arrangements. The experimental set-up was assembled on the same grid that hosts core A, however, it was located outside the graphite reflector surrounding the core. The position of the set-up within the core is shown on Figure 5.1.
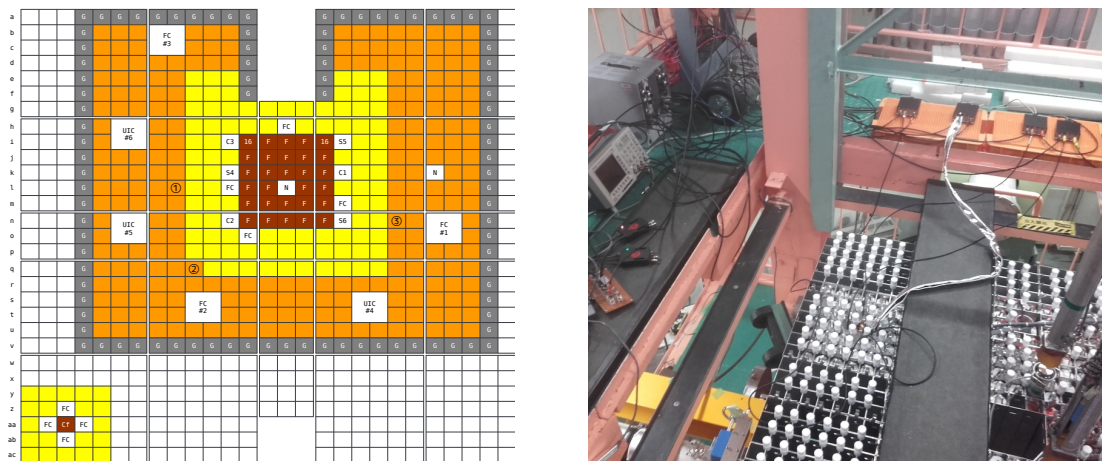
Figure 5.1: The location of the measurement set-up within core A of the Kyoto University Critical Assembly (KUCA).

In the following, the measurement set-up is described in detail. The description is best supported by images from the MCNP [25] model of the set-up shown on Figure 5.3, but actual photos of certain elements of the arrangement can also be seen on Figures 5.2 and 5.4. Since the facility was designed by the United States government, the sizes (and most other technical data) of its components are documented [88] in imperial units. Therefore, in the description that follows, the original documented values will be presented but approximate values in metric units will be presented as well. Note also that there are some minor differences between the MCNP [25] model shown below, and the actual measurement arrangement; these will be pointed out at the end of the section.

As seen on Figure 5.3, the measurement set-up consists of a 5×5 lattice of assemblies. Each assembly is loaded with rectangular cuboid plates with a $2 \,\text{in} \times 2 \,\text{in}$ ($\approx 50.8 \,\text{mm} \times 50.8 \,\text{mm}$) cross section and different thicknesses. Three different types of assemblies were built. We shall refer to these as *source assembly*, *detector assembly* and *moderator assembly*. Figure 5.4 shows actual pictures of these assemblies while being put together on site. In the following, the vertical structure of the assemblies and their positioning in the arrangement is described in detail.

The central grid element in the arrangement is the source assembly which hosted three ^{252}Cf samples. Each sample was enclosed in a cylindrical aluminium casing with an approximate diameter of 2 mm and an approximate height of 10 mm. The registered activities (including α-decay and spontaneous fission) of the three samples on September 6, 2019 were 48.9 kBq, 48.9 kBq and 14.7 kBq, respectively. This gives a total activity of 112.5 kBq and a total neutron emission rate of 12 930 s^{-1}. The samples were placed inside a 1/16 in ($\approx$1.59 mm) thick polyethylene plate as shown on Figure 5.2. This plate was then placed in the middle horizontal plane of the source assembly (which was also the middle plane of the entire set-up).

Two versions of the source assembly were built in order to create two measurement configurations. In both versions, the central polyethylene plate (enclosing the californium samples) was surrounded by additional 1/16 in ($\approx$1.59 mm) thick polyethylene plates from the top and the bottom. In one of the two versions, however, some of these polyethylene plates were replaced by 93.2 % enriched uranium-aluminum alloy plates of the same size. Figures 5.3 and 5.4 show only this second version. A more detailed description of the two configurations and the motivation behind creating them will be given in Section 5.3.
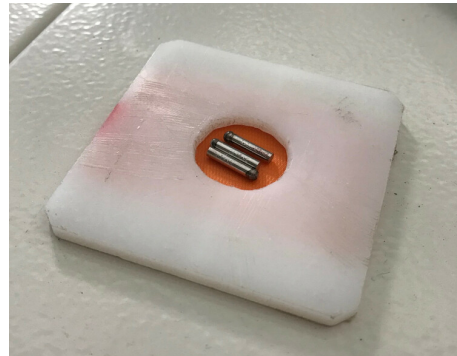
Figure 5.2: Three ^{252}Cf sources embedded into a polyethylene plate.

The central source assembly was surrounded symmetrically by four detector assemblies. They are labeled with A–D on Figures 5.3 and 5.4 (and these same labels will be used to refer to the signals of the corresponding detectors as well). Each assembly was hosting one thermal fission chamber of the same type. A detailed technical description of the detectors (along with the entire data acquisition chain) will be given in Section 5.4. The detectors were positioned vertically in a way that their sensitive region lies symmetrically around the plane of the californium sources. From the top and the bottom, they were surrounded with polyethylene blocks of appropriate thickness.

All the remaining positions in the grid were occupied by moderator assemblies. The moderator assemblies were entirely filled with 1/16 in ($\approx$1.59 mm) thick polyethylene plates. The primary purpose of the polyethylene in the moderator assemblies as well as in the other two types of assemblies was to thermalize fast fission neutrons, thus increasing the probability of detection in the fission chambers and the induced fission in the uranium-aluminum plates (when present).

5.3   Configurations of the set-up

Equations (2.22) and (2.12) show that the detection rates are monotonically increasing functions of the amount of fissile material in the measured sample. Two measurement configurations containing different amounts of fissile material were created in the hope that a significant difference between the measured detection rates will be observed. The first configuration contained only the three samples of ^{252}Cf, located in the source assembly, as fissile material; this configuration will be labeled as Cf in the

(a) Horizontal view.

(b) Vertical view.
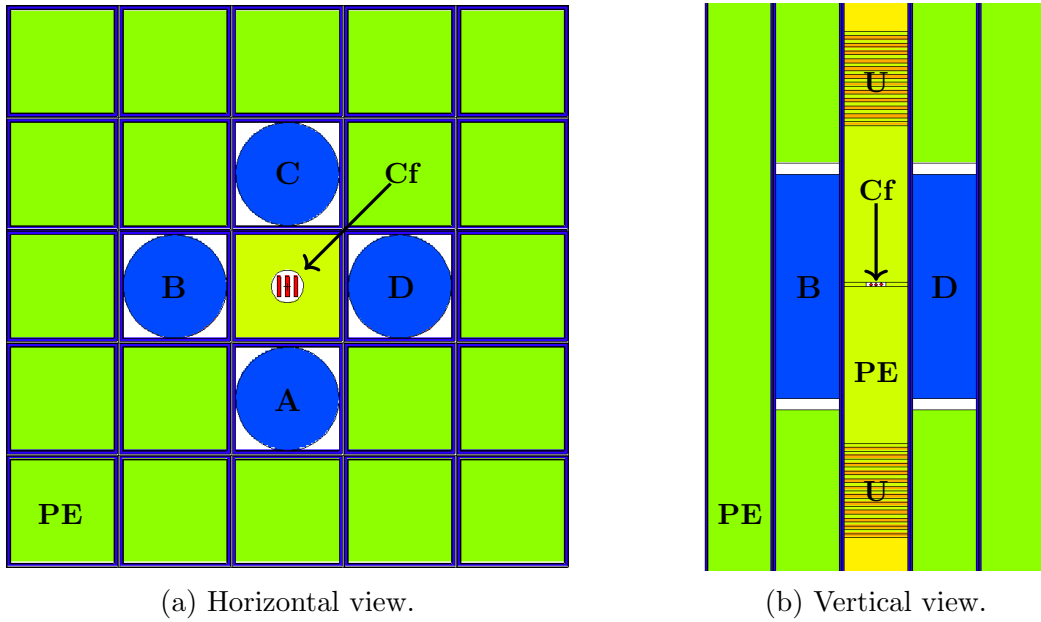
Figure 5.3: The MCNP model of the measurement set-up.

(a) Source assembly.

(b) Detector assembly.

(c) Moderator assembly.
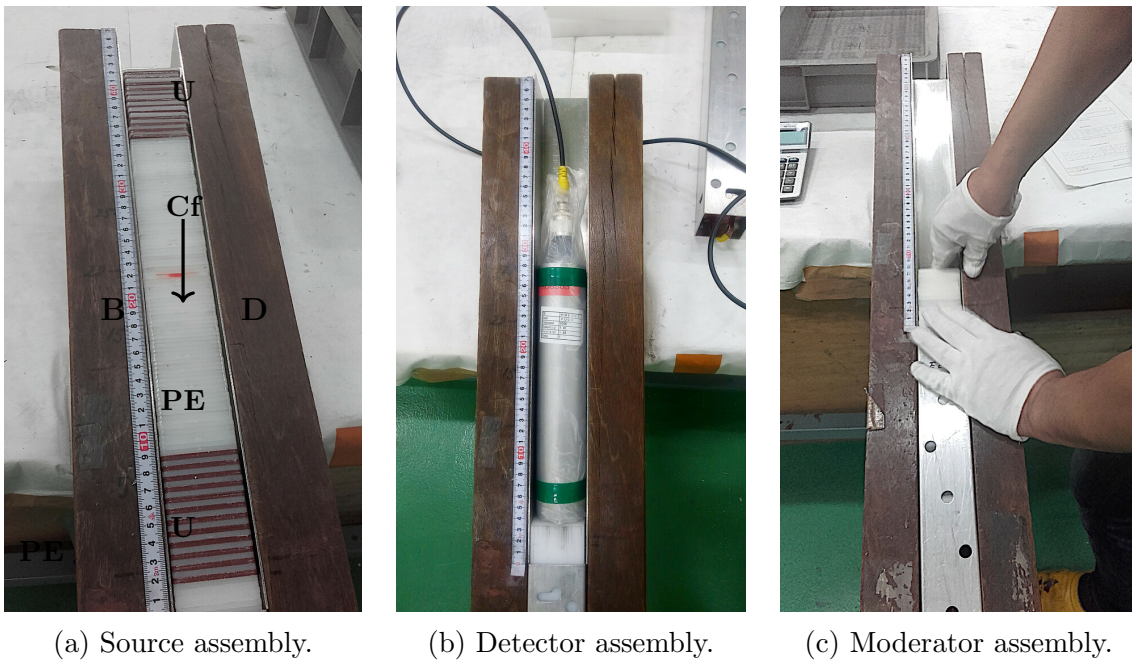
Figure 5.4: The three assemblies used in the measurement arrangement while being assembled.

subsequent sections. In the second configuration 90 % enriched ^{235}U plates were placed inside the source assembly symmetrically above and below the californium to serve as a secondary neutron source (induced fission caused by the primary neutrons from the californium); it will be labeled as Cf+U.

The number of neutrons produced additionally in induced fission is sensitive to the amount and location of the uranium in the system: the uranium must be far enough from the californium so that neutrons thermalize by the time they reach it; on the other hand, if too much polyethylene is replaced by uranium, the neutrons do not get moderated. The final positioning of the uranium-aluminum plates in configuration Cf+U has been determined by a simple numerical optimization using the MCNP model of the set-up. Seven variants of the central assembly has been created that contained different amounts of uranium at different distances from the californium; these are labeled with B–H on Figure 5.5 (label A shows the variant with no uranium at all, used in configuration Cf). Simulations were performed to estimate the singles, doubles and triples detection rates by using each variant of the source assembly.

The results are listed in Table 5.1, where the variants that were built in the end are marked with bold. One can immediately see that there is no significant difference between the detection rates in configuration Cf (with variant A) and Cf+U (variants B–H). This suggests that the measurements will not be able to show any difference either. In any case, for realizing configuration Cf+U, variant G has been chosen because it yields the highest triples to singles ratio.

While values in Table 5.1 refer to the detection rates observed in all four detectors cumulatively, Table 5.2 shows the singles rates from one detector, the doubles rates from a pair of detectors as well as the triples rates from three detectors, in the two configurations Cf and Cf+U. These will be compared with measured values in Section 5.8.

An important thing to notice, however, that the predicted value of the triples rate is very low. This is a consequence of the low detection efficiency of the system, which originates partly from the generally low internal efficiency of fission chambers (compared to other neutron detectors [38]) and partly from the low geometric efficiency due to the arrangement of the sample and the detectors. As a result, the triples rates are not expected to be measured with any good accuracy.

Table 5.1: Simulated values of the detection rates in the configuration shown on Figure 5.4.

configuration	detection rate (1/s)			triples to singles ratio (10^{-3})
	singles	doubles	triples	
A (Cf)	**80.697 ± 0.283**	**3.984 ± 0.063**	**0.208 ± 0.014**	**2.58**
B	79.773 ± 0.281	3.922 ± 0.062	0.202 ± 0.014	2.54
C	80.885 ± 0.283	4.029 ± 0.063	0.206 ± 0.014	2.55
D	79.092 ± 0.280	3.919 ± 0.062	0.203 ± 0.014	2.57
E	81.676 ± 0.284	4.130 ± 0.064	0.219 ± 0.015	2.68
F	81.513 ± 0.284	4.125 ± 0.064	0.215 ± 0.015	2.64
G (Cf+U)	**81.585 ± 0.284**	**4.137 ± 0.064**	**0.220 ± 0.015**	**2.70**
H	81.572 ± 0.284	4.147 ± 0.064	0.216 ± 0.015	2.65
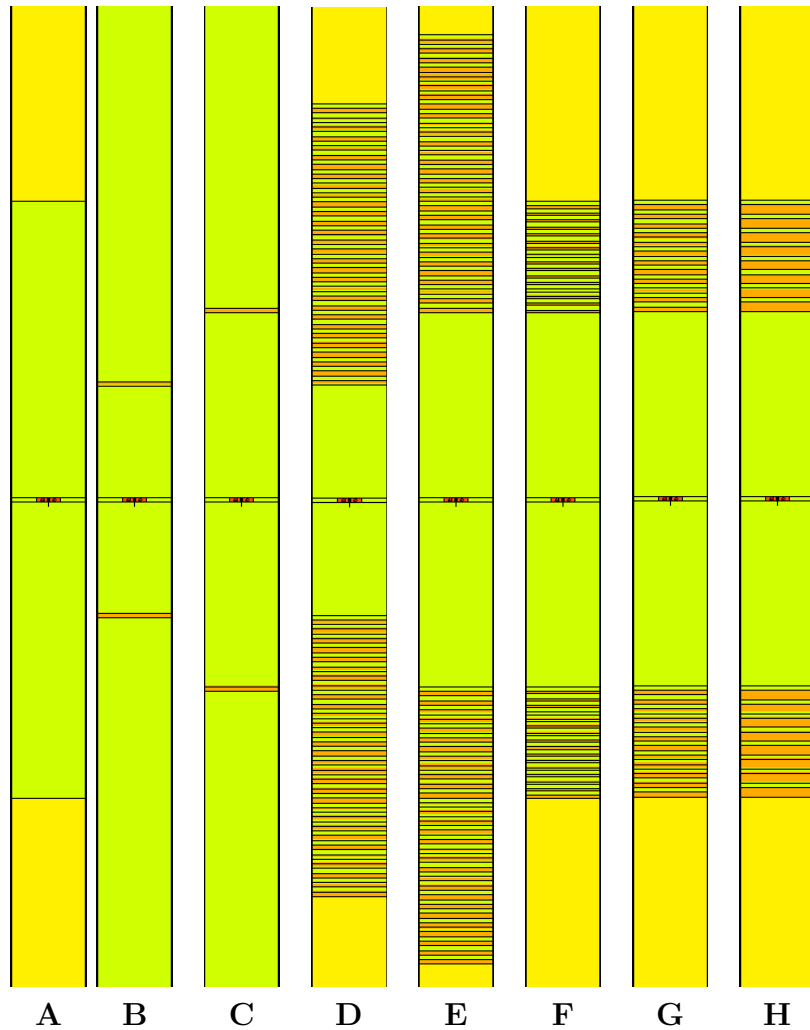
Figure 5.5: Variants of the central source assembly used for the optimization of the measurement arrangement.

Table 5.2: Simulated values of the detection rates in configurations Cf and Cf+U.

quantity	value (1/s)	
	Cf	Cf+U
singles (per 1 detector)	20.174 ± 0.141	20.396 ± 0.142
doubles (per 2 detectors)	0.996 ± 0.031	1.034 ± 0.032
triples (per 3 detectors)	0.088 ± 0.009	0.093 ± 0.010

Finally, it should be mentioned that certain assumptions had to be made when creating the MCNP model of the set-up. The two most important simplifications are the following:

1. The amount, chemical form and distribution of the californium within the three samples is not known. Therefore, the samples on the MCNP model were small cylinders filled with air, and a fixed isotropic neutron source (with the same multiplicity distribution as that of the spontaneous fission of ^{252}Cf) was defined and was distributed uniformly within the sample volume. As a consequence, (α, n) reactions on light materials as well as induced fission on the fissile isotopes of californium were not included in the model (see Section 2.3.2). However, both of these effects are expected to be negligible in the case of the small samples used in the measurement.

2. The internal structure of the fission chambers is not known, only their size and total fissile content. For this reason, each detector was represented by three vertically stacked homogeneous cylinders in the MCNP model. The central cylinder, representing the sensitive region of the detector, was filled evenly with the amount ^{235}U that is present on the sensitive layers according to the detector documentation. The remaining parts of the detector body were represented by an air cladding on the top and the bottom of the sensitive region. The effect of this homogenization is expected to have a small effect on the simulated detection efficiency.

Due to the above two simplifications, a difference is expected between the simulated and the measured detection rates. Moreover, the difference in the doubles rate is anticipated to be larger than in the case of the singles rate, since the former is more sensitive to the parameters of both the source and the detectors. However, the significance of this difference is not relevant, since the simulations were used only to design the measurement; conclusions on the applicability of the method will be drawn by comparing measured values.

5.4   Detectors and data acquisition system

Figure 5.6 shows the layout of the detection system. The output signal of the neutron detector is sent to a high-frequency pre-amplifier. The amplified voltage signal went through two paths. On one hand, it was sent to a high-resolution A/D converter to produce a sampled (digitized) continuous signal. On the other hand, it was submitted to a chain containing an amplifier, a discriminator and a counter to create a time series representing the times of detections. Both data sets were recorded into a binary file on the computer. In the following each element of this chain is described in detail.

For neutron detection Westinghouse WL-8073 type *dual range fission chambers* were used [89]. The outer casing of the detector is a cylindrical aluminum tube of height $9.75\,\mathrm{in}$ ($\approx 248\,\mathrm{mm}$) and diameter $2\,\mathrm{in}$ ($\approx 51\,\mathrm{mm}$). The filling gas is Argon-Nitrogen mixture at $760\,\mathrm{mmHg}$ ($\approx 101.3\,\mathrm{kPa}$) pressure. The neutron sensitive fissile deposit consists of $\mathrm{U_3O_8}$ compound enriched to more than $90\,\%$ in ^{235}U. The surface density of the deposit is $2\,\mathrm{mg/cm^2}$ whereas its total mass is $1.68\,\mathrm{g}$. No information is available
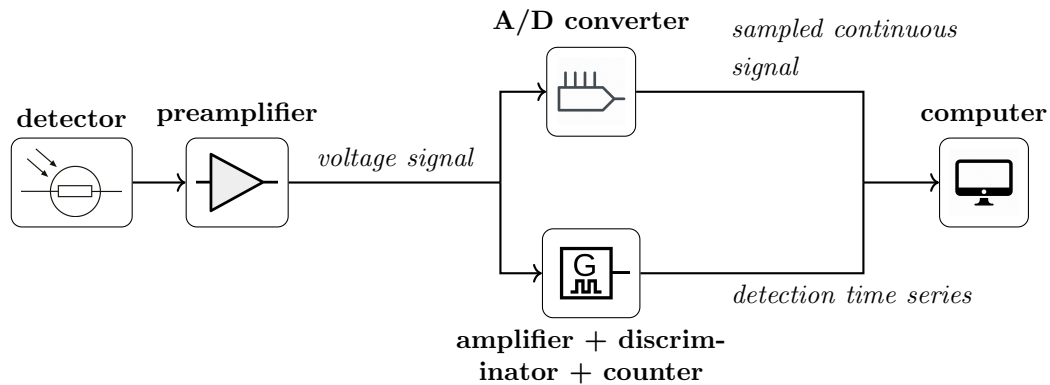
Figure 5.6: The layout of the detection and data acquisition chain.

on the structure (number, shape and size) of the electrodes and fissile coatings. This type of detector can be operated both as a counter (for low flux levels) or as an ionization chamber (for high flux levels). The nominal operating voltage is 300 V as a counter and 300 V–1000 V as an ionization chamber. During the measurements the detectors were operated at 300 V. At this value the total thermal neutron sensitivity is $0.7 \, \text{counts/neutron/cm}^2$, whereas pulses have an average amplitude of 0.2 mV as well as an average rise time of 0.2 μs.

The output signal of each detector is sent to an associated pre-amplifier. In order to suit the needs of the present (and future) measurements, six pre-amplifiers were designed and built [90] at the BME Institute of Nuclear Techniques of which four were used in the measurements. The pre-amplifiers produce a voltage signal ranging between -1 and 1 V. They have a small time constant (compared to the charge collection time of the detector), hence the shapes of the amplified voltage pulses reflect the shapes of the current pulses in the detector.

The amplified signal of the detector was sampled, digitized and recorded by a Red Pitaya STEMLab 125-14 multifunction instrument [91]. Each such device has two analogue input channels; hence, in order to process the signals of all four detectors simultaneously, two instruments were used in the measurements. The STEMLab 125-14 instrument is equipped with a high-performance analog-to-digital (A/D) converter, which provides a maximal sampling rate of 125 million samples per second (corresponding to a 8 ns maximal time resolution) and a fix 14 bit digital resolution. The device comes with an integrated field-programmable gate array (FPGA) unit which stores the digitized signal values in the internal RAM. A user-written C program is responsible for transferring the data from the RAM to an I/O device for long-time storage. To facilitate the data transfer, the instrument is equipped with a micro SD slot, a USB 2.0 port, a 1 GB ethernet port as well as with a WIFI dongle slot. In our case, we stored the signals in the (compressed) `time resolved signal` file format (described in Section 4.1.1) on a SanDisk Extreme Pro micro SD card with 32 GB capacity and 95 MB/s writing speed.

In order to obtain the times of individual pulses, the pre-amplified signals were also fed to a chain consisting of an amplifier, a single channel analyser and counter; this latter was a National Instruments myRIO device.

5.5 Recording the signals

As Table 5.2 shows, the detection rates are expected to be small in both measurement configurations. The low detection rate suggests that a rather long measurement time (lasting several hours) is required to achieve good statistics, especially in the case of the doubles rates. A nearly 14 hour-long measurement was performed in both configurations.

In the case of the continuous detector signals, the time resolution should be fine enough to resolve individual pulses. As seen from Figure 5.11, the characteristic width of the recorded pulses is around $10\,\mu s$. For this reason, a $40\,ns$ time resolution was used, samples such a typical pulse at 250 points. As mentioned at the end of the previous section, the signals were stored in the compressed `time resolved signal format`. Recall from Section 4.1.1 that this format maintains a value called `base line`, which represents an average value of the signal when there are no pulses. As a consequence, the sections between pulses can be represented in the stored signal by their lengths and the base line. The base lines determined for the four detectors in the two measurement configurations are given in Table 5.3. From this point, every voltage value presented in this chapter will be given with respect to the baseline.

Table 5.3: Base lines of the detector signals in the two measurement configurations.

| detector | base line value (mV) | |
	Cf	Cf+U
A	36.7	37.0
B	7.4	7.5
C	30.1	30.0
D	10.5	10.5

A simple algorithm was designed and implemented on the FPGA unit of the Red Pitaya instrument to transform the recorded voltage stream into the compressed `time resolved signal format`. The procedure utilizes the fact that sections separating individual pulses comprise mainly electronic noise, which is low in amplitude. The implementation of the algorithm is illustrated on Figure 5.7 using a simulated section of a detector signal, and is explained in the following. For each detector, a threshold value was chosen in a way that the fluctuating background does not cross it but the neutron induced pulses do. The threshold value was determined on-site by performing a short test measurement; the values applied are listed in Table 5.4 for all four detectors in both measurement configurations. The FPGA unit stored each digitized signal value in an internal memory buffer but it transferred to the RAM only those parts of the signal which were above the predefined threshold value together with their close neighbourhood. More precisely, whenever 3 consecutive values exceeded the threshold, the 43 preceding values (40 values under the threshold and 3 exceeding it) were saved to the RAM. Each subsequent value was saved to RAM until 250 consecutive values did not exceed the threshold. This means that aside from the part that is above the threshold, $1.6\,\mu s$ was recorded from each pulse before crossing the threshold upwards, and $10\,\mu s$ after crossing the threshold downwards. This time span is large enough to contain the

whole pulse emerging from the background including its rising and decaying section.
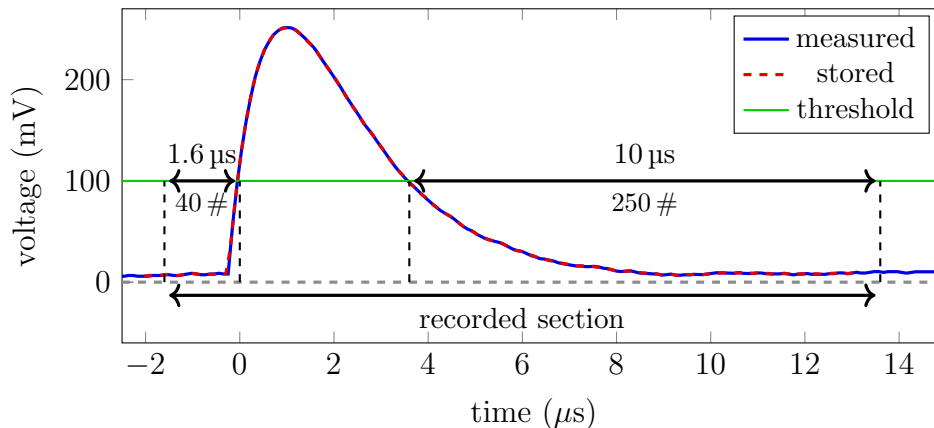
Figure 5.7: Illustration of the signal compression technique.

Table 5.4: Threshold values applied to discriminate the background fluctuation from the useful parts of the signals.

detector	threshold (mV)	
	Cf	Cf+U
A	65.8	66.2
B	70.4	71.4
C	61.4	65.8
D	70.8	71.0

The myRIO device, which was used as a dedicated counter in the data acquisition chain (see Figure 5.6) provided readily usable time series data for analysis. However, a similar time series data has been produced by postprocessing the recorded continuous signals as well. A simple computer program has been written, that implements a discriminator–counter logic: given a threshold value, the programs cans through the continuous signals and determines the times of level crossings. The pulse counting analysis have been performed using both sets of detection times. The reason for creating the second set is twofold. First, it ensures that the continuous signal analysis and pulse counting is performed on the exact same signal, which makes the two results more comparable. Second, when the detection times are produced from recorded continuous signals, it allows us to perform post processing steps on the signal, before submitting it to the discriminator–counter logic. As we shall see later, better results could be achieved using this second set of times.

5.6 The characteristics of the recorded signals

An inspection of the recorded continuous detector signals has revealed that it consists of short signals sections, separated by compressed parts, which in the majority of

the time contain a single pulse. Figure 5.8 shows examples of recorded sections, which show pulses that might easily be induced by different particles. The two pulses in the first row have large amplitudes hence they are likely been induced by neutrons; the other two in the second row have small amplitudes and might be induced by either an α or a γ particle.
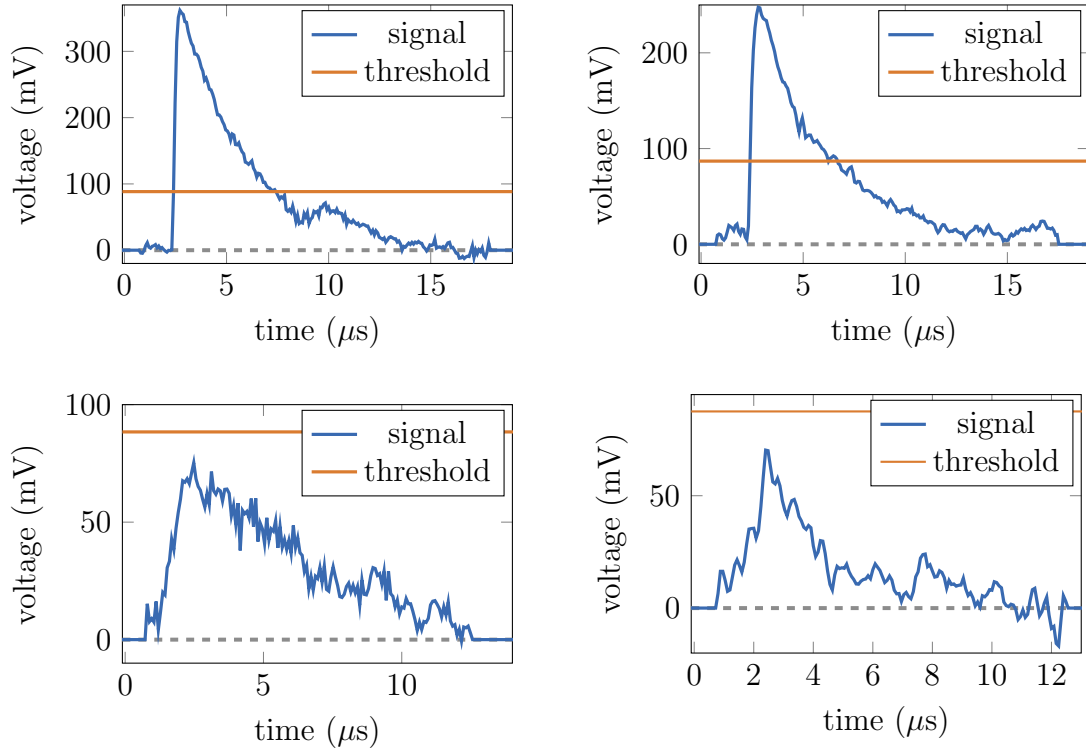
Figure 5.8: Examples of recorded pulses. The pulses in the first row have larger amplitudes and are likely induced by neutrons. The pulses in the second row have smaller amplitudes and might be induced by α or γ particles. The orange lines represent the threshold values used to discriminate against non-neutron pulses when calculating the average neutron induced pulse.

In order to derive a detection time series data from the continuous signals, an appropriate threshold level needs to be used that can discriminate against non-neutron pulses. Additionally, as we will see later, it was necessary to remove small pulses even from the continuous signals used for moment analysis to get values of the detection rates that compare well with reference values obtained with pulse counting. In order to determine the suitable threshold values, the pulse height distribution of the recorded signals has been estimated. As an illustration, Figure 5.9 shows the pulse height distribution observed in the signals of the detector A and B in the Cf configuration. One can see that the vast majority of the pulses have small amplitudes somewhere in the range of 70–90 mV. The threshold values were selected by choosing the inflection point in the distribution (shown as dashed line on the Figure). The list of threshold values can bee seen in Table 5.5.

(a) Detector A.
(b) Detector B.
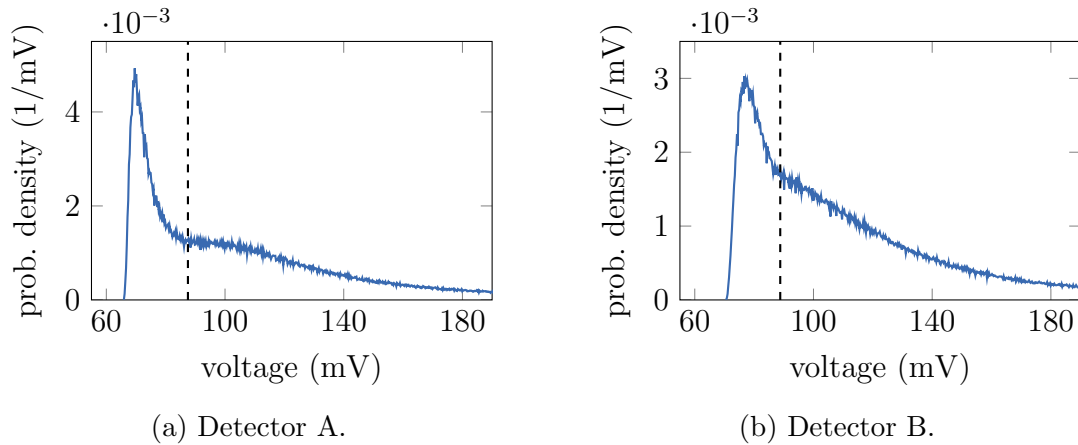
Figure 5.9: The pulse height distribution observed in the signals of detector A and B in the Cf measurement configuration. The dashed lines represent the threshold values used to discriminate against non-neutron pulses when calculating the average neutron induced pulse.

Table 5.5: Threshold values used to discriminate against non-neutron pulses when calculating the average neutron induced pulse.

detector	threshold (mV)	
	Cf	Cf+U
A	87.5	87.2
B	88.8	93.6
C	79.6	86.9
D	70.8	71.0

5.7   Estimation of the calibration factors

Whether we perform multiplicity counting by analysing continuous signals or by counting discrete pulses, the detection rates are not the quantities we directly measure. In the case of continuous signal analysis, the primary measured quantities are the moments of the signals which, as described in Section 3.5, can be converted to detection rates in the knowledge of the factor $\langle a \rangle I$, the area under a single neutron impulse. In the case of discrete pulse counting, one needs the doubles and triples gate fraction factors, denoted as f_d and f_t in Equations (2.21) and (2.22), to compensate for losses of correlated counts in the doubles and triples detection rates originating from the finiteness of the counting window.

Because our aim is to compare the detection rates obtained with these two approaches, it is important that we calculate their correct values. In the following, the estimation of the gate fraction factors as well as the are under the neutron pulses is described.

5.7.1   The gate fractions

There are several ways of estimating the gate fractions [1]. Here, a semi-empirical approach is chosen. Equation 2.20 provides an analytical formula for a quantity f, which is related to the doubles and triples gate fractions as $f_d = f$ and $f_t = f^2$. f is expressed as a function of the counting gate width τ_{gate}, the predelay τ_{pre} and the die-away time θ. The first two are parameters of the multiplicity counter and are chosen freely; their values used in this measurement will be given later in Section 5.8. The die-away time is, however, a property of the experimental set-up and needs to be determined either by measurement or by simulation.

It is generally known that the decay of the Rossi-alpha distribution of the detector counts is closely related to the die-away time [1]. Since the Rossi-alpha distribution characterizes the covariance function of the detector counts, we shall use its continuous equivalent, the covariance function of the continuous detector signals, to estimate the die-away time. Assuming a pure exponential die-away time and an exponentially decaying pulse shape with decay parameter θ_{pulse}, the concrete form of the covariance function can be calculated using the general expression (A.3.2), and it takes the form

$$\text{Cov}(s) = c \left(\theta \, e^{-|s|/\theta} - \theta_{\text{pulse}} \, e^{-|s|/\theta_{\text{pulse}}} \right). \tag{5.1}$$

By fitting this function to a measured cross covariance function of two signals, the θ die-away time can be determined and can be inserted into Equation 2.20 to give an estimate of f. Table ?? shows the value of f.

5.7.2   The area under the pulse

The estimation of the area $\langle a \rangle I$ under neutron induced pulses comes with two difficulties. First, contrary to the theoretical model introduced in Chapter 3, not every neutron induced has the same shape; as we have seen in Section 5.6, the shapes of the individual pulses shows a great variation. Second, pulses recorded by the detector might be induced by particles other than neutrons (most likely by alpha particles in

Table 5.6: The list of the die-away times and the doubles gate fractions used in Section 5.8.2 for the correction of doubles detection rates obtained from pulse counting.

detector pair	θ (µs)		f (-)	
	Cf	Cf+U	Cf	Cf+U
A–B	176.26	108.66	0.945	0.912
C–D	109.87	119.51	0.913	0.920
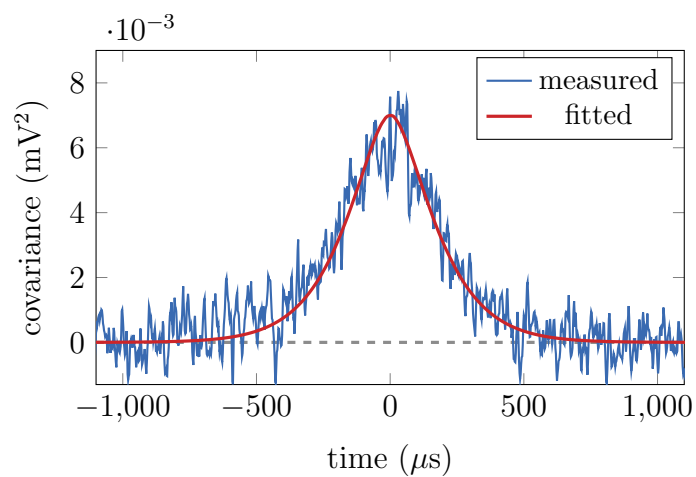
Figure 5.10: Illustration of fitting a function of the form (5.1) to the measured cross covariance function of two detector signals.

the case of fission chambers). In fact, the pulse height distribution on Figure 5.9 shows that the majority of the recorded pulses have such a small amplitude.

For this reason, a simple procedure has been designed to provide an proper estimate of $\langle a \rangle I$. The procedure relies on the fact that the observed count rate was so low, that the majority of the recorded signal sections contained a single pulse only. A program has been written that takes a threshold value as an input parameter. Given a recorded signal, the program scans through it and selects every section on which the signal crosses the predefined threshold value. The recorded sections are then aligned together in a way that the times they cross the threshold coincides. Finally, the corresponding points of the sections are averaged to form a average impulse. Because of the discrimination against low amplitude pulses, this average pulse makes a good approximation of neutron induced pulses. Figure 5.11 shows the average neutrons pulses of detectors A–D in the Cf measurement configuration determined with the above procedure. One can see that despite small differences, they are rather similar to each other.
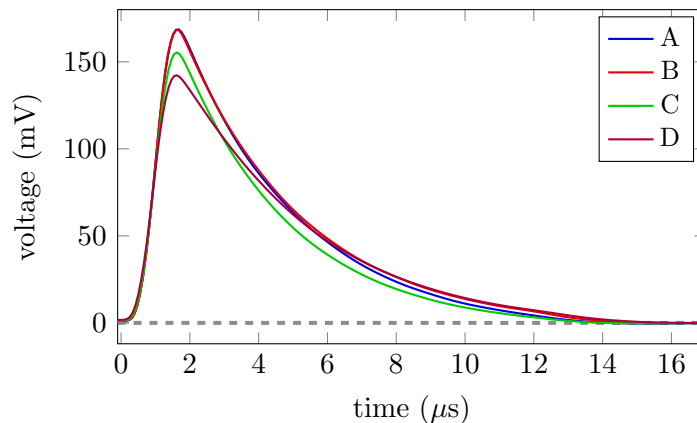
Figure 5.11: Average neutron pulses estimated from the signals of detectors A–D in the Cf measurement configuration.

In the possession of the average neutron pulses, it is now straightforward to calculate $\langle a \rangle I$ by integrating it numerically. The obtained integrals are listed in Table 5.7 for each detector in both measurement configurations. Actually, two sets of values are shown in the table. One set, labeled as original, was obtained from the signals without altering them. The second set, labeled as smoothed was obtained by smoothing the original signals using a simple running average algorithm. Both values were used to recover the detection rates from the moments of the continuous signals and it was found that only the smoothed version was able to provide correct results. For this reason, results will be provided only using this second set of integrals.

5.8   Estimation of the detection rates

In order to estimate the detection rates with pulse counting, a simple program has been written that implements the logic of the multiplicity shift register, described in Section 2.3.7. This program has been used to analyse the detection time series obtained both from the myRIO counter device as well as that created by the computer program

Table 5.7: Integrals of the average neutron pulses in the two measurement configurations.

case	detector	pulse integral (mV s)	
		Cf	Cf + U
original	A	$4.30 \cdot 10^{-3} \pm 1.7 \cdot 10^{-7}$	$4.30 \cdot 10^{-3} \pm 1.8 \cdot 10^{-7}$
	B	$4.34 \cdot 10^{-3} \pm 1.6 \cdot 10^{-7}$	$4.56 \cdot 10^{-3} \pm 1.7 \cdot 10^{-7}$
	C	$3.73 \cdot 10^{-3} \pm 1.4 \cdot 10^{-7}$	$3.91 \cdot 10^{-3} \pm 1.6 \cdot 10^{-7}$
	D	$3.83 \cdot 10^{-3} \pm 1.3 \cdot 10^{-7}$	$3.93 \cdot 10^{-3} \pm 1.4 \cdot 10^{-7}$
smoothed	A	$4.47 \cdot 10^{-3} \pm 1.8 \cdot 10^{-7}$	$4.49 \cdot 10^{-3} \pm 1.8 \cdot 10^{-7}$
	B	$4.60 \cdot 10^{-3} \pm 1.7 \cdot 10^{-7}$	$4.83 \cdot 10^{-3} \pm 1.9 \cdot 10^{-7}$
	C	$3.90 \cdot 10^{-3} \pm 1.5 \cdot 10^{-7}$	$4.18 \cdot 10^{-3} \pm 1.7 \cdot 10^{-7}$
	D	$4.12 \cdot 10^{-3} \pm 1.4 \cdot 10^{-7}$	$4.18 \cdot 10^{-3} \pm 1.4 \cdot 10^{-7}$

from the continuous signals. The detection rates were estimated with a $\theta_{\mathrm{gate}} = 10\,\mathrm{ms}$ gate width parameter and a $\theta_{\mathrm{pre}} = 10\,\mathrm{\mu s}$ predelay parameter.

The moments of the continuous detector signals have been calculated with the analysis tool described in Section 4.1.3. During analysis, the signals have been divided into sections of size $N = 200000$; with the 48 ns time resolution, this corresponds to a length of $T = 8\,\mathrm{ms}$ in time. From the moments, the detection rates were obtained using the expressions in Section 3.5.

Here, we note that the triples rate could not be estimated not only because the detection efficiency in the system is low, but also because of hardware limitations. The estimation of the covariance or bicovariance functions of the signals requires that they are perfectly synchronized in time. This synchronization is ensured when the signals are recorded by the same A/D converter. However, the Red Pitaya devices we used have only two inputs, which means that only two pairs of signals, namely A–B and C–D were synchronized. As a consequence, the calculation of the bicovariance function of three signals was not possible at all. But even in the case of covariance function, it could be estimated only for the two paris A–B and C–D.

5.8.1 Singles rate

The singles detection rate was estimated for all four detectors separately. The results are summarized in Table 5.8. The third and fourth columns contain the reference singles rates obtained with pulse counting by the myRIO device as well as by the multiplicity counting software. It is seen that in the majority of cases, the two results are close to each other. A significant difference can be observed in the estimated rates of detector D in both configurations as well as in the rate of detector C in the Cf configuration. The analysis of the pulse height distribution of the unaltered continuous signals has revealed the reason behind the deviation observed in the case of detector D: the signal of this detector was extremely noisy. As a result, false counts were registered by the myRIO device, whereas the noise level of the signal analysed by the software has been reduced by smoothing. The measured detection rates are 5–15 % smaller than the values predicted by the simulations in 5.3.

The fifth and sixth columns contain singles rates extracted from the mean value of the detector signals. The rates in the sixth column, labeled as "unfiltered", were obtained from the raw, unaltered continuous signals and are about 20–30 % larger, than the reference values. The deviation is clearly a consequence of the small amplitude pulses induced by alpha particles: these increase the estimated singles rate by inevitably contributing to the mean value of the signal, however, they are discriminated against in the process of pulse counting.

As it was suggested in Section 4.2.5, the contribution of a constant non-neutron background can be easily compensated by performing a background measurement without the neutron source and estimating the contribution of the background to the mean value. Unfortunately, no such background measurement has been made during the experiment. There is, however, an alternative solution which, which is based on the same principle that was used to determine the integral of the neutron induced pulses. Recalling that almost all recorded section in the signal contained a single pulse only, one can remove the small amplitude pulses by scanning the signal using a threshold value and dropping every section where the signal does not cross the threshold value. Using the threshold values listed in Table 5.5, a second set of continuous signals have been produced and analysed as well. The singles rates obtained from this set are shown in the sixth column of Table 5.8 under the label "filtered". One can immediately see that they are much closer to the reference values than the unfiltered versions. Nevertheless, they are still systematically higher by 1–10 %, which indicates that not all non-neutrons pulses have been removed. It is anticipated that in the possession of a background measurement, a more effective correction can be made, as it was demonstrated with simulated signals in Section 4.2.5.

In general, one can observe that there is no significant difference between the singles rates measured in the two configurations, as it was expected based on the simulation results presented in Section 5.3.

Table 5.8: Estimated values of the singles rates obtained from pulse counting and from the mean value of the detector signal.

configuration	detector	singles rate (s^{-1})			
		discrete pulse counting		continuous signal analysis	
		NI myRIO	program	unfiltered	filtered
Cf	A	17.019 ± 0.018	17.071 ± 0.018	25.253 ± 0.704	18.282 ± 0.704
	B	17.029 ± 0.018	17.837 ± 0.018	26.714 ± 0.837	19.720 ± 0.838
	C	19.791 ± 0.019	19.759 ± 0.019	31.629 ± 0.920	21.316 ± 0.920
	D	27.391 ± 0.022	21.584 ± 0.020	24.199 ± 0.777	24.198 ± 0.777
Cf+U	A	17.370 ± 0.018	17.475 ± 0.018	26.483 ± 0.806	18.753 ± 0.806
	B	17.627 ± 0.018	16.211 ± 0.018	25.004 ± 0.775	18.047 ± 0.775
	C	19.949 ± 0.019	16.823 ± 0.018	29.881 ± 0.964	18.837 ± 0.964
	D	27.440 ± 0.023	21.793 ± 0.020	24.154 ± 0.800	24.152 ± 0.800

5.8.2 Doubles rate

The doubles detection rate was estimated only for the detector pairs A–B and C–D. The results are summarized in Table 5.9. The columns of the table have the same meaning as in the case of the singles rate. Accordingly, columns three and four contain doubles rates estimated with pulse counting on the detection time series data produced by the myRIO device as well as by the program analysing the continuous signals. For detector pair A–B, the values agree within statistical uncertainty. There is, however, a significant difference in the values for detectors C–D. Clearly, this is the result of the large noise levels observed in detector D, which also caused the extremely large value in the singles rate. However, one can notice in the fourth column that the application of the noise filtering decreases the observed value of the doubles rate.

Column five shows values obtained from the moments of the raw, unaltered continuous signals. Just as in the case of the singles rate, the values shown here are systematically larger than the reference values. However, when the low amplitude pulses are filtered out from the signal, the obtained detection rates become identical with the reference values within statistical uncertainty, as it can be observed in the sixth column of the table. The explanation of this phenomenon is, however, less obvious than in the case of the singles rate. The simulations in Sections 4.2.4 and 4.2.5 show that the doubles estimation is insensitive to the presence of both a Gaussian white noise as well as a Poissonian pulse source (like the alpha background of the fission chamber). The observed difference between the values of columns five and six therefore indicates that the components removed from the signal have a nonzero covariance, that is, they are not pure white noise or pulses from the alpha background. A closer investigation of this effect might be the topic of a future research activity.

Table 5.9: Estimated values of the doubles rates.

configuration	detector	doubles rate (s^{-1})			
		discrete pulse counting		continuous signal analysis	
		NI myRIO	program	uncorrected	corrected
Cf	A–B	0.319 ± 0.018	0.291 ± 0.019	0.432 ± 0.009	0.305 ± 0.006
	C–D	0.540 ± 0.027	0.451 ± 0.023	0.428 ± 0.009	0.420 ± 0.008
Cf+U	A–B	0.304 ± 0.020	0.309 ± 0.019	0.433 ± 0.009	0.304 ± 0.007
	C–D	0.538 ± 0.028	0.383 ± 0.022	0.467 ± 0.011	0.376 ± 0.008

5.9 A final remark

We shall end this Chapter by showing an example of the cross covariance function of the signals of detectors A and B. Figure 5.10 shows two versions of this function: one was obtained with the standard pulse counting technique, while the other one was calculated from the continuous signals of the detectors; they show a good agreement. The significance of this result becomes apparent when one considers the physical content of the covariance function: its value at time t quantifies the correlation between

detection events that are at a distance t. The fact that such an information on discrete detection events can be recovered from a continuous process, where no discrete events appear explicitly, is somewhat remarkable.
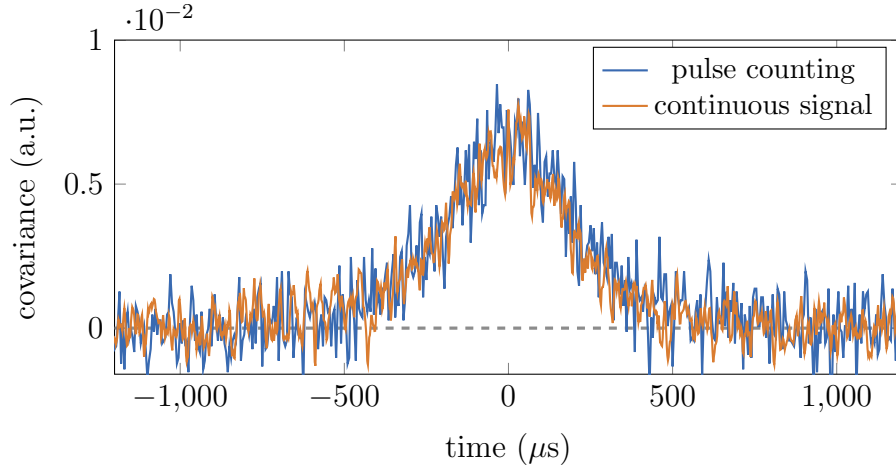
Figure 5.12: The cross covariance functions of the signals of the detector pair A–B obtained both by continuous signal analysis as well as by pulse counting.

Chapter 6

Summary

The topic of this thesis is the development and investigation of an alternative version of neutron multiplicity counting, which – contrary to the traditional approach with pulse counting – is based on the analysis of the continuous voltage signals of neutron detectors (primarily fission chambers). The motivation for creating this new form of the measurement is that the practical applicability of the traditional method is limited to low count rates due to dead time losses arising in the counting circuits. Being inherently free from this type of dead time, the new method can be an effective tool for measuring spent nuclear fuel, which usually comes with extremely high neutron and gamma count rates.

The thesis is divided into two parts. The first part, covered by Chapter 2, gives a brief overview on nuclear safeguards and material measurement techniques in general, and provides a detailed description of the traditional form of neutron multiplicity counting including its theory as well as certain aspects of its practical implementation. A mathematical formalism for describing continuous detector signals (on which the newly proposed version of multiplicity counting is based) is summarized here as well. The second part, covered by Chapters 3–5, discusses three aspects of the establishing the new technique.

Chapter 3 describes the theoretical background of the method. The evolution of the theoretical model went through three stages. In the first stage, certain low-order one-point moments (including the mean, and covariance) of the signals have been calculated by assuming that emitted neutrons are detected instantly. It was shown that the singles, doubles and triples detection rates can be recovered from the measured one-point moments. In the second stage, the same moments have been recalculated by assuming that every neutron is detected with a random time delay with respect to its emission. It was found that doubles and triples detection rates, in this case, can be recovered only when the average delay is shorter than the length of the voltage pulses, which occurs in fast detection systems. In the third stage, while maintaining the assumption of the delayed detection, certain two- and three-point moments (including the covariance and bicovariance functions) of the signals are calculated. It is shown that using these moments, the doubles and triples rates can be recovered at arbitrarily large time delays, hence in thermal detection systems as well. Finally, formulas are presented that express the singles, doubles and triples detection rates with the appropriate moments calculated from the continuous signals of a large detector array.

Chapter 4 presents a computational study for assessing the performance of the method. In order to provide a unified way of storing and transferring continuous detector signals (simulated and measured ones as well) on a computer, a dedicated file format has been defined. A program has been written for simulating detector signals in a multiplicity counting measurement. The program allows the user to specify the neutron emission statistics of the sample as well as the characteristics of the pulse induced by individual neutron detections. Besides that, another program has been created that can estimate the moments of recorded detector signals. The behaviour of the two programs have been verified by simulating a set of signals and comparing the recovered detection rates with analytical reference values. Then a large set of measurements have been simulated and analyzed in order to assess the impact of various parameters (the measurement time, the detection efficiency, the electronic noise as well as the non-neutron pulses) on the performance of the method. It was found that while the measurement time and the detection efficiency have a strong impact on the accuracy of the estimated detection rates, the effect of the electronic noise on the singles and doubles rate estimates and the effect of non-neutron pulses on the doubles rate estimate is negligible. Although non-neutron pulses introduce a bias into the singles estimate, this can easily be corrected with a background measurement. Finally, the performance of the traditional and the new method of multiplicity counting is compared by simulating measurements at different sample emission intensities and estimating the detection rates both from the moments of the continuous signals as well as with the pulse counting approach. It was found that at large intensities, the traditional approach underestimates the detection rates due to dead time losses, whereas the values obtained with the new method agree with the reference analytic values.

Chapter 5 reports on experimental activities for demonstrating the practical use of the method. A measurement set-up, containing four fission chambers, a ^{252}Cf source and ^{235}U plates, has been designed and built at the KUCA facility of the Kyoto University. Monte Carlo simulations were performed to optimize the arrangement of the elements of the set-up. An FPGA based fast data acquisition system was assembled to record the voltage signals of the detectors with 8 ns time resolution. The appropriate moments of the signals were estimated with the software described in Chapter 4 and the singles and doubles detection rates were calculated using the formulas presented in Chapter 3. The triples rates could not be estimated due to the low detection efficiency of the measurement set-up. To serve as a reference, the detection rates were estimated with a traditional pulse counting approach as well. By comparing the results, it has been shown that the new method is able to recover the singles and doubles rates from the signals.

Thesis propositions

The new scientific results presented in the thesis can be summarized in the form of the following propositions:

Proposition 1. I have upgraded the preliminary theory of a new form of neutron multiplicity counting, which is based on estimating the one-point (in time) moments of continuous detector signals. While the original model assumed that neutrons are detected instantly after their emission, I have introduced a random time delay before the detection to account for the migration of neutrons in the system. I have derived expressions for several one-point moments (including the mean value and the covariance) using a master equation formalism. Based on analytic considerations, I have shown that the singles, doubles and triples rates in this upgraded model can be recovered from the one-point moments of the signals in fast detection systems, where the average time delay is short compared to the length of a typical voltage impulse, hence pulses generated by the same emission event tend to overlap in time. At the same time I have shown that in thermal detection systems, which are predominantly used for measurements and in which the average time delay is much larger than the length of a typical voltage impulse, the information on the doubles and triples rates vanishes from the one-point moments of the signal, because pulses generated by the same emission event are dispersed in time. As a result, in such systems only the singles rate can be retrieved [P1–P3, P8].

Proposition 2. I have further extended the theory described in Proposition 1. Besides using the one-point moments of the detector signals, I have introduced the use of their two- and three-point (in time) moments as well, because they are able describe the temporal correlations between different points of the signals. I have derived expressions for several two- and three-point moments (including the covariance function and the bicovariance function) using a master equation formalism. I have calculated the integrals of these moments with respect to their parameters and I have shown that their values (with one exception) are independent of the time delay, because the integration process brings temporally dispersed pulses generated by the same emission event into overlap. As a consequence, I was able to show based on analytic considerations that – contrary to the one-point moments – the information on the doubles and triples rates does not vanish from the integrals of the two- and three-point moments, even when the average time delay becomes large compared to the length of the voltage pulses. As a result, using the two- and three-point moments the doubles and triples rates can be recovered even in thermal detection systems. [P4, P8]

Proposition 3. I have established a practical procedure for extracting the singles, doubles and triples detection rates from the recorded continuous signals of a large array of detectors. I have designed a numerical algorithm for estimating the one-, two- and three-point (in time) moments, described in Propositions 1 and 2, of the recorded continuous signals in an efficient way. Using the expressions of these moments provided by the theoretical models of Propositions 1 and 2, I have derived a set of equations that express the singles, doubles and triples detection rates with the moments estimated from all possible combinations of the signals, thus fully utilizing the information available in them. By using this procedure to analyse simulated detector signals, I have shown that it is capable of producing estimates for the singles and doubles detection rates and that these estimates agree with predictions from the theory. The ability to recover the triples rate could not be confirmed due to the numerical instability of the estimator. [P5–P7, P9–P11]

Proposition 4. By analysing a large number of simulated measurements using the procedure described in Proposition 3, I have investigated the effect of the following parameters on the value and/or accuracy of the estimated detection rates: the measurement time, the detector efficiency, the amplitude of an electronic white noise as well as the presence of small-amplitude parasitic pulses induced by a non-neutron source with Poisson statistics. I have shown that the measurement time and the detection efficiency have a strong impact on both the value and the relative uncertainty of the singles and doubles estimates; the effect of the electronic noise on both parameters is practically negligible; non-neutron pulses do not affect the doubles rate, but introduce a bias into the singles estimate which can, however, be easily corrected for. Finally, I have demonstrated that while the traditional pulse counting approach underestimates the values of the singles and doubles rates at large count rates due to dead time losses, values provided by the new method agree with predictions from the theory. As a result, the new method is a viable alternative of the traditional procedure. [P10, P11]

Proposition 5. In order to demonstrate the practical use of the new method of neutron multiplicity counting specified in Propositions 1 and 2, I have designed and analysed a measurement. Among other elements, the measurement set-up contained four thermal fission chambers and a spontaneously fissioning ^{252}Cf sample. I have performed Monte Carlo simulations to find an optimal arrangement that provides the highest detection rates. Using the procedure described in Proposition 3, I have analysed the measured detector signals to estimate the singles and doubles rates; the triples rate was not determined due to the low detection efficiency of the set-up as well as to the hardware limitations of the data acquisition system. Reference values of the detection rates were obtained from the same measurement using the traditional pulse counting approach. By comparing the two sets of values, I have shown that the singles rate received from the analysis of continuous signals slightly overestimates the reference values due to pulses generated by the inherent alpha background of the fission chambers. On the other hand, the agreement in the case of the doubles rates is satisfactory. [P5–P7, P9–P11]

Bibliography

[1] N. Ensslin, W. C. Harker, M. S. Krick, D. G. Langner, M. M. Pickrell, and J. E. Stewart, "Application guide to neutron multiplicity counting," *Los Alamos Report LA-13422-M*, 1998.

[2] S. Croft and A. Favalli, "Dead time corrections for neutron multiplicity counting," *Nuclear Instruments and Methods in Physics Research Section A: Accelerators, Spectrometers, Detectors and Associated Equipment*, vol. 686, pp. 115–116, 2012.

[3] D. Reilly, N. Ensslin, H. Smith Jr, and S. Kreiner, *Passive nondestructive assay of nuclear materials*, ch. "The Origin of Neutron Radiation". Washington DC, United States: Nuclear Regulatory Commission, Office of Nuclear Regulatory Research; Los Alamos National Lab., NM (United States), 1991.

[4] D. Henzlova, R. Kouzes, R. McElroy, P. Peerani, M. Aspinall, K. Baird, A. Bakel, M. Borella, M. Bourne, L. Bourva, *et al.*, "Current status of helium-3 alternative technologies for nuclear safeguards," tech. rep., Los Alamos National Lab.(LANL), Los Alamos, NM (United States), 2015.

[5] L. Pál, I. Pázsit, and Zs. Elter, "Comments on the stochastic characteristics of fission chamber signals," *Nuclear Instruments and Methods in Physics Research Section A: Accelerators, Spectrometers, Detectors and Associated Equipment*, vol. 763, pp. 44–52, 2014.

[6] *The Evolution of IAEA Safeguards*, no. 2 in International Nuclear Verification Series, (Vienna, Austria), International Atomic Energy Agency, 1998.

[7] J. Doyle, *Nuclear safeguards, security and nonproliferation: achieving security with technology and policy.* Elsevier, 2011.

[8] "Treaty on the Non-Proliferation of Nuclear Weapons (NPT)." URL: `https://www.un.org/disarmament/wmd/nuclear/npt/text/` (accessed: March, 2021).

[9] *IAEA Safeguards Glossary: 2001 Edition*, no. 3 in International Nuclear Verification Series, (Vienna, Austria), International Atomic Energy Agency, 2002.

[10] J. Vidaurre-Henry, *Handbook on International Nuclear Safeguards*. Integrated Support Center for Nuclear Nonproliferation and Nuclear Security, 2016.

[11] T. Gozani, "Active nondestructive assay of nuclear materials: principles and applications," tech. rep., Science Applications, Inc., Palo Alto, CA (USA); Monsanto Research Corp., 1981.

[12] R. Dierckx and W. Hage, "Neutron signal multiplet analysis for the mass determination of spontaneous fission isotopes," *Nuclear Science and Engineering*, vol. 85, no. 4, pp. 325–338, 1983.

[13] N. Ensslin, "Active neutron multiplicity counting," *Los Alamos Report LA-UR-07-140*, 1998.

[14] S. Croft, L.-A. Bourva, D. Weaver, and H. Ottmar, "Effective mass of ^{240}Pu, ^{238}Pu and ^{242}Pu in relation to passive neutron coincidence and multiplicity counting," *Journal of Nuclear Materials Management*, pp. 10–19, 2001.

[15] L. G. Evans, B. Goddard, W. S. Charlton, and P. Peerani, "An analysis technique for active neutron multiplicity measurements based on first principles," tech. rep., Los Alamos National Lab.(LANL), Los Alamos, NM (United States), 2012.

[16] B. Goddard, W. Charlton, and P. Peerani, "First principle active neutron coincidence counting measurements of uranium oxide," *Nuclear Instruments and Methods in Physics Research Section A: Accelerators, Spectrometers, Detectors and Associated Equipment*, vol. 739, pp. 1–5, 2014.

[17] B. Goddard, S. Croft, A. Lousteau, and P. Peerani, "Evaluation of Am–Li neutron spectra data for active well type neutron multiplicity measurements of uranium," *Nuclear Instruments and Methods in Physics Research Section A: Accelerators, Spectrometers, Detectors and Associated Equipment*, vol. 830, pp. 256–264, 2016.

[18] I. Pázsit, A. Enqvist, and L. Pál, "A note on the multiplicity expressions in nuclear safeguards," *Nuclear Instruments and Methods in Physics Research Section A: Accelerators, Spectrometers, Detectors and Associated Equipment*, vol. 603, no. 3, pp. 541–544, 2009.

[19] M. M. Ferrer, P. Peerani, M. R. Looman, and L. Dechamp, "Design and performances of the scrap neutron multiplicity counter," *Nuclear Instruments and Methods in Physics Research Section A: Accelerators, Spectrometers, Detectors and Associated Equipment*, vol. 574, no. 2, pp. 297–314, 2007.

[20] H. O. Menlove, "HENC performance evaluation and plutonium calibration," *Los Alamos Report, LA-13362-MS*, 1997.

[21] H. O. Menlove, "Manual for the epithermal neutron multiplicity detector (ENMC) for measurement of impure MOX and plutonium samples," *Los Alamos Report, LA-14088-M*, 2004.

[22] H. O. Menlove, "Manual for the portable handheld neutron counter (PHNC) for neutron survey and the measurement of plutonium samples," *Los Alamos Report, LA-14257-M*, 2005.

[23] J. L. Dolan, M. Flaska, A. Poitrasson-Riviere, A. Enqvist, P. Peerani, D. L. Chichester, and S. A. Pozzi, "Plutonium measurements with a fast-neutron multiplicity counter for nuclear safeguards applications," *Nuclear Instruments and Methods in Physics Research Section A: Accelerators, Spectrometers, Detectors and Associated Equipment*, vol. 763, pp. 565–574, 2014.

[24] D. A. Brown, M. Chadwick, R. Capote, A. Kahler, A. Trkov, M. Herman, A. Sonzogni, Y. Danon, A. Carlson, M. Dunn, *et al.*, "ENDF/B-VIII. 0: The 8th major release of the nuclear reaction data library with CIELO-project cross sections, new standards and thermal scattering data," *Nuclear Data Sheets*, vol. 148, pp. 1–142, 2018.

[25] D. B. Pelowitz, "MCNPX user's manual version 2.7. 0-LA-CP-11-00438," *Los Alamos National Laboratory*, 2011.

[26] K. Böhnel, "The effect of multiplication on the quantitative determination of spontaneously fissioning isotopes by neutron correlation analysis," *Nuclear Science and Engineering*, vol. 90, no. 1, pp. 75–82, 1985.

[27] W. Hage and D. M. Cifarelli, "On the factorial moments of the neutron multiplicity distribution of fission cascades," *Nuclear Instruments and Methods in Physics Research Section A: Accelerators, Spectrometers, Detectors and Associated Equipment*, vol. 236, no. 1, pp. 165–177, 1985.

[28] W. Hage and D. M. Cifarelli, "Correlation analysis with neutron count distributions in randomly or signal triggered time intervals for assay of special fissile materials," *Nuclear Science and Engineering*, vol. 89, no. 2, pp. 159–176, 1985.

[29] G. Grimmett and D. Stirzaker, *Probability and random processes*. Oxford university press, 2001.

[30] I. Pázsit and S. A. Pozzi, "Calculation of gamma multiplicities in a multiplying sample for the assay of nuclear materials," *Nuclear Instruments and Methods in Physics Research Section A: Accelerators, Spectrometers, Detectors and Associated Equipment*, vol. 555, no. 1-2, pp. 340–346, 2005.

[31] A. Enqvist, I. Pázsit, and S. Pozzi, "The number distribution of neutrons and gamma photons generated in a multiplying sample," *Nuclear Instruments and Methods in Physics Research Section A: Accelerators, Spectrometers, Detectors and Associated Equipment*, vol. 566, no. 2, pp. 598–608, 2006.

[32] A. Favalli, S. Croft, and P. Santi, "Point model equations for neutron correlation counting: Extension of böhnel's equations to any order," *Nuclear Instruments and Methods in Physics Research Section A: Accelerators, Spectrometers, Detectors and Associated Equipment*, vol. 795, pp. 370–375, 2015.

[33] S. Croft and A. Favalli, "Incorporating delayed neutrons into the point-model equations routinely used for neutron coincidence counting in nuclear safeguards," *Annals of Nuclear Energy*, vol. 99, pp. 36–39, 2017.

[34] I. Pázsit and L. Pál, "Multiplicity theory beyond the point model," *Annals of Nuclear Energy*, 2021. DOI: `https://doi.org/10.1016/j.anucene.2020.108119`.

[35] T. E. Harris *et al.*, *The theory of branching processes*, vol. 6. Springer Berlin, 1963.

[36] C. Dubi, T. Ridnick, I. Israelashvili, J. Bagi, and J. Huszti, "A method for the estimation of fissile mass by measuring the number of neutron signals within a specific time interval," *Nuclear Instruments and Methods in Physics Research Section A: Accelerators, Spectrometers, Detectors and Associated Equipment*, vol. 673, pp. 111–115, 2012.

[37] D. M. Cifarelli and W. Hage, "Models for a three-parameter analysis of neutron signal correlation measurements for fissile material assay," *Nuclear Instruments and Methods in Physics Research Section A: Accelerators, Spectrometers, Detectors and Associated Equipment*, vol. 251, no. 3, pp. 550–563, 1986.

[38] G. F. Knoll, *Radiation detection and measurement.* John Wiley & Sons, 2010.

[39] A. Enqvist, S. A. Pozzi, M. Flaska, and I. Pázsit, "Initial evaluation for a combined neutron and gamma ray multiplicity counter," *Nuclear Instruments and Methods in Physics Research Section A: Accelerators, Spectrometers, Detectors and Associated Equipment*, vol. 621, no. 1-3, pp. 493–497, 2010.

[40] T. H. Shin, M. Y. Hua, M. J. Marcath, D. L. Chichester, I. Pázsit, A. Di Fulvio, S. D. Clarke, and S. A. Pozzi, "Neutron multiplicity counting moments for fissile mass estimation in scatter-based neutron detection systems," *Nuclear Science and Engineering*, vol. 188, no. 3, pp. 246–269, 2017.

[41] A. Di Fulvio, T. Shin, A. Basley, C. Swenson, C. Sosa, S. Clarke, J. Sanders, S. Watson, D. Chichester, and S. Pozzi, "Fast-neutron multiplicity counter for active measurements of uranium oxide certified material," *Nuclear Instruments and Methods in Physics Research Section A: Accelerators, Spectrometers, Detectors and Associated Equipment*, vol. 907, pp. 248–257, 2018.

[42] K. Frame and et. al, "Development of a liquid scintillator neutron multiplicity counter (LSMC)," *Nuclear Instruments and Methods in Physics Research A*, vol. 579, p. 192, 2007.

[43] D. L. Chichester and et. al., "Statistical estimation of the performance of a fast-neutron multiplicity system for nuclear material accountancy," *Nuclear Instruments and Methods in Physics Research A*, vol. 784, p. 448, 2015.

[44] A. di Fulvio and et. al., "Passive assay of plutonium metal plates using a fast-neutron multiplicity counter," *Nuclear Instruments and Methods in Physics Research A*, vol. 855, p. 92, 2017.

[45] H. Menlove, J. Baca, M. Krick, K. Kroncke, and D. Langner, "Plutonium scrap multiplicity counter operation manual," tech. rep., Los Alamos National Lab., NM (United States), 1993.

[46] N. Dytlewski, M. Krick, and N. Ensslin, "Measurement variances in thermal neutron coincidence counting," *Nuclear Instruments and Methods in Physics Research Section A: Accelerators, Spectrometers, Detectors and Associated Equipment*, vol. 327, no. 2-3, pp. 469–479, 1993.

[47] L. Pál and I. Pázsit, "On some problems in the counting statistics of nuclear particles: Investigation of the dead time problems," *Nuclear Instruments and Methods in Physics Research Section A: Accelerators, Spectrometers, Detectors and Associated Equipment*, vol. 693, pp. 26–50, 2012.

[48] H. Menlove and J. Swansen, "A high-performance neutron time correlation counter," *Nuclear Technology*, vol. 71, no. 2, pp. 497–505, 1985.

[49] S. Croft, R. McElroy, S. Philips, M. Villani, and L. Evans, "Dead time behaviors in passive neutron correlation counting," in *Waste Management Symposia, WM*, vol. 7, 2007.

[50] B. Harker and M. Krick, "INCC software users manual," *LANL Report LA-UR-99-1291*, 1998.

[51] S. Croft and A. Favalli, "Extension of the Dytlewski-style dead time correction formalism for neutron multiplicity counting to any order," *Nuclear Instruments and Methods in Physics Research Section A: Accelerators, Spectrometers, Detectors and Associated Equipment*, vol. 869, pp. 141–152, 2017.

[52] S. Degweker, "Effect of deadtime on the statistics of time correlated pulses—application to the passive neutron assay problem," *Annals of Nuclear Energy*, vol. 16, no. 8, pp. 409–416, 1989.

[53] S. Degweker, "Solution of the markov chain for the dead time problem," *Annals of Nuclear Energy*, vol. 24, no. 5, pp. 375–386, 1997.

[54] S. Degweker, "An exact solution for a non-extending dead time problem in passive neutron assay," *Annals of Nuclear Energy*, vol. 25, no. 15, pp. 1267–1273, 1998.

[55] S. Degweker, "A markov chain approach for deriving the statistics of time-correlated pulses in the presence of non-extendible dead time," *Annals of Nuclear Energy*, vol. 24, no. 1, pp. 1–20, 1997.

[56] L. Holzleitner and M. T. Swinhoe, "Dead-time correction for any multiplicity using list mode neutron multiplicity counters: A new approach–low and medium count-rates," *Radiation Measurements*, vol. 46, no. 3, pp. 340–356, 2011.

[57] C. Dubi, I. Israelashvili, and T. Ridnik, "Analytic model for dead time effect in neutron multiplicity counting," *Nuclear Science and engineering*, vol. 176, no. 3, pp. 350–359, 2014.

[58] S. Hsue, T. Crane, W. Talbert Jr, and J. C. Lee, "Nondestructive assay methods for irradiated nuclear fuels," tech. rep., Los Alamos Scientific Lab., N. Mex.(USA), 1978.

[59] J. Phillips, J. K. Halbig, D. Lee, S. Beach, T. Bement, E. Dermendjiev, C. Hatcher, K. Kaieda, and E. Medina, "Application of nondestructive gamma-ray and neutron techniques for the safeguarding of irradiated fuel materials," tech. rep., Los Alamos Scientific Lab., NM (USA), 1980.

[60] *Safeguards Techniques and Equipment: 2011 Edition*, no. 1 in International Nuclear Verification Series, (Vienna, Austria), International Atomic Energy Agency, 2011.

[61] H. O. Menlove, A. H. Menlove, and S. J. Tobin, "Verification of plutonium content in spent fuel assemblies using neutron self-interrogation," tech. rep., Los Alamos National Lab.(LANL), Los Alamos, NM (United States), 2009.

[62] H. O. Menlove and D. Beddingfield, "Passive neutron reactivity measurement technique," in *Proceedings of the Institute of Nuclear Materials Management Annual Meeting*, 1997.

[63] S. J. Tobin, W. S. Charlton, M. L. Fensin, H. O. Menlove, A. Hoover, B. Quiter, A. Rajasingam, M. Swinhoe, S. Thompson, W. Charlton, *et al.*, "Determining plutonium in spent fuel with nondestructive assay techniques," tech. rep., Los Alamos National Lab.(LANL), Los Alamos, NM (United States), 2009.

[64] L. G. Evans, S. J. Tobin, M. A. Schear, H. O. Menlove, S. Y. Lee, and M. T. Swinhoe, "Nondestructive determination of plutonium mass in spent fuel: prelliminary modeling results using the passive neutron albedo reactivity technique," tech. rep., Los Alamos National Lab.(LANL), Los Alamos, NM (United States), 2009.

[65] H. O. Menlove, S. Menlove, and S. Tobin, "Fissile and fertile nuclear material measurements using a new differential die-away self-interrogation technique," *Nuclear Instruments and Methods in Physics Research Section A: Accelerators, Spectrometers, Detectors and Associated Equipment*, vol. 602, no. 2, pp. 588–593, 2009.

[66] N. Campbell and V. Francis, "A theory of valve and circuit noise," *Journal of the Institution of Electrical Engineers-Part III: Radio and Communication Engineering*, vol. 93, no. 21, pp. 45–52, 1946.

[67] I. Lux and A. Baranyai, "Higher order campbell techniques for neutron flux measurement: I. theory," *Nuclear Instruments and Methods in Physics Research*, vol. 202, no. 3, pp. 469–475, 1982.

[68] I. Lux and A. Baranyai, "Higher order campbell techniques for neutron flux measurement: II. correlated campbelling," *Nuclear Instruments and Methods in Physics Research*, vol. 202, no. 3, pp. 477–480, 1982.

[69] B. Bärs, "Variance and higher order signal moments in neutron flux measurements," *Nuclear Instruments and Methods in Physics Research Section A: Accelerators, Spectrometers, Detectors and Associated Equipment*, vol. 275, no. 2, pp. 403–410, 1989.

[70] C. Jammes, B. Geslot, R. Rosa, G. Imel, and P. Fougeras, "Comparison of reactivity estimations obtained from rod-drop and pulsed neutron source experiments," *Annals of Nuclear Energy*, vol. 32, no. 10, pp. 1131–1145, 2005.

[71] C. Jammes, B. Geslot, and G. Imel, "Advantage of the area-ratio pulsed neutron source technique for ads reactivity calibration," *Nuclear Instruments and Methods in Physics Research Section A: Accelerators, Spectrometers, Detectors and Associated Equipment*, vol. 562, no. 2, pp. 778–784, 2006.

[72] B. Geslot, F. Berhouet, L. Oriol, S. Bréaud, C. Jammes, P. Filliatre, and J. Villard, "Development and manufacturing of special fission chambers for in-core measurement requirements in nuclear reactors," in *2009 1st International Conference on Advancements in Nuclear Instrumentation, Measurement Methods and their Applications*, pp. 1–4, IEEE, 2009.

[73] B. Geslot, T. C. Unruh, P. Filliatre, C. Jammes, J. Di Salvo, S. Bréaud, and J.-F. Villard, "Method to calibrate fission chambers in campbelling mode," *IEEE Transactions on nuclear science*, vol. 59, no. 4, pp. 1377–1381, 2012.

[74] S. Chabod, G. Fioni, A. Letourneau, and F. Marie, "Modelling of fission chambers in current mode—analytical approach," *Nuclear Instruments and Methods in Physics Research Section A: Accelerators, Spectrometers, Detectors and Associated Equipment*, vol. 566, no. 2, pp. 633–653, 2006.

[75] E. W. Pontes and A. Ferreira, "Using cumulants and spectra to model nuclear radiation detectors," *IEEE transactions on nuclear science*, vol. 53, no. 3, pp. 1292–1298, 2006.

[76] P. Filliatre, C. Jammes, B. Geslot, and R. Veenhof, "A Monte Carlo simulation of the fission chambers neutron-induced pulse shape using the GARFIELD suite," *Nuclear Instruments and Methods in Physics Research Section A: Accelerators, Spectrometers, Detectors and Associated Equipment*, vol. 678, pp. 139–147, 2012.

[77] P. Loiseau, B. Geslot, and J. André, "On the fission chamber pulse charge acquisition and interpretation at MINERVE," *Nuclear Instruments and Methods in Physics Research Section A: Accelerators, Spectrometers, Detectors and Associated Equipment*, vol. 707, pp. 58–63, 2013.

[78] Zs. Elter, "pyFC: a TRIM-based fission chamber pulse shape simulator documentation," tech. rep., Chalmers University of Technology, 2015. URL: `https://research.chalmers.se/en/publication/242459` (accessed: March, 2021).

[79] L. Pál and I. Pázsit, "Campbelling-type theory of fission chamber signals generated by neutron chains in a multiplying medium," *Nuclear Instruments and Methods in Physics Research Section A: Accelerators, Spectrometers, Detectors and Associated Equipment*, vol. 794, pp. 90–101, 2015.

[80] Y. Kitamura, I. Pázsit, and T. Misawa, "Determination of prompt neutron decay constant by time-domain fluctuation analyses of detector current signals," *Annals of Nuclear Energy*, vol. 120, pp. 691–706, 2018.

[81] Y. Kitamura and T. Misawa, "Delayed neutron effect in time-domain fluctuation analyses of neutron detector current signals," *Annals of Nuclear Energy*, vol. 123, pp. 119–134, 2019.

[82] R. P. Feynman, F. De Hoffmann, and R. Serber, "Dispersion of the neutron emission in U-235 fission," *Journal of Nuclear Energy (1954)*, vol. 3, no. 1-2, pp. 64–IN10, 1956.

[83] J. D. Orndoff, "Prompt neutron periods of metal critical assemblies," *Nuclear Science and Engineering*, vol. 2, no. 4, pp. 450–460, 1957.

[84] M. M. R. Williams, *Random processes in nuclear reactors*. Elsevier, 1974.

[85] I. Pázsit and L. Pál, *Neutron Fluctuations: A Treatise on the Physics of Branching Processes*. Elsevier, 2007.

[86] A. Papoulis and H. Saunders, "Probability, random variables and stochastic processes," 1989.

[87] Zs. Elter, G. de Izarra, P. Filliatre, C. Jammes, and I. Pázsit, "Performance of higher order Campbell methods, Part II: calibration and experimental application," *Nuclear Instruments and Methods in Physics Research Section A: Accelerators, Spectrometers, Detectors and Associated Equipment*, vol. 835, pp. 86–93, 2016.

[88] C. H. Pyeon, "Experimental benchmarks for accelerator-driven system (ADS) at kyoto university critical assembly," Tech. Rep. KURRI-TR-444, Research Reactor Institute, Kyoto University, 2013.

[89] Westinghouse Electric Corporation, Electronic Tube Division, Elmira, New York, *Westinghouse Dual Range Fission Chamber Type 8073 Data Sheet*, May 15, 1961. URL: `https://frank.pocnet.net/sheets/201/8/8073.pdf` (accessed: March, 2021.

[90] G. Klujber, I. Barth, and M. Szieberth, "Construction of a data acquisition system for recording the continuous signals of fission chambers (in Hungarian)," Tech. Rep. BME-NTI-887/2019, Institute of Nuclear Techniques, Budapest University of Technology and Economics, 2019.

[91] Red Pitaya d.d., Velika pot 22, 5250 Solkan, Slovenia, *Red Pitaya Stemlab Board – Data Sheet*. URL: `https://www.redpitaya.com/f130/red-pitaya-stemlab-board`, accessed: March, 2021.

[92] J. Lestone, "Watt parameters for the Los Alamos Model: Subroutine GETAB," *arXiv preprint arXiv:1410.1769*, 2014.

[93] Zs. Elter, M. Bakkali, C. Jammes, and I. Pázsit, "Performance of higher order Campbell methods, Part I: review and numerical convergence study," *Nuclear Instruments and Methods in Physics Research Section A: Accelerators, Spectrometers, Detectors and Associated Equipment*, vol. 821, pp. 66–72, 2016.

Appendix A

Detailed derivation of the moments

A.1 One point moments with instant detection

A.1.1 Distribution of one detector signal

The one-point distribution of the signal of one detector, say that labeled with 1, concerns the random variable $\{\boldsymbol{y}_1(t)\}$, which is characterized by the cumulative distribution function

$$F_1(y,t) = \mathbb{P}[\boldsymbol{y}_1(t) \leq y].$$

The procedure of calculating the moments of the signal takes four steps.

- In the first step we start by formulating an equation for the density function of the distribution defined as

$$p_1(y,t) = \frac{\partial F_1(y,t)}{\partial y}. \tag{A.1}$$

The equation is written by considering the probabilities of all events that change the value of the signal. As we shall see this equation has no solution so we need to transform it.

- In the second step by taking the Fourier transform of the density equation we derive an equation for the characteristic function defined as

$$\pi_1(\omega,t) = \int_{-\infty}^{\infty} \mathrm{e}^{\imath \omega y}\, p_1(y,t)\,\mathrm{d}y. \tag{A.2}$$

This equation can easily be solved. Since the characteristic function is the generating function of the ordinary moments it could be used to calculate expression of the ordinary moments. However, the selected moments are more conviniently

- In the third step, we calculate the stationary cumulant-generating function of the distribution which is defined as

$$\gamma_1(\omega) = \lim_{t \to \infty} \ln[\pi_1(\omega,t)]. \tag{A.3}$$

- In the fourth step we calculate any cumulant with

$$\kappa_k = \frac{1}{\imath^k} \left. \frac{\partial^k \gamma_1(\omega)}{\partial \omega^k} \right|_{\omega=0} \tag{A.4}$$

We shall see in subsequent section the calculation of any moment of of the detector signals follows the same four steps listed above. Although the function in question are replaced with the appropriate ones and the resulting equations are somewhat complicated, the transformations applied remain the same and the whole derivation process is a natural extension of the derivation presented here. For this reason, the derivation of the one point moments of one detector will be presented below with as much detail as possible. In the derivation of other moments in subsequent section we shall point out only details that are qualitatively different and the remaining part of the derivation will be omitted by referencing to this derivation.

As noted earlier, we start by formulating an expression for the density function p_1 of the signal defined in (A.1). If we recall that the detection process starts at time $t = 0$ consequently the value of the signal at earlier times is zero, it is clear that the density function for $t < 0$ takes the form

$$p_1(y, t) = \delta(y). \tag{A.5}$$

On the other hand, as we shall explain below, for $t \geq 0$ it obeys the Kolmogorov backward integral equation

$$\begin{aligned} p_1(y, t) = \mathrm{e}^{-Q_\mathrm{s} t}\, \delta(y) &+ \int_0^t Q_\mathrm{s}\, \mathrm{e}^{-Q_\mathrm{s} t'} \sum_{n=0}^{\infty} P(n) \sum_{k=0}^{n} \binom{n}{k} \varepsilon^k\, (1 - \varepsilon)^{n-k} \\ &\times \int_0^y U_k^{(1)}(y', t - t')\, p_1(y - y', t - t')\, \mathrm{d}y' \mathrm{d}t'. \end{aligned} \tag{A.6}$$

Here Q_s and $P(n)$ denote the intensity and multiplicity of the source and were defined earlier in Section 2.3.3; ε denotes the detection efficiency (more precisely: the probability of detecting a neutron) and was introduced in Section 3.1; finally the function $U_k^{(1)}$ is defined as

$$U_k^{(1)}(y, t) = \int_0^{\infty} \cdots \int_0^{\infty} h_1(y_1, t) \cdots h_1(y_k, t)\, \mathrm{d}y_k \cdots \mathrm{d}y_1, \tag{A.7}$$
$$\scriptsize y_1 + \cdots + y_k = y$$

where h_1 denotes the one-point density function of a single pulse and was defined in (3.6).

Before interpreting the Kolmogorov equation (A.6), we should consider the physical meaning of the the function $U_k^{(1)}$ given by (A.7). One can recognize that it is essentially the density function of k pulses induced by k neutrons originating from the same emission at time $t = 0$. As a k-fold convolution of h_1, it reflects the fact that pulses induced by more that one neutrons are independent and add up linearly.

With these in mind, Equation (A.6) can be interpreted in the following way. As an application of the law of total probability, the probability density of having a signal value y at time t (left-hand side) is expressed with the probabilities (or probability

densities) of events, that cause it (right-hand side). The two terms on the right-hand side correspond to two mutually exclusive events. The first term represents the event when no source emission occurs until time t with probability $\mathrm{e}^{-Q_s t}$, in which case the signal value at time t remains zero with probability density $\delta(y)$. The second term represents the event when there was at least one source emission until time t. In fact, its is a sum (or integral) over the probabilities (or probability densities) of a set of mutually exclusive events, each of which can be described as follows. The first emission occurs at time t' with probability density $Q_s \, \mathrm{e}^{-Q_s t'}$; during the emission n neutrons are released with probability $P(n)$; from the n neutrons k are detected and $n-k$ escape with probability $\binom{n}{k} \varepsilon^k \, (1-\varepsilon)^{n-k}$; the k pulses induced in the detector contribute by y' to the signal at time t with probability density $U_k^{(1)}(y', t-t')$; pulses from subsequent emissions contribute to it by $y - y'$ with probability density $p_1(y - y', t - t')$.

For practical reasons which will become apparent later, let us rewrite Equation (A.6) into a slightly different form. It can be shown (with a simple substitution of variables) that the arguments t' and $t - t'$ in the second term can be switched which yields

$$
\begin{aligned}
p_1(y, t) = {} & \mathrm{e}^{-Q_s t} \, \delta(y) + \int_0^t Q_s \, \mathrm{e}^{-Q_s(t-t')} \sum_{n=0}^{\infty} P(n) \sum_{k=0}^{n} \binom{n}{k} \varepsilon^k \, (1-\varepsilon)^{n-k} \\
& \times \int_0^y U_k^{(1)}(y', t') \, p_1(y - y', t') \, \mathrm{d}y' \mathrm{d}t'.
\end{aligned}
\tag{A.8}
$$

If we would solve (A.8), using the known form of the density function $p_1(y, t)$ we could easily calculate the characteristic function (A.2), from which the stationary cumulant-generating function as well as the corresponding cumulants could be obtained using (A.3) and (A.4). However, Equation (A.8) is an integral equation in both variables y and t and, whats more, it contains multiple convolutions in the variable y. As a result, no analytical solution of this equation can be found.

The alternative is to transform Equation (A.8) into another equation that we can solve analytically. Keeping in mind the convolution theorem being an effective way of simplifying convolution-expressions, let us take the Fourier transform of (A.8) with respect to y; formally this can be written as

$$
\begin{aligned}
\int_{-\infty}^{\infty} \mathrm{e}^{\imath \omega y} \, p(y, t) \, \mathrm{d}y = {} & \mathrm{e}^{-Q_s t} \int_{-\infty}^{\infty} \mathrm{e}^{\imath \omega y} \, \delta(y) \, \mathrm{d}y \\
& + \int_0^t Q_s \, \mathrm{e}^{-Q_s(t-t')} \sum_{n=0}^{\infty} P(n) \sum_{k=0}^{n} \binom{n}{k} \varepsilon^k \, (1-\varepsilon)^{n-k} \\
& \times \int_{-\infty}^{\infty} \mathrm{e}^{\imath \omega y} \left[\int_0^y U_k^{(1)}(y', t') \, p_1(y - y', t') \, \mathrm{d}y' \right] \mathrm{d}y \, \mathrm{d}t'.
\end{aligned}
\tag{A.9}
$$

Using the convolution theorem, we can write

$$
\int_{-\infty}^{\infty} \mathrm{e}^{\imath \omega y} \left[\int_0^y U_k^{(1)}(y', t') \, p_1(y - y', t') \, \mathrm{d}y' \right] \mathrm{d}y = \int_{-\infty}^{\infty} \mathrm{e}^{\imath \omega y} \, U_k^{(1)}(y, t') \, \mathrm{d}y \cdot \int_{-\infty}^{\infty} \mathrm{e}^{\imath \omega y} \, p_1(y, t') \mathrm{d}y
$$

and

$$
\int_{-\infty}^{\infty} \mathrm{e}^{\imath \omega y} \, U_k^{(1)}(y, t') \, \mathrm{d}y = \left[\int_{-\infty}^{\infty} \mathrm{e}^{\imath \omega y} \, h_1(y, t') \, \mathrm{d}y \right]^k.
$$

Furthermore, by noting that

$$\int_{-\infty}^{\infty} e^{\imath \omega y}\, \delta(y)\, \mathrm{d}y = 1$$

and accounting for the definitions (3.7) and (A.2), Equation (A.9) takes the form

$$\pi_1(\omega, t) = e^{-Q_s t} + \int_0^t Q_s\, e^{-Q_s(t-t')} \sum_{n=0}^{\infty} P(n) \sum_{k=0}^{n} \binom{n}{k} \varepsilon^k\, (1-\varepsilon)^{n-k} \tag{A.10}$$
$$\times \chi_1^k(\omega, t')\, \pi_1(\omega, t')\, \mathrm{d}t'.$$

This equation can be brought into slightly more compact form which shall also be advantageous for practical reasons later. Using the binomial theorem, one may write

$$\sum_{k=0}^{n} \binom{n}{k} \chi_1^k(\omega, t)\, \varepsilon^k\, (1-\varepsilon)^{n-k} = \{1 + \varepsilon\, [\chi_1(\omega, t) - 1]\}^n.$$

If we further introduce the function

$$c_1(x) = 1 + \varepsilon\, (x - 1) \tag{A.11}$$

and account for (??), Equation A.10 simplifies to

$$\pi_1(\omega, t) = e^{-Q_s t} + \int_0^t Q_s\, e^{-Q_s(t-t')}\, G\{c_1\, [\chi_1(\omega, t')]\}\, \pi_1(\omega, t')\, \mathrm{d}t'. \tag{A.12}$$

Like Equation (A.8) before, Equation (A.10) is also an integral equation, this time, however, for the characteristic function π_1. Comparing with (A.8) one immediately notices how much simpler this last equation is: integration occurs only with respect to the variable t; the former integrals of the other variable are now replaced by summations hidden in the function G.

Equation (A.10) can be solved analytically by casting it into a differential equation. Differentiating both sides with respect to t and rearranging the terms, we get

$$\frac{\partial \pi_1(\omega, t)}{\partial t} = Q_s\, G\{c_1\, [\chi_1(\omega, t)]\}\, \pi_1(\omega, t)$$
$$- Q_s \left[e^{-Q_s t} + \int_0^t Q_s\, e^{-Q_s(t-t')}\, G\{c_1\, [\chi_1(\omega, t')]\}\, \pi_1(\omega, t')\, \mathrm{d}t' \right]$$

which, after recognizing (A.12) in the second term of the right-hand side, simplifies to

$$\frac{\partial \pi_1(\omega, t)}{\partial t} = Q_s\, (G\{c_1\, [\chi_1(\omega, t)]\} - 1)\, \pi_1(\omega, t). \tag{A.13a}$$

The initial condition corresponding to this equation, using (A.5), reads as

$$\pi_1(\omega, t = 0) = \int_{-\infty}^{\infty} e^{\imath \omega y}\, p_1(y, 0)\, \mathrm{d}y = 1. \tag{A.13b}$$

It is easy to see that (A.13) has the solution

$$\pi_1(\omega, t) = \exp\left(Q_s \int_0^t (G\{c_1\, [\chi_1(\omega, t')]\} - 1)\, \mathrm{d}t' \right). \tag{A.14}$$

112

In the possession of the characteristic function π_1, we can now obtain the stationary cumulant-generating function using its definition (A.3):

$$\gamma_1(\omega) = Q_{\mathrm{s}} \int_0^\infty \left(G\left\{ c_1\left[\chi_1(\omega, t)\right]\right\} - 1 \right) \mathrm{d}t. \tag{A.15}$$

By substituting this expression into (A.4), we are able to calculate κ_k, the stationary cumulant of order k.

As noted in the beginning of Section 3.2, we are interested in three moments of the signal of one detector: its mean value κ_1, its variance κ_2 and its skewness κ_3. Performing the first step in the calculation of the moments, that is, differentiating the stationary cumulant-generating function with respect to ω, we get

$$\frac{\mathrm{d}\gamma_1(\omega)}{\mathrm{d}\omega} = Q_{\mathrm{s}} \int_0^\infty \varepsilon \frac{\partial \chi_1}{\partial \omega} \sum_{n=0}^\infty n \, P(n) \left[1 + \varepsilon\left(\chi_1 - 1\right)\right]^{n-1} \mathrm{d}t,$$

$$\frac{\mathrm{d}^2\gamma_1(\omega)}{\mathrm{d}\omega^2} = Q_{\mathrm{s}} \int_0^\infty \varepsilon \frac{\partial^2 \chi_1}{\partial \omega^2} \sum_{n=0}^\infty n \, P(n) \left[1 + \varepsilon\left(\chi_1 - 1\right)\right]^{n-1} \mathrm{d}t$$
$$+ \, Q_{\mathrm{s}} \int_0^\infty \varepsilon^2 \left(\frac{\partial \chi_1}{\partial \omega}\right)^2 \sum_{n=0}^\infty n\,(n-1) \, P(n) \left[1 + \varepsilon\left(\chi_1 - 1\right)\right]^{n-2} \mathrm{d}t$$

and

$$\frac{\mathrm{d}^3\gamma_1(\omega)}{\mathrm{d}\omega^3} = Q_{\mathrm{s}} \int_0^\infty \varepsilon \frac{\partial^3 \chi_1}{\partial \omega^3} \sum_{n=0}^\infty n \, P(n) \left[1 + \varepsilon\left(\chi_1 - 1\right)\right]^{n-1} \mathrm{d}t$$
$$+ \, 3\,Q_{\mathrm{s}} \int_0^\infty \varepsilon^2 \frac{\partial^2 \chi_1}{\partial \omega^2} \frac{\partial \chi_1}{\partial \omega} \sum_{n=0}^\infty n\,(n-1) \, P(n) \left[1 + \varepsilon\left(\chi_1 - 1\right)\right]^{n-2} \mathrm{d}t$$
$$+ \, Q_{\mathrm{s}} \int_0^\infty \varepsilon^3 \left(\frac{\partial \chi_1}{\partial \omega}\right)^3 \sum_{n=0}^\infty n\,(n-1)\,(n-2) \, P(n) \left[1 + \varepsilon\left(\chi_1 - 1\right)\right]^{n-3} \mathrm{d}t.$$

where, for the sake of compactness, we have omitted the arguments (ω, t) of χ_1. Finally, let us divide the derivatives with the appropriate power of the imaginary unit $\imath$ at evaluate them at $\omega = 0$. Noticing that, based on (3.7), $\chi(\omega = 0, t) = 1$, furthermore using (**??**) and substituting the moments (3.8) of the pulse symbolically, we get

$$\kappa_1 = Q_{\mathrm{s}}\,\nu_1\,\varepsilon \int_0^\infty \mu_1(t)\,\mathrm{d}t,$$

$$\kappa_2 = Q_{\mathrm{s}}\,\nu_1\,\varepsilon \int_0^\infty \mu_2(t)\,\mathrm{d}t + Q_{\mathrm{s}}\,\nu_2\,\varepsilon^2 \int_0^\infty \mu_1^2(t)\,\mathrm{d}t,$$

$$\kappa_3 = Q_{\mathrm{s}}\,\nu_1\,\varepsilon \int_0^\infty \mu_3(t)\,\mathrm{d}t + 3\,Q_{\mathrm{s}}\,\nu_2\,\varepsilon^2 \int_0^\infty \mu_2(t)\,\mu_1(t)\,\mathrm{d}t + Q_{\mathrm{s}}\,\nu_3\,\varepsilon^3 \int_0^\infty \mu_1^3(t)\,\mathrm{d}t.$$

If, additionally, we account for the definitions (2.22) of the detection rates, these ex-

pressions become

$$\kappa_1 = S \int_0^\infty \mu_1(t)\,\mathrm{d}t, \tag{A.17a}$$

$$\kappa_2 = S \int_0^\infty \mu_2(t)\,\mathrm{d}t + 2\,D \int_0^\infty \mu_1^2(t)\,\mathrm{d}t, \tag{A.17b}$$

$$\kappa_3 = S \int_0^\infty \mu_3(t)\,\mathrm{d}t + 6\,D \int_0^\infty \mu_2(t)\,\mu_1(t)\,\mathrm{d}t + 6\,T \int_0^\infty \mu_1^3(t)\,\mathrm{d}t. \tag{A.17c}$$

At this point it might worth to take a look at the physical meaning of the above expressions of the moments. The κ_1 mean value (first order moment) of the signal originates from one "source": the first moment μ_1 of one pulse (single). The κ_2 variance (second order moment) of the signal, on the other hand, originates from two "sources": the second moment μ_2 of one pulse (single) or the joint second moment μ_1^2 of two distinct pulses (doubles). Finally, the κ_3 skewness (third order moment) of the signal originates from three "sources": the third moment μ_3 of one pulse (single), the joint third moment $\mu_2\,\mu_1$ of two distinct pulses (doubles) or the joint third moment μ_1^3 of three distinct pulses (triples).

Finally, when we insert the explicit form of the moments of the pulse (3.8) into Equation (A.17) then, by introducing the notation

$$I_n = \int_0^\infty f^n(t)\,\mathrm{d}t, \tag{A.18}$$

the cumulants of the signal take the particularly compact forms

$$\kappa_1 = S \langle a \rangle\,I_1, \tag{A.19a}$$
$$\kappa_2 = \left[S \langle a^2 \rangle + 2\,D \langle a \rangle^2 \right] I_2, \tag{A.19b}$$
$$\kappa_3 = \left[S \langle a^3 \rangle + 6\,D \langle a^2 \rangle \langle a \rangle + 6\,T \langle a \rangle^3 \right] I_3. \tag{A.19c}$$

A.1.2 One point distribution of two detector signals

The one-point distribution of the signal of two detectors, say those labeled with 1 and 2, concerns the random variable $\{\boldsymbol{y}_1(t), \boldsymbol{y}_2(t)\}$, which is characterized by the cumulative distribution function

$$F_{1,1}(y_1, y_2, t) = \mathbb{P}[\boldsymbol{y}_1(t) \le y_1, \boldsymbol{y}_2(t) \le y_2].$$

As noted earlier, the procedure of calculating the joint moments of two signals follows the same steps as calculation of the moments of one signal: starting from a Kolmogorov backward integral equation for the density function, we derive an expression for the stationary cumulant-generating function, from which the desired moments can be obtained by simple differentiation. For this reason, the derivation of the joint moments below will be given in much less detail, focusing mainly on the differences compared to the derivation in the previous subsection.

Again, we start by formulating expressions for the density function which, in this case, will be defined as

$$p_{1,1}(y_1, y_2, t) = \frac{\partial^2 F_{1,1}(y_1, y_2, t)}{\partial y_1\,\partial y_2}.$$

With similar considerations as before, the density function for $t < 0$ takes the form

$$p_{1,1}(y_1, y_2, t) = \delta(y_1)\,\delta(y_2),$$

whereas for $t \geq 0$ it obeys the Kolmogorov backward integral equation

$$\begin{aligned}
p_{1,1}(y_1, y_2, t) = \mathrm{e}^{-Q_{\mathrm{s}}t}\,\delta(y_1)\,\delta(y_2) + Q_{\mathrm{s}}\int_0^t \mathrm{e}^{-Q_{\mathrm{s}}t'} \\
\times \sum_{n=0}^{\infty} P(n) \sum_{k_0+k_1+k_2=n} \frac{n!}{k_0!\,k_1!\,k_2!}\,\varepsilon^{k_1}\varepsilon^{k_2}(1-2\varepsilon)^{k_0} \\
\times \int_0^{y_2}\int_0^{y_1} U_{k_1}^{(1)}(y_1', t-t')\,U_{k_2}^{(1)}(y_2', t-t') \\
\times p_{1,1}(y_1-y_1', y_2-y_2', t-t')\,\mathrm{d}y_1'\mathrm{d}y_2'\mathrm{d}t'
\end{aligned} \tag{A.20}$$

Here $U^{(1)}$ is the same as in (A.7) and the interpretation of Equation A.20 is also similar to that of (A.6). The two terms on the right-hand side again correspond to two mutually exclusive events: the first represents the event when there is no source emission until time t, whereas the second represents the set of events when there is at least one source emission until time t. The major difference compared to Equation (A.6) lies inside the second term. In this case, following the release of n neutrons from the source at time t', k_1 are detected by the first detector and k_2 by the other, whereas $k_0 = n-k_1-k_2$ escape; this has a probability $\frac{n!}{k_0!\,k_1!\,k_2!}\,\varepsilon^{k_1}\varepsilon^{k_2}(1-2\varepsilon)^{k_0}$. Then, by time t, the pulses induced in the first detector contribute to its current by y_1' with probability density $U_{k_1}^{(1)}(y_1', t-t')$, whereas the pulses induced in the second detector contribute to its current by y_2' with probability density $U_{k_2}^{(1)}(y_2', t-t')$; pulses from further emissions contribute by $y_1 - y_1'$ and $y_2 - y_2'$ with probability density $p_{1,1}(y_1-y_1', y_2-y_2', t-t')$.

Since, again, no analytical solution to the integral Equation (A.20) can be given, we take its two-dimensional Fourier-transform with respect to the variables y_1 and y_2 to transform it to a simpler equation, this time for the characteristic function

$$\pi_{1,1}(\omega_1, \omega_2, t) = \int_{-\infty}^{\infty}\int_{-\infty}^{\infty} \mathrm{e}^{\imath(\omega_1 y_1+\omega_2 y_2)}\,p_{1,1}(y_1, y_2, t)\,\mathrm{d}y_1\mathrm{d}y_2. \tag{A.21}$$

After simplification, we get

$$\begin{aligned}
\pi_{1,1}(\omega_1, \omega_2, t) = \mathrm{e}^{-Q_{\mathrm{s}}t} + Q_{\mathrm{s}}\int_0^t \mathrm{e}^{-Q_{\mathrm{s}}(t-t')} \\
\times \sum_{n=0}^{\infty} P(n) \sum_{k_0+k_1+k_2=n} \frac{n!}{k_0!\,k_1!\,k_2!}\,\varepsilon^{k_1}\varepsilon^{k_2}(1-2\varepsilon)^{k_0} \\
\times \chi_1^{k_1}(\omega_1, t')\,\chi_1^{k_2}(\omega_2, t')\,\pi_{1,1}(\omega_1, \omega_2, t')\,\mathrm{d}t'
\end{aligned}$$

for $t \geq 0$ which, following similar considerations as before, can be reduced to

$$\begin{aligned}
\pi_{1,1}(\omega_1, \omega_2, t) = \mathrm{e}^{-Q_{\mathrm{s}}t} + Q_{\mathrm{s}}\int_0^t \mathrm{e}^{-Q_{\mathrm{s}}(t-t')} \\
\times G\left\{c_2\left[\chi_1(\omega_1, t'), \chi_1(\omega_2, t')\right]\right\}\pi_{1,1}(\omega_1, \omega_2, t')\,\mathrm{d}t',
\end{aligned} \tag{A.22}$$

115

where we have introduced the function

$$c_2(x_1, x_2) = 1 + \varepsilon\,(x_1 - 1) + \varepsilon\,(x_2 - 1). \tag{A.23}$$

Differentiating (A.22) with respect to t and performing simplifications yield the differential equation

$$\frac{\partial \pi_{1,1}(\omega_1, \omega_2, t)}{\partial t} = Q_{\mathrm{s}}\,(G\,\{c_2\,[\chi_1(\omega_1, t), \chi_1(\omega_2, t)]\} - 1)\,\pi_{1,1}(\omega_1, \omega_2, t)$$

with the initial condition

$$\pi_{1,1}(\omega_1, \omega_2, t = 0) = \int_{-\infty}^{\infty}\int_{-\infty}^{\infty} \mathrm{e}^{\imath(\omega_1 y_1 + \omega_2 y_2)}\,p_{1,1}(y_1, y_2, 0)\,\mathrm{d}y_1\mathrm{d}y_2 = 1.$$

The solution of the above differential equation for $t \geq 0$ can immediately be written as

$$\pi_{1,1}(\omega_1, \omega_2, t) = \exp\left(Q_{\mathrm{s}}\int_0^t (G\,\{c_2\,[\chi_1(\omega_1, t'), \chi_1(\omega_2, t')]\} - 1)\,\mathrm{d}t'\right). \tag{A.25}$$

Using (A.25), the stationary cumulant-generating function

$$\gamma_{1,1}(\omega_1, \omega_2) = \lim_{t\to\infty} \ln[\pi_{1,1}(\omega_1, \omega_2, t)] \tag{A.26}$$

can be obtained and takes the form

$$\gamma_{1,1}(\omega_1, \omega_2) = Q_{\mathrm{s}}\int_0^{\infty} (G\,\{c_2\,[\chi_1(\omega_1, t), \chi_1(\omega_2, t)]\} - 1)\,\mathrm{d}t. \tag{A.27}$$

From this expression, the stationary cumulant of order (m, n) is calculated as follows:

$$\kappa_{m,n} = \frac{1}{\imath^{(m+n)}}\,\frac{\partial^{(m+n)}}{\partial\omega_1^m \partial\omega_2^m}\,\gamma(\omega_1, \omega_2)\bigg|_{\omega_1 = \omega_2 = 0} \tag{A.28}$$

As noted in the beginning of Section 3.2, we are interested in two of the above cumulants: the cross-covariance $\kappa_{1,1}$ of the two signals and $\kappa_{2,1}$, which does not have its own name. By inserting (A.27) into (A.28), after similar considerations as in the case of the moments of one signal, we obtain

$$\kappa_{1,1} = 2\,D\int_0^{\infty} \mu_1^2(t)\,\mathrm{d}t, \tag{A.29a}$$

$$\kappa_{2,1} = 2\,D\int_0^{\infty} \mu_2(t)\,\mu_1(t)\,\mathrm{d}t + 6\,T\int_0^{\infty} \mu_1^3(t)\,\mathrm{d}t, \tag{A.29b}$$

The interpretation of the above equations is analogous to that of (A.17). The $\kappa_{1,1}$ covariance (second order moment) of two signals originates from one "source": the joint second moment $\mu_1^2(t)$ of two distinct pulses (doubles) each from a different detector. $\kappa_{2,1}$ (third order moment) originates from two "sources": the joint third moment $\mu_2\,\mu_1$ of two distinct pulses (doubles) each from a different detector and the joint third moment μ_1^3 of three distinct pulses (triples) of which two comes from one detector and one comes from the other.

Again, when we use the explicit form of the moments of the pulse (3.8) and account for (A.18), the expressions can be rewritten into the compact forms

$$\kappa_{1,1} = 2\,D\,\langle a\rangle^2\,I_2, \tag{A.30a}$$

$$\kappa_{2,1} = \left[2\,D\,\langle a^2\rangle\langle a\rangle + 6\,T\,\langle a\rangle^3\right]I_3. \tag{A.30b}$$

A.1.3 One point distribution of three detector signals

The one-point distribution of the signal of three detectors, those labeled with 1, 2 and 3, concerns the random variable $\{\boldsymbol{y}_1(t), \boldsymbol{y}_2(t), \boldsymbol{y}_3(t)\}$, which is characterized by the cumulative distribution function

$$F_{1,1,1}(y_1, y_2, y_3, t) = \mathbb{P}[\boldsymbol{y}_1(t) \leq y_1, \boldsymbol{y}_2(t) \leq y_2, \boldsymbol{y}_3(t) \leq y_3].$$

The procedure of calculating the joint moments of three signals follows, again, the same four steps as the calculation of the moments earlier, and is a straightforward analogy of the derivations presented so far in this section. Therefore, the derivation below will contain even less details as the one in the previous subsection: key expressions will be presented without any particular explanation or commentary.

The density function

$$p_{1,1,1}(y_1, y_2, y_3, t) = \frac{\partial^3 F_{1,1,1}(y_1, y_2, y_3, t)}{\partial y_1 \, \partial y_2 \, \partial y_3} \tag{A.31}$$

for $t < 0$ takes the form

$$p_{1,1,1}(y_1, y_2, y_3, t) = \delta(y_1)\,\delta(y_2)\,\delta(y_3),$$

whereas for $t \geq 0$ it obeys the Kolmogorov backward integral equation

$$p_{1,1,1}(y_1, y_2, t) = \mathrm{e}^{-Q_\mathrm{s}t}\,\delta(y_1)\,\delta(y_2)\,\delta(y_3) + Q_\mathrm{s}\int_0^t \mathrm{e}^{-Q_\mathrm{s}t'}$$

$$\times \sum_{n=0}^{\infty} P(n) \sum_{k_0+k_1+k_2+k_3=n} \frac{n!}{k_0!\,k_1!\,k_2!\,k_3!}\,\varepsilon^{k_1}\varepsilon^{k_2}\varepsilon^{k_3}(1-3\varepsilon)^{k_0}$$

$$\times \int_0^{y_3}\int_0^{y_2}\int_0^{y_1} U_{k_1}^{(1)}(y_1', t - t')\,U_{k_2}^{(1)}(y_2', t - t')\,U_{k_3}^{(1)}(y_3', t - t')$$

$$\times p_{1,1,1}(y_1 - y_1', y_2 - y_2', y_3 - y_3', t - t')\,\mathrm{d}y_1'\mathrm{d}y_2'\mathrm{d}y_3'\mathrm{d}t'.$$

The characteristic function

$$\pi_{1,1,1}(\omega_1, \omega_2, \omega_3, t) = \int_{-\infty}^{\infty}\int_{-\infty}^{\infty}\int_{-\infty}^{\infty} \mathrm{e}^{\iota(\omega_1 y_1 + \omega_2 y_2 + \omega_3 y_3)}\,p_{1,1,1}(y_1, y_2, y_3, t)\,\mathrm{d}y_1\mathrm{d}y_2\mathrm{d}y_3 \tag{A.32}$$

for $t \geq 0$ satisfies the differential equation

$$\frac{\partial \pi_{1,1,1}(\omega_1, \omega_2, \omega_3, t)}{\partial t} = Q_\mathrm{s}\left(G\left\{c_3\left[\chi_1(\omega_1, t), \chi_1(\omega_2, t), \chi_1(\omega_3, t)\right]\right\} - 1\right)$$

$$\times \pi_{1,1,1}(\omega_1, \omega_2, \omega_3, t)$$

with the initial condition

$$\pi_{1,1,1}(\omega_1, \omega_2, \omega_3, t = 0) = 1$$

and with

$$c_3(x_1, x_2, x_3) = 1 + \varepsilon\,(x_1 - 1) + \varepsilon\,(x_2 - 1) + \varepsilon\,(x_3 - 1). \tag{A.33}$$

The solution of the above differential equation for $t \geq 0$ reads as

$$\pi_{1,1,1}(\omega_1, \omega_2, \omega_3, t) = \exp \left(Q_s \int_0^t \left(G \left\{ c_3 \left[\chi_1(\omega_1, t'), \chi_1(\omega_2, t'), \chi_1(\omega_3, t') \right] \right\} - 1 \right) dt' \right).$$

Using this expression, the stationary cumulant-generating function

$$\gamma_{1,1,1}(\omega_1, \omega_2, \omega_3) = \lim_{t \to \infty} \ln[\pi_{1,1,1}(\omega_1, \omega_2, \omega_3, t)] \tag{A.34}$$

is obtained in the form

$$\gamma_{1,1,1}(\omega_1, \omega_2, \omega_3, t) = Q_s \int_0^\infty \left(G \left\{ c_3 \left[\chi_1(\omega_1, t), \chi_1(\omega_2, t), \chi_1(\omega_3, t) \right] \right\} - 1 \right) dt, \tag{A.35}$$

from which the stationary cumulant of order (m, n, l) can be calculated as

$$\kappa_{m,n,l} = \frac{1}{\imath^{(m,n,l)}} \left. \frac{\partial^3 \gamma_{1,1,1}(\omega_1, \omega_2, \omega_3)}{\partial \omega_1^m \, \partial \omega_2^n \, \partial \omega_3^l} \right|_{\omega_1 = \omega_2 = \omega_3 = 0} \tag{A.36}$$

As noted in the beginning of Section 3.2, the only moment of interest here is $\kappa_{1,1,1}$, the cross-bicovariance of three signals. By inserting (A.35) into (A.36), after similar considerations as in the case of the moments of one signal, we arrive to the expressions

$$\kappa_{1,1,1} = 6 \, T \, \langle a \rangle^3 \int_0^\infty \mu_1^3(t) \, dt. \tag{A.37}$$

The interpretation of this equation is analogous to that of (A.17) and (**??**). The $\kappa_{1,1,1}$ bicovariance (third order moment) of three signals originates from one "source": the joint third moment μ_1^3 of three distinct pulses (triples) each from a different detector.

Again, when we use the explicit form of the moments of the pulse (3.8) and account for (A.18), the expression can be rewritten into the compact form

$$\kappa_{1,1,1} = 6T \, \langle a \rangle^3 \, I_3. \tag{A.38}$$

A.2 One point moments with delayed detection

A.2.1 Distribution of one detector signal

By substituting (3.31) into the general expressions (3.20 of the moments, we obtain

$$\kappa_1 = S \, \langle a \rangle \int_0^\infty I_1(t) \, dt,$$

$$\kappa_2 = S \, \langle a^2 \rangle \int_0^\infty I_2(t) \, dt + 2 \, D \, \langle a \rangle^2 \int_0^\infty I_1^2(t) \, dt,$$

$$\kappa_3 = S \, \langle a^3 \rangle \int_0^\infty I_3(t) \, dt + 6 \, D \, \langle a^2 \rangle \langle a \rangle \int_0^\infty I_1(t) \, I_2(t) \, dt + 6 \, T \, \langle a \rangle^3 \int_0^\infty I_1^3(t) \, dt,$$

where we have introduced the function

$$I_n(t) = \int_0^\infty f^n(t - \tau) \, u(\tau) \, d\tau. \tag{A.40}$$

The physical interpretation of these equations is the same as that of (3.20). However, they can be recast into much compact forms. The integral in the first term of the right-hand sides of all three equations can be simplified. By applying the convolution theorem and accounting for the fact that the integral of the density function u is unity, one can write

$$\int_0^\infty I_n(t)\,\mathrm{d}t = \int_0^\infty \int_0^\infty f^n(t-\tau)\,u(\tau)\,\mathrm{d}\tau\mathrm{d}t = \int_0^\infty f^n(t)\,\mathrm{d}t = I_n,$$

where the quantity I_n was already defined earlier in (A.18). The physical content of this last equations is that the moments of a single randomly delayed pulse are invariant to the value of the delay. The integrals in the other terms of the above equations, however, cannot be simplified in a similar way, because the moments of more than one randomly delayed pulses are not invariant to their delay. Instead, let us introduce the notations

$$\xi_{1,1} = \frac{1}{I_2}\int_0^\infty I_1^2(t)\,\mathrm{d}t, \quad \xi_{1,2} = \frac{1}{I_3}\int_0^\infty I_1(t)\,I_2(t)\,\mathrm{d}t, \quad \xi_{1,1,1} = \frac{1}{I_3}\int_0^\infty I_1^3(t)\,\mathrm{d}t. \quad \text{(A.41)}$$

With these considerations the expressions of the moments take the following form:

$$\kappa_1 = S\,\langle a\rangle\,I_1, \tag{A.42a}$$
$$\kappa_2 = \left[S\,\langle a^2\rangle + 2\,D\,\langle a\rangle^2\,\xi_{1,1}\right]\,I_2, \tag{A.42b}$$
$$\kappa_3 = \left[S\,\langle a^3\rangle + 6\,D\,\langle a\rangle\langle a^2\rangle\,\xi_{1,2} + 6\,T\,\langle a\rangle^3\,\xi_{1,1,1}\right]\,I_3. \tag{A.42c}$$

A.2.2 Distribution of two detector signals

If we substitute (3.31) into the general expressions (A.29 of the moments then, by using (A.40), we obtain

$$\kappa_{1,1} = 2\,D\,\langle a\rangle^2\int_0^\infty I_1^2(t)\,\mathrm{d}t,$$
$$\kappa_{2,1} = 2\,D\,\langle a\rangle\langle a^2\rangle\int_0^\infty I_1(t)\,I_2(t)\,\mathrm{d}t + 6\,T\,\langle a\rangle^3\int_0^\infty I_1^3(t)\,\mathrm{d}t.$$

The physical content of these equations is the same as that of (**??**). By further accounting for (A.41), they can be recast into the form

$$\kappa_{1,1} = 2\,D\,\langle a\rangle^2\,\xi_{1,1}\,I_2, \tag{A.43a}$$
$$\kappa_{2,1} = \left[2\,D\,\langle a\rangle\langle a^2\rangle\,\xi_{1,2} + 6\,T\,\langle a\rangle^3\,\xi_{1,1,1}\right]\,I_3. \tag{A.43b}$$

A.2.3 Distribution of three detector signals

If we substitute (3.31) into the general expression (A.37 of the moment then, by using (A.40), we obtain

$$\kappa_{1,1,1} = 6\,T\,\langle a\rangle^3\int_0^\infty I_1^3(t)\,\mathrm{d}t.$$

The physical content of this equation is the same as that of (A.37). By further accounting for (A.41), they can be recast into the form

$$\kappa_{1,1,1} = 6\,T\,\langle a\rangle^3\,\xi_{1,1,1}\,I_3. \tag{A.44}$$

A.3 Two and three point moments with delayed detection

A.3.1 Two-point distribution of one detector signal

The two-point distribution of the signal of one detector, say that labeled with 1, concerns the random variable $\{\boldsymbol{y}_1(t), \boldsymbol{y}_1(t-\theta)\}$, which is characterized by the cumulative distribution function

$$F_2(y_1, y_2, t, \theta) = \mathbb{P}\left[\boldsymbol{y}_1(t) \leq y_1, \boldsymbol{y}_1(t - \theta) \leq y_2\right].$$

As we must already be used to it, the calculation of the two-point moments of the detector signal follows the same four steps as the calculation of the one-point moments discussed in Sections 3.2 and 3.3: starting from a Kolmogorov backward integral equation for the density function, we derive an expression for the stationary cumulant-generating function, from which the desired moments can be obtained by differentiation. However, as we shall see in this section, accounting for the temporal correlations introduces certain qualitatively new elements to the equations, which are thus in no way straightforward extensions of their one-point versions. For this reason, as we did with the one-points moments of one detector signal back in Section 3.2, below we provide a detailed derivation of the two-point moments of the signal (although still less detailed than for its one-point version). In the case of other two- or three point moments discussed in the forthcoming subsections, we shall again return to the practice of showing only the key steps from the derivations.

As usual, we start by formulating equations for the density function, which in this case is defined as

$$p_2(y_1, y_2, t, \theta) = \frac{\partial^2 F_2(y_1, y_2, t, \theta)}{\partial y_1 \partial y_2}. \tag{A.45}$$

If we recall that the detection process starts at time $t = 0$, hence the value of the signal at earlier times is zero, it is easy to see that for $\theta \geq 0$ and $t < \theta$ the density function takes the form

$$p_2(y_1, y_2, t, \theta) = p_1(y_1, t)\, \delta(y_2), \tag{A.46}$$

where p_1 is the one-point density function of the signal defined in (A.1). On the other hand, as it will be explained below, for $t \geq \theta$ the density function obeys the Kolmogorov backward equation

$$
\begin{aligned}
p_2(y_1, y_2, t, \theta) = {}& \mathrm{e}^{-Q_{\mathrm{s}}t}\, \delta(y_1)\, \delta(y_2) \\
& + \int_0^t Q_{\mathrm{s}}\, \mathrm{e}^{-Q_{\mathrm{s}}t'} \sum_{n=0}^{\infty} P(n) \sum_{k=0}^{n} \binom{n}{k} \varepsilon^k \, (1 - \varepsilon)^{(n-k)} \\
& \times \Bigg[\Delta(t' - \theta) \int_0^{y_2} \int_0^{y_1} U_k^{(2)}(y_1', y_2', t - t', \theta)\, p_2(y_1 - y_1', y_2 - y_2', t - t', \theta)\, \mathrm{d}y_1' \mathrm{d}y_2' \\
& + \Delta(\theta - t')\delta(y_2) \int_0^{y_1} U_k^{(1)}(y_1', t - t')\, p_1(y_1 - y_1', t - t')\, \mathrm{d}y_1' \Bigg] \mathrm{d}t'.
\end{aligned}
\tag{A.47}
$$

Here, again, Q_s and $P(n)$ denote the intensity and multiplicity of the source defined in Section 2.3.3; ε denotes the detection efficiency (the probability of detecting a neutron) introduced in Section 3.1; Δ denotes the Heaviside step function and was defined in (3.5); the function $U_k^{(2)}$ is defined as

$$U_k^{(2)}(y_1, y_2, t, \theta) = \int_0^\infty \cdots \int_0^\infty \cdot \int_0^\infty \cdots \int_0^\infty$$
$$\scriptstyle y_{1,1}+\cdots+y_{1,k}=y_1 \quad y_{2,1}+\cdots+y_{2,k}=y_2$$
$$h_2(y_{1,1}, y_{2,1}, t, \theta) \cdots h_2(y_{1,k}, y_{2,k}, t, \theta)\, \mathrm{d}y_{2,k} \cdots \mathrm{d}y_{2,1} \cdot \mathrm{d}y_{1,k} \cdots \mathrm{d}y_{1,1}. \tag{A.48}$$

The physical content of the function (A.48) is analogous to that of its one-point version (A.7): it is the two-point density function of k pulses induced by k neutrons originating from the same emission at time $t = 0$. As a k-fold convolution of h_2, it again reflects the fact that pulses induced by more that one neutrons are independent and add up linearly.

Equation (A.47), just like its one-point version Equation (A.6), is an application of the law of total probability and can be interpreted in the following way. The first term represents the event when no source emission occurs until time t with probability $\mathrm{e}^{-Q_s t}$, in which case the signal value at both times t and $t - \theta$ remains zero with probability density $\delta(y_1)\,\delta(y_2)$. The second term sums (or integrates) over the probabilities (or probability densities) of events each of which can be described as follows. The first emission occurs at time t' with probability $Q_s\, \mathrm{e}^{-Q_s t'}$. During the emission n neutrons are released with probability $P(n)$; from the n neutrons, k are detected and $n-k$ escape with probability $\binom{n}{k}\varepsilon^k\,(1-\varepsilon)^{n-k}$. In specifying the contribution of the pulses to the signal induced by the detected neutrons, two cases are distinguished (see the two terms in the square brackets) based on the value of t' (the time of first emission) relative to $t - \theta$. In the first case, when $t - \theta \geq t'$, the k pulses contribute by y_1' and y_2' to the value of the signal at times t and $t - \theta$ with a probability density $U_k^{(2)}(y_1', y_2', t-t', \theta)$; pulses from subsequent emissions contribute to it by $y_1 - y_1'$ and $y_2 - y_2'$ with a probability density $p_2(y_1 - y_1', y_2 - y_2', t-t', \theta)$. In the second case, when $t - \theta < t'$, the value of the signal is zero at time $t - \theta$ with a probability density $\delta(y_2)$; the k pulses contribute to the signal value at time t by y_1' with a probability density $U_k^{(1)}(y_1', t - t')$; pulses from subsequent emissions contribute to it by $y_1 - y_1'$ with probability density $p_1(y_1 - y_1', t-t')$.

Since no analytical solution of Equation (A.47) can be found, we transform it again to another equation for the characteristic function

$$\pi_2(\omega_1, \omega_2, t, \theta) = \int_{-\infty}^\infty \int_{-\infty}^\infty \mathrm{e}^{i(y_1\omega_1 + y_2\omega_2)}\, p_2(y_1, y_2, t, \theta)\, \mathrm{d}y_1 \mathrm{d}y_2.$$

by taking its two-dimensional Fourier transform with respect to the variables y_1 and y_2. Application of the convolution theorem and performing the same transformations as in the case of the one-point version yields the integral equation

$$\begin{aligned}
\pi_2(\omega_1, \omega_2, t, \theta) = {}& \mathrm{e}^{-Q_s t} + \int_0^t Q_s\, \mathrm{e}^{-Q_s(t-t')} \\
& \times \left[\Delta(t' - \theta)\, G\{c_1[\chi_2(\omega_1, \omega_2, t', \theta)]\}\, \pi_2(\omega_1, \omega_2, t', \theta) \right. \\
& \left. + \Delta(\theta - t')\, G\{c_1[\chi_1(\omega_1, t')]\}\, \pi_1(\omega_1, t') \right] \mathrm{d}t',
\end{aligned} \tag{A.49}$$

121

where the functions G, c_1, π_1, χ_1, χ_2 are defined in (**??**), (A.11), (A.2), (3.30) and (3.46), respectively.

In order to solve Equation (A.49) we again cast it into a differential equation. By differentiating both sides with respect to t, after rearranging the terms we get

$$\frac{\partial \pi_2(\omega_1, \omega_2, t, \theta)}{\partial t} = Q_\mathrm{s}\,\Delta(t - \theta)\,(G\{c_1[\chi_2(\omega_1, \omega_2, t, \theta)]\} - 1)\,\pi_2(\omega_1, \omega_2, t, \theta)$$
$$+ Q_\mathrm{s}\,\Delta(\theta - t)\,(G\{c_1[\chi_1(\omega_1, t)]\} - 1)\,\pi_1(\omega_1, t)$$

which, for $t > \theta$, reduces to

$$\frac{\partial \pi_2(\omega_1, \omega_2, t, \theta)}{\partial t} = Q_\mathrm{s}\,(G\{c_1[\chi_2(\omega_1, \omega_2, t, \theta)]\} - 1)\,\pi_2(\omega_1, \omega_2, t, \theta). \tag{A.50a}$$

The initial condition corresponding to this equation, using (A.46), reads as

$$\pi_2(\omega_1, \omega_2, t = \theta, \theta) = \pi_1(\omega_1, \theta). \tag{A.50b}$$

It is easy to see that (A.50) has the solution

$$\pi_2(\omega_1, \omega_2, t, \theta) = \pi_1(\omega_1, \theta)\,\exp\left[Q_\mathrm{s}\int_\theta^t (G\{c_1[\chi_2(\omega_1, \omega_2, t', \theta)]\} - 1)\,\mathrm{d}t'\right].$$

In the possession of the characteristic function π_2, we can now obtain the stationary cumulant-generating function

$$\gamma_2(\omega_1, \omega_2, \theta) = \lim_{t\to\infty} \ln[\pi_2(\omega_1, \omega_2, t, \theta)],$$

which takes the form

$$\gamma_2(\omega_1, \omega_2, \theta) = \gamma_1(\omega_1, \theta) + Q_\mathrm{s}\int_\theta^\infty (G\{c_1[\chi_2(\omega_1, \omega_2, t, \theta)]\} - 1)\,\mathrm{d}t, \tag{A.51}$$

where γ_1 is the one-point stationary cumulant-generating function defined in (A.3). Using this equation, the two-point stationary cumulant of order (m, n) can be calculated as

$$\kappa_{m,n}(\theta) = \frac{1}{\imath^{(m+n)}}\left.\frac{\partial^{(m+n)}\gamma_2(\omega_1, \omega_2, \theta)}{\partial\omega_1^m\,\partial\omega_2^n}\right|_{\omega_1=\omega_2=0}. \tag{A.52}$$

As noted in the beginning of Section 3.4, the only moment of interest here is the auto-covariance function $\mathrm{Cov}_2(\theta)$, defined in (3.41a), which is identical to the cumulant $\kappa_{1,1}(\theta)$. Substituting (A.51) into (A.52) and performing the required operations yields the result

$$\mathrm{Cov}_2(\theta) = Q_\mathrm{s}\,\nu_1\,\varepsilon\int_\theta^\infty \mu_{1,1}(t, \theta)\,\mathrm{d}t + Q_\mathrm{s}\,\nu_2\,\varepsilon^2\int_\theta^\infty \mu_1(t)\,\mu_1(t - \theta)\,\mathrm{d}t,$$

where μ_1 and $\mu_{1,1}$, the moments of the pulse, were defined in (3.31) and (3.48), respectively. If we also account for the definitions (2.22) of the detection rates, the covariance function takes the form

$$\mathrm{Cov}_2(\theta) = S\int_\theta^\infty \mu_{1,1}(t, \theta)\,\mathrm{d}t + 2\,D\int_\theta^\infty \mu_1(t)\,\mu_1(t - \theta)\,\mathrm{d}t. \tag{A.53}$$

Let us take a look at the physical meaning of this last equation. The auto-covariance function of the signal has two components: the first one is the "auto-covariance function" $\mu_{1,1}$ of one pulse (single), whereas the second one is the "cross-covariance function" $\mu_1\,\mu_1$ of two distinct pulses (doubles).

If we now substitute the explicit forms of μ_1 and $\mu_{1,1}$ into (A.53) then, by introducing

$$I_{m,n}(t,s) = \int_0^\infty f^m(t-\tau)\,f^n(s-\tau)\,u(\tau)\,\mathrm{d}\tau \tag{A.54}$$

further using (A.40), we get

$$\mathrm{Cov}_2(\theta) = S\,\langle a^2\rangle \int_\theta^\infty I_{1,1}(t,t-\theta)\,\mathrm{d}t + 2\,D\,\langle a\rangle^2 \int_\theta^\infty I_1(t)\,I_1(t-\theta)\,\mathrm{d}t.$$

This equation can be rewritten into a slightly simpler form. First note that, by accounting for the fact that $f(t)=0$ for $t<0$, the lower boundary of the integral in both terms on the right-hand side can be changed from θ to 0 without changing its value. In the first term, by applying the convolution theorem and accounting for the fact that the integral of the density function u is unity, we can write

$$\int_0^\infty I_{1,1}(t,t-\theta)\,\mathrm{d}t = \int_0^\infty \int_0^\infty f(t-\tau)\,f(t-\theta-\tau)u(\tau)\,\mathrm{d}\tau\mathrm{d}t = \int_0^\infty f(t)\,f(t-\theta)\,\mathrm{d}t.$$

The second term, on the other hand, cannot be simplified in a similar way. With these considerations, $\mathrm{Cov}_2(\theta)$ now takes the form

$$\mathrm{Cov}_2(\theta) = S\,\langle a^2\rangle \int_0^\infty f(t)\,f(t-\theta)\,\mathrm{d}t + 2\,D\,\langle a\rangle^2 \int_0^\infty I_1(t)\,I_1(t-\theta)\,\mathrm{d}t. \tag{A.55}$$

As noted in the beginning of Section 3.4, we are mostly interested in the integral Cov_2 of the auto-covariance function defined in (3.44), which can formally be written as

$$\mathrm{Cov}_2 = S\,\langle a^2\rangle \int_0^\infty \int_0^\infty f(t)\,f(t-\theta)\,\mathrm{d}t\mathrm{d}\theta + 2\,D\,\langle a\rangle^2 \int_0^\infty \int_0^\infty I_1(t)\,I_1(t-\theta)\,\mathrm{d}t\mathrm{d}\theta.$$

This equation can also be brought to a simpler form. By applying the convolution theorem to the integral in the second term and accounting for (A.40), we can write

$$\int_0^\infty \int_0^\infty I_1(t)\,I_1(t-\theta)\,\mathrm{d}t\mathrm{d}\theta = \left[\int_0^\infty I_1(t)\,\mathrm{d}t\right]^2 = I_1^2.$$

In the case of the integral in the first term, let us first switch the order of the integration with respect to t and θ. Then notice that, by recalling that $f(t)=0$ for $t<0$, the upper limit of the integral with respect to θ can be changed from ∞ to t without altering its value. Finally, by introducing the function $F(t) = \int_0^t f(t')\,\mathrm{d}t'$ and noting that $\lim_{t\to\infty} F(t) = F(\infty) = I_1$, we can write

$$\int_0^t \int_0^\infty f(t)\,f(t-\theta)\,\mathrm{d}t\mathrm{d}\theta = \int_0^\infty f(t)\,F(t)\,\mathrm{d}t = \frac{1}{2}\int_0^\infty \frac{\mathrm{d}}{\mathrm{d}t}F^2(t)\,\mathrm{d}t = \frac{1}{2}\,F^2(\infty) = \frac{1}{2}\,I_1^2.$$

With these considerations the integral Cov_2 of the covariance function takes the particularly simple form

$$\mathrm{Cov}_2 = \frac{1}{2}\left[S\,\langle a^2\rangle + 2\,D\,\langle a\rangle^2\right]\,I_1^2. \tag{A.56}$$

123

A.3.2   Two-point distribution of two detector signals

The two-point distribution of the signal of two detectors, say those labeled with 1 and 2, concerns the random variable $\{\boldsymbol{y}_1(t), \boldsymbol{y}_2(t - \theta)\}$, which is characterized by the cumulative distribution function

$$F_{1,1}(y_1, y_2, t, \theta) = \mathbb{P}\left[\boldsymbol{y}_1(t) \leq y_1, \boldsymbol{y}_2(t - \theta) \leq y_2\right].$$

The procedure of calculating the moments of this distribution is a rather straight-forward extension of that of the two-point moments of one signal and the one-point moments of two signals. For this reason, most details of the derivation will be omitted and only the key formulas will be presented without any particular commentary.

The density function, which in this case is defined as

$$p_{1,1}(y_1, y_2, t, \theta) = \frac{\partial^2}{\partial y_1 \partial y_2} F_{1,1}(y_1, y_2, t, \theta), \tag{A.57}$$

for $\theta \geq 0$ and $t < \theta$ takes the form

$$p_{1,1}(y_1, y_2, t, \theta) = p_1(y_1, t)\, \delta(y_2),$$

whereas for $t \geq \theta$ obeys the Kolmogorov backward integral equation

$$
\begin{aligned}
p_{1,1}(y_1, y_2, t, \theta) =\ & \mathrm{e}^{-Q_\mathrm{s} t}\, \delta(y_1)\, \delta(y_2) \\
& + Q_\mathrm{s} \int_0^t \mathrm{e}^{-Q_\mathrm{s} t'} \sum_{n=0}^{\infty} P(n) \sum_{k_0 + k_1 + k_2 = n} \frac{n!}{k_0!\, k_1!\, k_2!}\, \varepsilon^{k_1} \varepsilon^{k_2} \\
& \times \left[\Delta(t' - \theta) \int_0^{y_2} \int_0^{y_1} U_{k_1}^{(1)}(y_1', t - t')\, U_{k_2}^{(1)}(y_2', t - t' - \theta) \right. \\
& \times\ p_{1,1}(y_1 - y_1', y_2 - y_2', t - t', \theta)\, \mathrm{d}y_1' \mathrm{d}y_2' \\
& \left. + \Delta(\theta - t')\, \delta(y_2) \int_0^{y_1} U_{k_1}^{(1)}(y_1', t - t')\, p_1(y_1 - y_1', t - t')\, \mathrm{d}y_1' \right] \mathrm{d}t',
\end{aligned}
\tag{A.58}
$$

The interpretation of Equation (A.58) is analogous to that of (A.20) and (A.47).

After taking the two-dimensional Fourier transform of the above equation with respect to y_1 and y_2, we find that the characteristic function

$$\pi_{1,1}(\omega_1, \omega_2, t, \theta) = \int_{-\infty}^{\infty} \int_{-\infty}^{\infty} \mathrm{e}^{\imath(y_1 \omega_1 + y_2 \omega_2)}\, p_{1,1}(y_1, y_2, t, \theta)\, \mathrm{d}y_1 \mathrm{d}y_2 \tag{A.59}$$

satisfies the differential equation

$$\frac{\partial\, \pi_{1,1}(\omega_1, \omega_2, t, \theta)}{\partial t} = Q_\mathrm{s}\left(G\{c_2[\chi_1(\omega_1, t'), \chi_1(\omega_2, t' - \theta)]\} - 1\right) \pi_{1,1}(\omega_1, \omega_2, t, \theta)$$

for $t \geq \theta$, with the initial condition

$$\pi_2(\omega_1, \omega_2, t = \theta, \theta) = \pi_1(\omega_1, \theta).$$

The solution of this differential equation reads as

$$\begin{aligned}
\pi_{1,1}(\omega_1, \omega_2, t, \theta) &= \pi_1(\omega_1, \theta) \\
&\times \exp\left[Q_s \int_\theta^t \left(G\{c_2[\chi_1(\omega_1, t'), \chi_1(\omega_2, t' - \theta)]\} - 1 \right) \mathrm{d}t' \right].
\end{aligned} \tag{A.60}$$

Using (A.60) the stationary cumulant generating function

$$\gamma_{1,1}(\omega_1, \omega_2, \theta) = \lim_{t \to \infty} \ln[\pi_{1,1}(\omega_1, \omega_2, t, \theta)] \tag{A.61}$$

can be obtained and takes the form

$$\gamma_{1,1}(\omega_1, \omega_2, \theta) = \gamma_1(\omega_1, \theta) + Q_s \int_\theta^\infty \left(G\{c_2[\chi_1(\omega_1, t), \chi_1(\omega_2, t - \theta)]\} - 1 \right) \mathrm{d}t, \tag{A.62}$$

from which the cumulant of order (m, n) can be calculated as

$$\kappa_{m,n}(\theta) = \left. \frac{\partial^{(m+n)} \gamma_{1,1}(\omega_1, \omega_2, \theta)}{\partial \omega_1^m \, \partial \omega_2^n} \right|_{\omega_1 = \omega_2 = 0}. \tag{A.63}$$

As noted in the beginning of Section 3.4, the only moment of interest here is the cross-covariance function $\mathrm{Cov}_{1,1}(\theta)$, defined in (3.42), which is identical to the cumulant $\kappa_{1,1}(\theta)$. Substituting (A.62) into (A.63), after similar considerations as in the case of the two-point moments of one detector, we get

$$\mathrm{Cov}_{1,1}(\theta) = 2\,D \int_\theta^\infty \mu_1(t)\,\mu_1(t - \theta)\, \mathrm{d}t,$$

where μ_1, the moment of the pulse, was defined in (3.31). The interpretation of this equation is analogous to that of (A.53). The cross-covariance function of the signal has one component: the "cross-covariance function" $\mu_1 \mu_1$ of two distinct pulses (doubles) each from a different detector.

By substituting the explicit form of μ_1 and performing the same simplifications as in the case of the auto-covariance function Cov_2, we obtain

$$\mathrm{Cov}_{1,1}(\theta) = 2\,D \langle a \rangle^2 \int_0^\infty I_1(t)\,I_1(t - \theta)\, \mathrm{d}t. \tag{A.64}$$

Again, the main quantity of interest is the integral $\mathrm{Cov}_{1,1}$ of the cross-covariance function, defined in (3.44) which, after simplification, takes the form

$$\mathrm{Cov}_{1,1} = D \langle a \rangle^2 I_1^2. \tag{A.65}$$

A.3.3   Three-point distribution of one detector signal

The three-point distribution of the signal of one detector, say that labeled with 1, concerns the random variable $\{\boldsymbol{y}_1(t), \boldsymbol{y}_1(t - \theta)\}, \boldsymbol{y}_1(t - \theta - \rho)\}$, which is characterized by the cumulative distribution function

$$F_3(y_1, y_2, y_3, t, \theta, \rho) = \mathbb{P}\left[\boldsymbol{y}_1(t) \le y_1, \boldsymbol{y}_1(t - \theta) \le y_2, \boldsymbol{y}_1(t - \theta - \rho) \le y_3 \right].$$

Since the procedure of calculating the moments of this distribution is a straightforward analogy of that of the two-point distribution of one signal, we shall again omit most of the details of the derivation.

The density function, which in this case is defined as

$$p_3(y_1, y_2, y_3, t, \theta, \rho) = \frac{\partial^3 F_3(y_1, y_2, y_3, t, \theta, \rho)}{\partial y_1 \, \partial y_2 \, \partial y_3} \tag{A.66}$$

for $\theta, \rho \geq 0$ and $t < \theta + \rho$ takes the form

$$p_3(y_1, y_2, y_3, t, \theta, \rho) = p_2(y_1, y_2, t, \theta) \, \delta(y_3),$$

whereas for $t \geq \theta + \rho$ it obeys the Kolmogorov backward integral equation

$$
\begin{aligned}
p_3(y_1, y_2, y_3, t, \theta, \rho) &= \mathrm{e}^{-Q_s t} \, \delta(y_1) \, \delta(y_2) \, \delta(y_3) \\
&+ Q_s \int_0^t \mathrm{e}^{-Q_s t'} \sum_{n=0}^{\infty} P(n) \sum_{k=0}^{n} \binom{n}{k} \varepsilon^k \, (1 - \varepsilon)^{n-k} \\
&\times \Bigg[\Delta[t' - (\theta + \rho)] \int_0^{y_3} \int_0^{y_2} \int_0^{y_1} U_k^{(3)}(y_1', y_2', y_3', t - t', \theta, \rho) \\
&\times p_3(y_1 - y_1', y_2 - y_2', y_3 - y_3', t - t', \theta, \rho) \, \mathrm{d}y_1' \mathrm{d}y_2' \mathrm{d}y_3' \\
&+ \Delta[(\theta + \rho) - t'] \delta(y_3) \int_0^{y_2} \int_0^{y_1} U_k^{(2)}(y_1', y_2', t - t', \theta) \\
&\times p_2(y_1 - y_1', y_2 - y_2', t - t', \theta) \, \mathrm{d}y_1' \mathrm{d}y_2' \Bigg] \mathrm{d}t',
\end{aligned}
\tag{A.67}
$$

where $U_k^{(3)}$ is defined as

$$
\begin{aligned}
U_k^{(3)}(y_1, y_2, y_3, t, \theta, \rho) &= \underbrace{\int_0^{\infty} \cdots \int_0^{\infty}}_{y_{1,1} + \cdots + y_{1,k} = y_1} \cdot \underbrace{\int_0^{\infty} \cdots \int_0^{\infty}}_{y_{2,1} + \cdots + y_{2,k} = y_2} \cdot \underbrace{\int_0^{\infty} \cdots \int_0^{\infty}}_{y_{3,1} + \cdots + y_{3,k} = y_3} \\
&\times h^{(3)}(y_{1,1}, y_{2,1}, y_{3,1}, t, \theta, \rho) \cdots h^{(3)}(y_{1,k}, y_{2,k}, y_{3,k}, t, \theta, \rho) \\
&\times \mathrm{d}y_{3,k} \cdots \mathrm{d}y_{3,1} \cdot \mathrm{d}y_{2,k} \cdots \mathrm{d}y_{2,1} \cdot \mathrm{d}y_{1,k} \cdots \mathrm{d}y_{1,1}.
\end{aligned}
\tag{A.68}
$$

The interpretation of (A.67) and (A.68) is analogous to that of (A.47) and (A.48).

After taking the two-dimensional Fourier transform of the above equation with respect to y_1 and y_2, we find that the characteristic function

$$
\begin{aligned}
\pi_3(\omega_1, \omega_2, \omega_3, t, \theta, \rho) &= \int_{-\infty}^{\infty} \int_{-\infty}^{\infty} \int_{-\infty}^{\infty} \mathrm{e}^{\imath(y_1 \omega_1 + y_2 \omega_2 + y_3 \omega_3)} \\
&\times p_3(y_1, y_2, y_3, t, \theta, \rho) \, \mathrm{d}y_1 \mathrm{d}y_2 \mathrm{d}y_3.
\end{aligned}
\tag{A.69}
$$

satisfies the differential equation

$$\frac{\partial}{\partial t} \pi_3(\omega_1, \omega_2, \omega_3, t, \theta, \rho) = Q_s \left(G\{c_1[\chi_3(\omega_1, \omega_2, \omega_3, t, \theta, \rho)]\} - 1 \right) \pi_3(\omega_1, \omega_2, \omega_3, t, \theta, \rho)$$

for $t \geq \theta + \rho$, with the initial condition

$$\pi_3(\omega_1, \omega_2, \omega_3, t = \theta + \rho, \theta, \rho) = \pi_2(\omega_1, \omega_2, \theta + \rho, \theta).$$

The solution of this differential equation reads as

$$\pi_3(\omega_1, \omega_2, \omega_3, t, \theta, \rho) = \pi_2(\omega_1, \omega_2, \theta + \rho, \theta)$$

$$\times \exp\left[Q_s \int_{\theta+\rho}^{t} \left(G\{c_1[\chi_3(\omega_1, \omega_2, \omega_3, t', \theta, \rho)]\} - 1 \right) \mathrm{d}t' \right]. \tag{A.70}$$

Using (A.70) the stationary cumulant generating function

$$\gamma_3(\omega_1, \omega_2, \omega_3, \theta, \rho) = \lim_{t\to\infty} \ln[\pi_3(\omega_1, \omega_2, \omega_3, t, \theta, \rho)] \tag{A.71}$$

can be obtained and takes the form

$$\gamma_3(\omega_1, \omega_2, \omega_3, \theta, \rho) = \gamma_2(\omega_1, \omega_2, \theta + \rho, \theta) \tag{A.72}$$

$$+ Q_s \int_{\theta+\rho}^{\infty} \left(G\{c_1[\chi_3(\omega_1, \omega_2, \omega_3, t, \theta, \rho)]\} - 1 \right) \mathrm{d}t. \tag{A.73}$$

from which the cumulant of order (m, n, l) can be calculated as

$$\kappa_{m,n,l}(\theta, \rho) = \left. \frac{\partial^{(m+n+l)} \gamma_3(\omega_1, \omega_2, \omega_3, \theta, \rho)}{\partial \omega_1^m \, \partial \omega_2^n \, \partial \omega_2^l} \right|_{\omega_1=\omega_2=\omega_3=0}. \tag{A.74}$$

As noted in the beginning of Section 3.4, the only moment of interest here is the auto-bicovariance function $\mathrm{Cov}_3(\theta, \rho)$, defined in (3.41b), which is identical to the cumulant $\kappa_{1,1,1}(\theta, \rho)$. Substituting (A.72) into (A.74), after similar considerations as in the case of the two-point moments of one detector, we get

$$\mathrm{Cov}_3(\theta, \rho) = S \int_{\theta+\rho}^{\infty} \mu_{1,1,1}(t, \theta, \rho) \, \mathrm{d}t$$

$$+ 2D \int_{\theta+\rho}^{\infty} [\mu_1(t) \, \mu_{1,1}(t, \rho)$$

$$+ \mu_1(t - \theta) \, \mu_{1,1}(t, \theta + \rho) + \mu_1(t - \theta - \rho) \, \mu_{1,1}(t, \theta)] \, \mathrm{d}t$$

$$+ 6T \int_{\theta+\rho}^{\infty} \mu_1(t) \, \mu_1(t - \theta) \, \mu_1(t - \theta - \rho) \, \mathrm{d}t,$$

where μ_1, $\mu_{1,1}$ and $\mu_{1,1,1}$, the moments of the pulse, were defined in (3.31), (3.48) and (3.51), respectively. The interpretation of this equation is analogous to that of (A.53). The auto-bicovariance function of the signal has three components: the "auto-bicovariance function" $\mu_{1,1,1}$ of one pulse (single), the "cross-bicovariance function" $\mu_1 \, \mu_{1,1}$ of two distinct pulses (doubles) and the "cross-bicovariance function" $\mu_1 \, \mu_1 \, \mu_1$ of three distinct pulses (triples).

By substituting the explicit forms of μ_1, $\mu_{1,1}$ and $\mu_{1,1,1}$ and performing the same simplifications as in the case of the auto-covariance function Cov_2, we obtain

$$\mathrm{Cov}_3(\theta, \rho) = S \langle a^3 \rangle \int_0^{\infty} f(t) \, f(t - \theta) \, f(t - \theta - \rho) \, \mathrm{d}t$$

$$+ 2D \langle a^2 \rangle \langle a \rangle \int_0^{\infty} [I_1(t) \, I_{1,1}(t - \theta, t - \theta - \rho)$$

$$+ I_1(t - \theta) \, I_{1,1}(t, t - \theta - \rho) + I_1(t - \theta - \rho) \, I_{1,1}(t, t - \theta)] \, \mathrm{d}t \tag{A.75}$$

$$+ 6T \langle a \rangle^3 \int_0^{\infty} I_1(t) \, I_1(t - \theta) \, I_1(t - \theta - \rho) \, \mathrm{d}t.$$

Again, the main quantity of interest is the integral Cov_3 of the cross-covariance function, defined in (3.45). Using similar considerations as in the case of Cov_3, one can show that the integrals in the first and last terms simplify to

$$\int_0^\infty \int_0^\infty \int_0^\infty f(t)\, f(t-\theta)\, f(t-\theta-\rho)\, \mathrm{d}t \mathrm{d}\theta \mathrm{d}\rho = \frac{1}{6}\, I_1^3$$

and

$$\int_0^\infty \int_0^\infty \int_0^\infty I_1(t)\, I_1(t-\theta)\, I_1(t-\theta-\rho)\, \mathrm{d}t \mathrm{d}\theta \mathrm{d}\rho = \frac{1}{6}\, I_1^3.$$

The integrals in the second term cannot be simplified in a similar manner. A possible explanation is that while the first and last terms represent a "pure auto-bicovariance" and "pure cross-bicovariance", the second term represents a "mix of auto- and cross-covariances" which is not invariant to a time shift (such a mixed term could not exist in the two-point version of this moment, Cov_2). Instead let us introduce the notations

$$\xi_A = \frac{6}{I_1^3} \int_0^\infty \int_0^\infty \int_0^\infty I_1(t)\, I_{1,1}(t-\theta, t-\theta-\rho)\, \mathrm{d}t \mathrm{d}\theta \mathrm{d}\rho, \tag{A.76a}$$

$$\xi_B = \frac{6}{I_1^3} \int_0^\infty \int_0^\infty \int_0^\infty I_1(t-\theta)\, I_{1,1}(t, t-\theta-\rho)\, \mathrm{d}t \mathrm{d}\theta \mathrm{d}\rho, \tag{A.76b}$$

$$\xi_C = \frac{6}{I_1^3} \int_0^\infty \int_0^\infty \int_0^\infty I_1(t-\theta-\rho)\, I_{1,1}(t, t-\theta)\, \mathrm{d}t \mathrm{d}\theta \mathrm{d}\rho, \tag{A.76c}$$

With these considerations, Cov_3 takes the particularly compact form

$$\mathrm{Cov}_3 = \frac{1}{6} \left[S\, \langle a^3 \rangle + 2\, D\, \langle a \rangle \langle a^2 \rangle (\xi_A + \xi_B + \xi_C) + 6\, T\, \langle a \rangle^3 \right] I_1^3. \tag{A.77}$$

A.3.4 Three-point distribution of three detector signals

The three-point distribution of the signal of three detectors, those labeled with 1, 2 and 3, concerns the random variable $\{\boldsymbol{y}_1(t), \boldsymbol{y}_2(t-\theta)\}, \boldsymbol{y}_3(t-\theta-\rho)\}$, which is characterized by the cumulative distribution function

$$F_{1,1,1}(y_1, y_2, y_3, t, \theta, \rho) = \mathbb{P}\left[\boldsymbol{y}_1(t) \leq y_1, \boldsymbol{y}_2(t-\theta) \leq y_2, \boldsymbol{y}_3(t-\theta-\rho) \leq y_3 \right].$$

Since the derivation of the moments of this distribution is a straightforward extension of that of the two-point distribution of two signals and three-point distribution of three signals, we shall only provide the final results.

The cross-bicovariance function of three signals, defined in (3.43), takes the form

$$\mathrm{Cov}_{1,1,1}(\theta, \rho) = 6\, T \int_{\theta+\rho}^\infty \mu_1(t)\, \mu_1(t-\theta)\, \mu_1(t-\theta-\rho)\, \mathrm{d}t$$

or, by substituting the explicit form of μ_1 from (3.31):

$$\mathrm{Cov}_{1,1,1}(\theta, \rho) = 6\, T\, \langle a \rangle^3 \int_0^\infty I_1(t)\, I_1(t-\theta)\, I_1(t-\theta-\rho)\, \mathrm{d}t. \tag{A.78}$$

The integral $\mathrm{Cov}_{1,1,1}$ of this function, defined in (3.45), reads as

$$\mathrm{Cov}_{1,1,1} = T\, \langle a \rangle^3\, I_1^3. \tag{A.79}$$

Appendix B

Calculation of the time delay distribution

B.1 Example of a realistic time delay and detector pulse shape

The quantities $\xi_{1,1}$, $\xi_{1,2}$ and $\xi_{1,1,1}$, defined by (3.33), are analogous to the gate factors of traditional multiplicity counting. They play a role similar to the gate factors f_d and f_t of the traditional multiplicity counting, and this analogy will be supported with some qualitative and quantitative investigations below. It is seen that, unlike in the theory of traditional multiplicity counting, these appear more straightforward from the theory. For any given detector pulse shape $f(t)$ and amplitude distribution $w(a)$, and known time delay distribution $u(\tau)$, the defining integrals can be calculated either analytically or numerically. The difficulty lies in the knowledge of the latter, whose determination requires further derivations. Similarly to traditional multiplicity counting, the time delay function, which is the basis of the gate factors, is not solely a property of the detector, but also of the experimental set-up, and, unlike in traditional multiplicity counting, a function of the (unknown) sample properties. For an illustration, in the next subsection, the time delay distribution will be calculated for the case of fast neutron detection from an item, where the only reason of the random detection time is the random velocity of the neutrons arising from a sample emitting neutrons with a given energy spectrum.

B.2 Time delay distribution: general

It is now a relevant question to ask into which of the above categories the realistic time delays and detector pulse shapes will fall. The pulse shape widths of fission chambers depend on the type and manufacture of the detector, and vary with the gas pressure and detector geometries. The pulses are rather short, in general in the range of some tens of ns. Regarding the fluctuations in the detection times, we shall make an estimate based on the assumption that both neutron emission and detection is instantaneous (after that the neutrons hit the detector), but neutrons from the item will travel with different speeds due to the energy spectrum of source neutrons. The

different speed will lead to different arrival times. To take an example (neglecting relativistic effects), it takes about $13\,\text{ns}$ for a $5\,\text{MeV}$ neutron to travel a distance of $40\,\text{cm}$, whereas the same time for a $2\,\text{MeV}$ neutron is $20.4\,\text{ns}$, the difference being less than $8\,\text{ns}$. This is very much on the same scale as the detector pulse width, hence the gate factors should be reasonably large.

In the continuation we shall assume that the neutrons are emitted from the sample with a given energy spectrum, and derive a general formula for the arrival time distribution corresponding to the given energy spectrum. In reality, the source event is a spontaneous fission, with a characteristic energy spectrum, whereas the neutrons generated in the internal multiplication before leaving the sample will have a different spectrum, corresponding to induced fission in the same material. However, we shall neglect this spectral difference. It will also be assumed that the energies of the neutrons from a fission event are independent of each other, and hence the corresponding arrival time distributions will also be independent (as it was assumed in the previous parts of the paper).

Before actually employing the concrete energy spectrum $f(E)$ of a given material, it is useful to derive a general formula for the of distribution of the arrival time τ in terms of the energy spectrum. The task is simply the calculation of the distribution of the function of a continuous random variable with a given distribution. This calculation is expedited if we notice that both variables have a positive support, i.e. the accessible values of E and τ satisfy the following conditions:

$$0 < E < \infty \quad \text{and} \quad 0 < \tau < \infty, \tag{B.1}$$

as well as that there is a strictly monotonic relationship between E and τ. Then, we can use the fact that if there exists a function g such that

$$\tau = g(E), \tag{B.2}$$

furthermore g

1. is monotonic;

2. is continuously differentiable;

3. has a non-zero derivative everywhere,

then the distribution $u(\tau)$ can be expressed from the relationships[1]

$$u(\tau)d\tau = f(E)dE \tag{B.3}$$

and hence

$$u(\tau) = f(E)\,|dE/d\tau| \tag{B.4}$$

where

$$|dE/d\tau| = m\,\frac{s^2}{\tau^3} \tag{B.5}$$

---

[1]The formula provided here does not refer to the most general case, only when g satisfies the above listed conditions.

Assuming that the flight distance from the item to the detector is constant, denoted by s, then the relationship between E and τ is given by

$$E = \frac{m}{2}v^2 \qquad \text{and} \qquad v = \frac{s}{\tau}, \quad \text{hence} \qquad E(\tau) = \frac{m}{2}\frac{s^2}{\tau^2}, \tag{B.6}$$

where m is the rest mass of the neutron. Note that in order to express the energy in units of eV, the value of the mass should be substituted by $m = m'/c^2$, where m' is the mass in units of eV/c^2 and c is the speed of light. Using these expressions, one obtains the relationship

$$u(\tau; s) = m\frac{s^2}{\tau^3}f\left(\frac{m}{2}\frac{s^2}{\tau^2}\right) \tag{B.7}$$

With this last expression, the density function of the time delay can be calculated for any source spectrum given in an analytical form.

B.3 Time delay distribution: Watt spectrum

The energy distribution of fission neutrons is usually described by the Watt-spectrum, which is parametrized by two rate parameters a and b, which also uniquely identify the isotope [92]. The density function of the distribution is:

$$f(x) = \frac{\exp\left(-\dfrac{ab}{4}\right)}{a\sqrt{\dfrac{\pi ab}{4}}}\exp\left(-\frac{x}{a}\right)\sinh\left(\sqrt{b\,x}\right) \qquad x > 0. \tag{B.8}$$

If the energy x has units of eV, then a must have units of eV, whereas b must have units of $1/eV$.

Substituting (B.8) into the general expression (B.7), we obtain:

$$u(\tau; s) = \frac{\exp\left(-\dfrac{ab}{4}\right)}{a\sqrt{\dfrac{\pi ab}{4}}}m\frac{s^2}{\tau^3}\exp\left(-\frac{m}{2\,a}\frac{s^2}{\tau^2}\right)\sinh\left(\sqrt{\frac{b\,m}{2}}\frac{s}{\tau}\right) \qquad s, \tau > 0. \tag{B.9}$$

Figure B.1 shows these density functions for some typical values of their parameters.

B.4 Choice of the pulse shape function

In many applications, a double exponential function normalized to a unit amplitude is used with two scale parameters α and β ($0 < \beta < \alpha$):

$$f(t; \alpha, \beta) = \frac{1}{C}\left(e^{-t/\alpha} - e^{-t/\beta}\right) \qquad t > 0, \tag{B.10}$$

where β is the pulse rise time and α is the pulse fall time. In the quantitative work in the forthcoming, we shall use such a pulse shape function. Once the pulse shape is
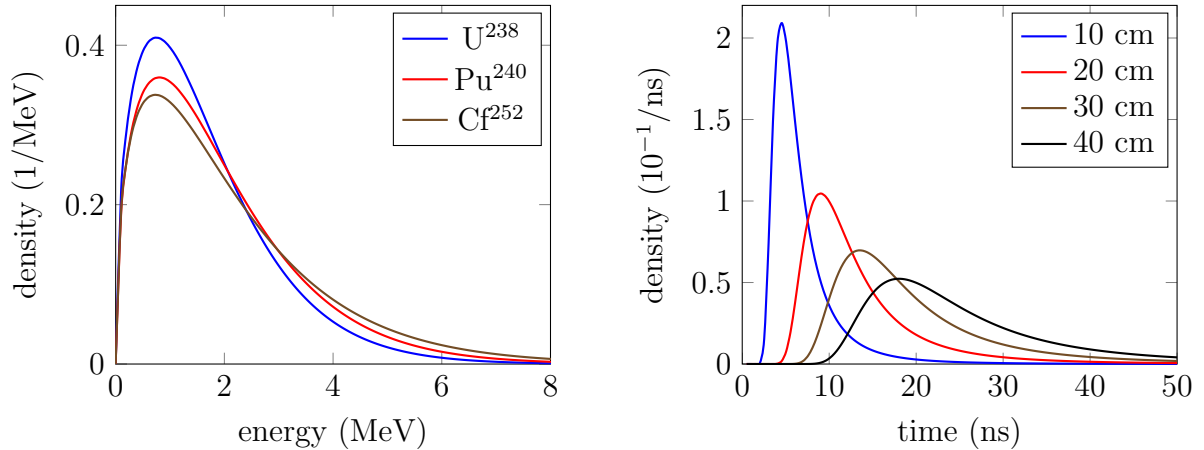
(a) The distribution of the energy of neutrons from spontaneous fission of different isotopes. Watt parameter values are taken from [25, Appendix H.].

(b) The distribution of the travelling time of neutrons originating from the spontaneous fission of Pu^{240} for different travelling distances.

Figure B.1

fixed, the integral parameters I_n, $i = 1, 2, 3$, defined in (3.21) can be calculated, with the following results:

$$I_1 = \frac{\alpha - \beta}{C} \qquad I_2 = \frac{(\alpha - \beta)^2}{2(\alpha + \beta)C^2} \qquad I_3 = \frac{2(\alpha - \beta)^3}{3(2\alpha + \beta)(\alpha + 2\beta)C^3}. \qquad \text{(B.11)}$$

In the expressions above, C is a normalization factor with the following definition:

$$C = \left(\frac{\beta}{\alpha}\right)^{\beta/(\alpha - \beta)} - \left(\frac{\beta}{\alpha}\right)^{\alpha/(\alpha - \beta)} \qquad \text{(B.12)}$$

B.5   Calculation of the gate factors

With the above choice of the detector pulse shape and the calculated distribution of time delay, everything is given to calculate the gate factors $\xi_{i,j,k}$ of Eq. (3.33). In view of the involved form of the integrand functions, especially the time delay function (B.9), an analytical calculation is not possible. Instead, these integrals were evaluated numerically. For a fixed source and detector characteristics, the dependence of the values of the ξ factors on the source-detector distance was investigated. Since according to Fig. B.1, the neutron spectrum (and hence, the travelling time density) is similar for the different spontaneously fissioning isotopes, we choose the Pu^{240} for this calculation, due to its practical relevance. As for the detector characteristics, we chose $\alpha = 20$ ns and $\beta = 5$ ns as scale parameters in the pulse shape function (B.10), which is a typical value for fission chambers and results in an approximate pulse width of 100 ns [93].

The results are shown in Figure B.2. It is seen that the gate factors remain reasonably high up to a distance of 1 m between the source and the detector, although for this case $\xi_{1,1,1}$ is already down to about 0.1. Together with other deteriorating circumstances not accounted for here, such as the finite detection emission and detection

time, in practice, a distance of a couple of tens centimetres appears to be a maximum when the method is applicable in its present form.
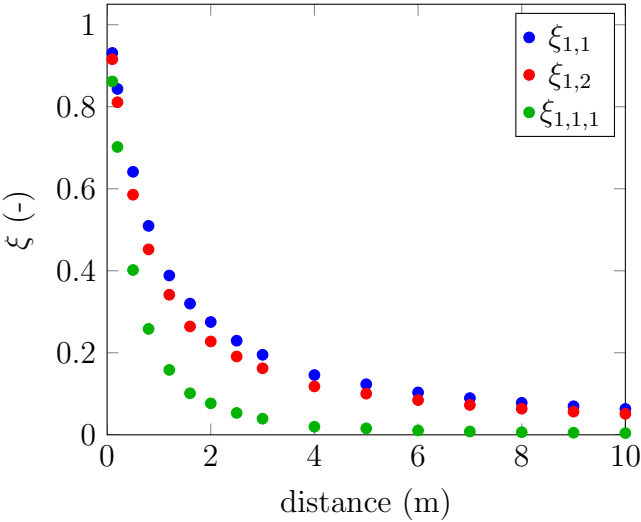

Figure B.2: The values of the ξ factors at different source-detector distances ranging from 0.1 m to 10 m.